DOKUZ EYLÜL UNIVERSITY
GRADUATE SCHOOL OF NATURAL AND APPLIED SCIENCES

FOUNDATION ANALYSIS OF A 14 STORY HIGH BUILDING ACCORDING TO İZMİR LOCAL TECHNICAL ADVISORY TALL BUILDINGS

by

Mustafa ŞAHİN

November, 2015

İZMİR

FOUNDATION ANALYSIS OF A 14 STORY HIGH BUILDING ACCORDING TO İZMİR LOCAL TECHNICAL ADVISORY TALL BUILDINGS

A Thesis Submitted to the
Graduate School of Natural and Applied Sciences of Dokuz Eylül University
In Partial Fulfillment of the Requirements for the Degree of Master of Science in Civil Engineering, Geotechnical Engineering Program

by

Mustafa ŞAHİN

November, 2015

İZMİR

M.Sc. THESIS EXAMINATION RESULT FORM

We have read the thesis entitled **"FOUNDATION ANALYSIS OF A 14 STORY HIGH BUILDING ACCORDING TO IZMIR LOCAL TECHNICAL ADVISORY TALL BUILDINGS"** completed by **MUSTAFA ŞAHİN** under supervision of **PROF. DR. GÜRKAN ÖZDEN** and we certify that in our opinion it is fully adequate, in scope and in quality, as a thesis for the degree of Master of Science.

Prof. Dr. Gürkan ÖZDEN

Supervisor

Recep BİRGÜL

(Jury Member)

Hikmet H. ÇATAL

(Jury Member)

Prof. Dr. Ayşe OKUR
Director
Graduate School of Natural and Applied Sciences

ACKNOWLEDGEMENT

I would like to express my deepest gratitude to my advisor, Prof. Dr. Gürkan ÖZDEN, for his excellent guidance, caring, patience, and providing me with an excellent atmosphere for doing research. His guidance helped me in all the time throughout research and writing period this thesis.

I would also thank all academic staff of Geotechnical Department of Civil Engineering at Dokuz Eylül University for their contributions.

I would like to thank Cemal COŞAK and Çağrıhan SARIAVCI for their great encouragement and support in my thesis.

First and foremost, I would like to thank my wife Senem for standing beside me throughout my career and writing this thesis. She has been my inspiration and motivation for continuing to improve my knowledge and move my career forward.

Mustafa ŞAHİN

FOUNDATION ANALYSIS OF A 14 STORY HIGH BUILDING ACCORDING TO İZMİR LOCAL TECHNICAL ADVISORY TALL BUILDINGS

ABSTRACT

The goal of this study is to investigate use of İzmir Local Technical Advisory for Tall Buildings by means of analyses of the foundation system of a sample building. The building is considered to be situated on the east coast of İzmir Bay Area and its inertial soil-structure interaction analyses were made. Computations were performed obeying the procedure as defined by NEHRP. The dynamic stiffness of the pile group was obtained according to Makris-Gazetas approach. A software was developed for this purpose and achieved results were compared with those from the DYNAN software. The flexible behavior of the foundation was taken into consideration by distributing the computed group stiffness within the foundation zones. Influence of this zonation approach on the building period required application of an iterative procedure. Iterations continued until computed dynamic group stiffness values with respect to the building period converged. The D1, D2 and D3 level response spectra produced according to the DLH Technical Standard were utilized as the target spectra while performing dynamic analyses of the buildings being designed in the area. The acceleration-time records that were necessary in this respect were selected from the PEER Ground Motion Database. The ground motions at the foundation level of the building were computed through one-dimensional site response analyses. Variation of shear wave velocity with depth was deduced using geophysical field tests whereas other conventional soil mechanics data were acquired based on the soil mechanics laboratory test results. Such data obtained at various locations and depth levels were used while establishing the idealized soil profile. Two different rock levels were assumed in the idealized soil profile during dynamic analyses. These were the engineering bedrock and the seismic rock levels yielding two sets of ground motion records at the foundation level. The results of time-domain structural analyses were then compared. It was found that the analyses that were made using engineering bedrock level ground motion set yielded results that stay on the unsafe side.

Keywords: Inertial, site response analysis, impedance, spring stiffness, bedrock.

ONDÖRT KATLI BİR YAPI TEMELİNİN YÜKSEK BİNALAR İÇİN İZMİR YEREL TEKNİK ÖNERMESİNE GÖRE ANALİZİ

ÖZ

Bu çalışmanın amacı İzmir Yüksek Yapılar Teknik Önermesi'nin örnek bir yapının temel sistemi analizinde kullanımının incelenmesidir. İzmir Körfezi'nin doğu kıyısında yer aldığı kabul edilen 14 katlı bir yüksek binanın zemin-yapı etkileşim analizleri yapılmış; bu kapsamda sadece atalet etkileşimi analizleri gerçekleştirilmiştir. Hesaplar NEHRP tarafından tarif edilen yönteme göre yapılmıştır. Analizlerde kazık grubu dinamik rijitliği Makris ve Gazetas yaklaşımına göre elde edilmiştir. Bunun için bir yazılım geliştirilmiş; elde edilen sonuçlar DYNAN yazılımı sonuçları ile karşılaştırılmıştır. Temelin elastik davranışı, kazık grubu dinamik rijitliklerinin temel alanı içinde zonlanarak kullanılmasıyla dikkate alınmıştır. Bu kabulün yapı periyoduna olan etkisi iteratif bir analizi gerektirmiştir. İterasyon sırasında kazık grubu dinamik rijitliği yapı periyoduna bağlı olarak hesaplanarak yakınsama sağlanana kadar yenilenmiştir. Yüksek Yapılar Teknik Önermesi'ne göre bölgede yapılmakta olan dinamik analizlerde DLH Teknik Yönetmeliği'nde tanımlanmış D1, D2 ve D3 deprem seviyelerine karşı gelen spektrumlar hedef spektrum olarak kullanılmaktadır. Bu yöntemle gerekli ivme-zaman kayıtları PEER veritabanından seçilmiştir. Çalışma alanında temel seviyesindeki yer hareketi kaydının elde edilmesi amacıyla, bir boyutlu dinamik zemin davranışı analizleri yapılmıştır. Kayma dalgasının derinlikle değişim verileri jeofizik arazi deneylerinden, diğer zemin parametreleri ise zemin mekaniği laboratuar deneylerinden elde edilmiştir. Arazideki farklı konum ve derinliklerden elde edilen parametreler idealize bir zemin profili oluşturulmasında kullanılmıştır. Analizlere esas zemin profili için iki farklı kaya seviyesi kabul edilmiştir. Bunlar; Mühendislik Taban Kayası ve Sismik Kaya seviyeleridir. Bu iki farklı zemin profili için temel seviyesinde iki ayrı grup ivme kaydı elde edilmiştir. Bu iki grup kayıt üst yapının zaman tanım alanındaki analizlerinde kullanılarak sonuçlar karşılaştırılmıştır. Elde edilen sonuçlara göre Mühendislik Taban Kaya Seviyesi'ne göre yapılan analizler güvensiz tarafta kalan sonuçlar vermektedir.

Anahtar kelimeler: Atalet, zemin davranışı analizi, empedans, yay rijitliği, anakaya.

CONTENTS

Page

THESIS EXAMINATION RESULT FORM i

ACKNOWLEDGEMENT ii

ABSTRACT iii

ÖZ iv

LIST OF FIGURES vi

LIST OF TABLES xii

CHAPTER ONE – INTRODUCTION 1

1.1 Background 1

1.2 Organization of the Thesis 2

CHAPTER TWO – SITE SPECIFIC GEOTECHNICAL INVESTIGATION AND DYNAMIC SITE RESPONSE ANALYSES 4

2.1 Introduction 4

2.2 Measurement of Dynamic Soil Properties 4

2.2.1 Multichannel Analysis of Surface Waves (MASW) 5

2.2.2 Down-Hole Test 5

2.2.3 SPAC (Spatial Auto-Correlation) Method 5

2.2.4 Laboratory Methods 6

2.3 Nonlinear Dynamic Site Response Analysis 6

2.3.1 Modeling Soil Profile 7

2.3.2 Material Model 8

2.3.3 Selecting Input Rock Motion 12

2.4 Site Response Analyses 13

CHAPTER THREE - SOIL STRUCTURE INTERACTION ANALYSIS........ 14

3.1 Introduction 14

3.2 Inertial Interaction 14

3.2.1 Factors Affecting the Inertial Interaction 15

3.2.2 Impedance Function of the Foundation-Soil Interface 16

3.2.3 Elastic Solution of the Foundation Dynamic Stiffness............................ 18

3.2.4 Effect of Non-Uniform Soil Over the Foundation Dynamic Stiffness.... 24

3.2.5 Effect of Soil Nonlinearity 26

3.2.6 Effect of Flexible Foundation... 26

3.2.7 Pile Group Dynamic Stiffness 32

3.2.7.1 Lateral Dynamic Stiffness of a Single Pile 33

3.2.7.2 Vertical and Rocking Dynamic Stiffness of a Single Pile 35

3.2.7.3 Lateral Dynamic Stiffness of Pile Group.. 36

3.2.7.4 Vertical and Rocking Dynamic Stiffness of Pile Group.................. 38

3.3 Calculation Foundation Dynamic Stiffness by means of a Computer Algorithm 39

3.4 Kinematic Interaction 40

3.4.1 Shallow Foundations at the Ground Surface 42

3.4.2 Embedded Shallow Foundations 43

3.4.3 Pile Foundations 45

3.4.4 Application of Transfer Function 45

CHAPTER FOUR - CASE STUDY: 14 STORY REINFORCED CONCRETE BUILDING SSI ANALYSIS 47

4.1 Introduction 47

4.2 Technical Advisories for Tall Buildings in the İzmir New Town Center 47

4.3 Site Soil and Structure Definition 48

4.4 Idealized Soil Profile 51
4.5 Site Response Analysis 55
4.5.1 Material Model 55
4.5.2 Selecting and Scaling of Earthquake Records 57
4.5.3 Deconvolution Analysis 62
4.6 Calculating Foundation Dynamic Stiffness 63
4.7 Structural Model 65
4.8 Time History Analysis 66

CHAPTER FIVE - RESULTS AND DISCUSSIONS 67

5.1 Introduction 67
5.2 Comparing the Method-I and Method-II in Terms of Spectral Plots 67
5.3 Calculation of the Foundation Dynamic Stiffness 73
5.3.1 Average Effective Velocity of the Profile 73
5.3.2 Foundation Type and Structure to Soil Stiffness Ratio 74
5.3.3 Calculation Translational and Rotational Foundation Dynamic Stiffness and Damping 74
5.3.3.1 NEHRP method 74
5.3.3.2 DYNAN Software 76
5.3.4 Calculation Pile Group Dynamic Stiffness and Damping 76
5.3.4.1 Using Developed Algorithm 76
5.3.4.2 Using DYNAN Software 81
5.4 Calculation Distributed Spring Stiffness 82
5.5 Time History Analyses of the Structure 84

CHAPTER SIX - CONCLUSIONS AND RECOMMENDATIONS 96

6.1 Conclusions 96

6.2 Recommendations for Future Studies... 98

REFERENCES... 99

APPENDICES 105

LIST OF FIGURES

Page

Figure 2.1 Multi-degree-of freedom lumped parameter model representation of horizontally layered soil deposit shaken at the base by a vertically propagating horizontal shear wave. 8

Figure 2.2 G/G_{max} and Damping curve correction method for high strain levels suggested by Stewart ve Kwok 11

Figure 3.1 Period Lengthening Ratio and Foundation Damping Factor for Sites Sorted by Confidence Level and Analytical Results from Veletsos and Nair (tr = Transverse, L = longitudinal) 16

Figure 3.2 The four foundation–soil systems whose impedances are given in tabular form. Numbers I–IV refer to corresponding tables 19

Figure 3.3 Representing overburden corrected Vs calculation. 25

Figure 3.4 Disk foundations with (a) rigid core considered by Iguchi and Luco (b) thin perimeter walls considered by Liou and Huang, and (c) rigid concentric walls considered by Riggs and Waas 27

Figure 3.5 Rocking stiffness and damping factors for flexible foundations; rigid core cases and perimeter wall case 28

Figure 3.6 Vertical spring distribution used to reproduce total rotational stiffness k_{yy}. A comparable geometry can be shown in the y-z plane (using foundation dimension 2B) to reproduce k_{xx} 29

Figure 3.7 Horizontal dynamic stiffness of the side-walls (embedment effect) 31

Figure 3.8 Schematic illustration of the developed 3-step procedure for computing the influence of Pile-1, deforming under harmonic lateral head loading, upon the adjacent Pile-2.. 32

Figure 3.9 Schematic representation of 2D radiation model: (a) ‘rigorous’ plane-strain model of Novak, (b) simplified plane-strain model of Gazetas and Dobry 34

Figure 3.10 Illustration superposition thechnique for pile to pile interaction.......... 37

Figure 3.11 Flowchart of the algorithm 40

Figure 3.12 Kinematic interaction with free-field motions indicated by dashed lines: (a) flexural stiffness of surface foundation prevents it from following vertical component of free-field displacement; (b) rigidity of block foundation prevents it from following horizontal component of free-field displacement; (c) axial stiffness of surface foundation prevents immediately underlying soil from deforming incoherently. 41
Figure 3.13 Illustration of foundation subjected to inclined shear waves: (a) schematic geometry; (b)transfer functions between FIM and free-field motion for wave passage using a semi-empirical model for incoherent waves. 42
Figure 3.14 Illustration of foundation subjected to vertically incident shear waves: (a) schematic geometry; and (b) transfer functions for horizontal foundation translation and rocking 44
Figure 4.1 Satellite view of the study area. 49
Figure 4.2 a) Structure section view, b) Architectural plan up to 4th story, c) Architectural plan up to 12th story 50
Figure 4.3 Piled raft foundation plan and section view... 51
Figure 4.4 Shear wave velocity variation with depth (according to the MASW, Downhole and SPAC tests)... 52
Figure 4.5 Averaged shear wave velocity profiles until 1400 m depth................. 53
Figure 4.6 Soil dynamic properties after 140 m depth 53
Figure 4.7 Idealized soil profile 54
Figure 4.8 Explanation of the analysis methods. Method-I represent the engineering bedrock assumption and Method-II considers the total alluvial profile. 55
Figure 4.9 Active fault map of the İzmir. 58
Figure 4.10 Explanation of the methods which were used for representing seismic bedrock and engineering bedrock assumptions. Schematically soil prism for the selected and scaled earthquakes. 60
Figure 4.11 Selected earthquakes from the Peer Strong Motion Database for soil class A and B according to D1 earthquake intensity level. 61

Figure 4.12 Selected earthquakes from the Peer Strong Motion Database for soil class A and B according to D2 earthquake intensity level. 62
Figure 4.13 Selected earthquakes from the Peer Strong Motion Database for soil class A and B according to D3 earthquake intensity level. 62
Figure 4.14 Linear link element definition in the SAP2000 64
Figure 5.1 Method-I and Method-II resulting response spectra for D1 earthquake intensity level 68
Figure 5.2 Method-I resulting response spectra with Method-II for D2 earthquake intensity level. 68
Figure 5.3 Method-I resulting response spectra with Method-II for D3 earthquake intensity level. 69
Figure 5.4 PGA values for Method-I and Method-II (D1).................................... 69
Figure 5.5 Max. strain values for Method-I and Method-II (D1) 70
Figure 5.6 PGA values for Method-I and Method-II (D2).................................... 70
Figure 5.7 Max. strain values for Method-I and Method-II (D2) 71
Figure 5.8 PGA values for Method-I and Method-II (D3).................................... 71
Figure 5.9 Max. strain values for Method-I and Method-II (D3) 72
Figure 5.10 Some important properties of the concrete pile group.......................... 77
Figure 5.11 Real part and imaginary partf of the group dynamic stiffness factors for the rigid capped pile group of the related structure (Developed algorithm)... 78
Figure 5.12 Pile group dynamic stiffness for the rigid capped pile group of the related structure in the frequency domain (Developed algorithm). 79
Figure 5.13 Pile group dapming for the rigid capped pile group of the related structure in the frequency domain (Developed algorithm). 79
Figure 5.14 Influence areas distribution of the foundation. 82
Figure 5.15 Side wall stiffness and damping contribution along the X axis direction 83
Figure 5.16 Side wall stiffness and damping contribution along the Y axis direction. 84

Figure 5.17 D1 level earthquake story maximum and minimum displacements for the Method-I and Method-II. (Structure behavior factor, R = 1.5, modal damping ratio constant at 0.05, RSN is the Record Sequence Number in the PEER database)... 85
Figure 5.18 D2 level earthquake story maximum and minimum displacements for the Method-I and Method-II. (Structure behavior factor, R = 4, modal damping ratio constant at 0.05, RSN is the Record Sequence Number in the PEER Database)... 87
Figure 5.19 D3 level earthquake story maximum and minimum displacements for the Method-I and Method-II. (Structure behavior factor, R = 4, modal damping ratio constant at 0.05, RSN is the Record Sequence Number in the PEER database)... 88
Figure 5.20 D1 level earthquake story maximum and minimum drift ratios for the Method-I and Method-II. (Max. Limit and Min. Limit represent the limit drift ratio of the stories according to Turkish Earthquake Code.) 89
Figure 5.21 D2 level earthquake story maximum and minimum drift ratios for the Method-I and Method-II. (Max. Limit and Min. Limit represent the limit drift ratio of the stories according to Turkish Earthquake Code.) 90
Figure 5.22 D3 level earthquake story maximum and minimum drift ratios for the Method-I and Method-II. (Max. Limit and Min. Limit represent the limit drift ratio of the stories according to Turkish Earthquake Code.) 91
Figure 5.23 D1 level earthquake story peak accelerations for the Method-I and Method-II. 92
Figure 5.24 D2 level earthquake story peak accelerations for the Method-I and Method-II. 93
Figure 5.25 D3 level earthquake story peak accelerations for the Method-I and Method-II. 94

LIST OF TABLES

Page

Table 2.1 Weight criterion for different approaches. 12
Table 2.2 1D, 2D and 3D site response analysis capable softwares. 13
Table 3.1 Elastic solutions for static stiffness of rigid footings at the ground Surface... 20
Table 3.2 Embedment correction factors for static stiffness of rigid footings 21
Table 3.3 Dynamic stiffness modifiers and radiation damping ratios for rigid footings.. 22
Table 3.4 Dynamic stiffness modifiers and radiation damping ratios for embedded footings.. 23
Table 3.5 Values of shear wave velocity and shear modulus reduction for various site classes and shaking amplitudes 26
Table 4.1 G/G_{max} and damping curves; the table on the left side is given for rock units located up to first 120 m thickness, the table on the right side is given for after 120 m thickness. 56
Table 4.2 D1 level selected earthquakes for Method-II. 59
Table 4.3 D2 level selected earthquakes for Method-II. 59
Table 4.4 D3 level selected earthquakes for Method-II. 59
Table 4.5 D1 level selected earthquakes for Method-I. 59
Table 4.6 D2 level selected earthquakes for Method-I. 59
Table 4.7 D3 level selected earthquakes for Method-I. 60
Table 4.8 Directional differences and station to fault rupture differences of the selected pairs of earthquakes. 61
Table 5.1 Max. PGA values and max. strain of the soil profile for the Method-I and Method-II 73
Table 5.2 Effective profile depth and average shear wave velocities 73
Table 5.3 Calculated values of the foundation dynamic stiffness and damping 75
Table 5.4 Calculated values of the foundation dynamic stiffness and damping 75
Table 5.5 Foundation stiffness, calculated by DYNAN software 76
Table 5.6 Pile group dynamic stiffness and damping calculated by the developed code. 80

Table 5.7 Piled raft foundation dynamic stiffness and damping calculated by the developed code. 80
Table 5.8 Overall group dynamic stiffness and damping values calculated by the DYNAN 81
Table 5.9 Side soil removed group dynamic stiffness and damping values calculated by the DYNAN 81
Table 5.10 Only side soil dynamic stiffness and damping values calculated by the DYNAN 81
Table 5.11 Spring stiffness correction factors and resulting stiffness of 1, 2, 3, 4 regions 83
Table 5.12 The foundation base link stiffness and dashpots for related local axis directions 84
Table 5.13 Comparision of base shear forces of the structures in terms of Method-I and Method-II for D1, D2, D3 earthquake intensity levels. (All values are in tonnes). 95
Table 5.14 Fist three mode periods of the structure for fixed base and flexible base models 95

CHAPTER ONE
INTRODUCTION

1.1 Background

The Soil Structure Interaction (SSI) analysis of structures has become an indispensable part of the structural design in recent years. The issue of soil structure interaction is a vital work for structures built on weaker soils in a high risk earthquake area. High buildings, bridge piers, important structures such as nuclear power plants interact with the ground. This interaction occurs due to the deformability of the soil material. The order of the soil-structure interaction vary based on factors such as structural properties, the number of stories, the basic shape of foundations, soil material properties, etc. For instance soil-structure interaction of low-rise buildings is negligible (Veletsos and Meek, 1974). Similarly, when the response of a structure built on weaker ground is compared with that of another structure built on a stiff rock site, the interaction effects are more pronounced for the first structure.

The soil-structure interaction causes an increase in the structural period, effective damping, displacements and P-Δ effects. On the other hand, it causes a reduction in the base shear force. Some codes permit to base shear force reduction up to 30% due to soil structure interaction.

This interaction between the soil and the structure can be modeled according to the direct approach or the subsystem approach (Whitman and Bielak 1980). The direct approach method uses the finite element method where soil medium and the superstructure exist in the same model (Lysmer et al., 1981; Borja et al., 1992). Today this type of effective commercial software that consider soil and structural nonlinearity at the same time are not available. In order to overcome this problem, Whitman proposed the substructure method and handled the problem in two parts that are so-called as “kinematic interaction and inertial interaction”.

One of practical SSI procedures available in the literature for inertial interaction was proposed by NEHRP as the Extension of the Equivalent Lateral Force Procedure. The other is the Extension of the Modal Analysis Simplified Procedure. For the design of major buildings, advanced time history analysis is preferred over the simplified method. Therefore, the selection of analytical methods plays a major role in the best representation of the soil-structure interaction. Also foundation type, foundation embedment, variation of soil properties with depth, hysteretic action in the soil and the best representation of soil dynamic properties directly affect analyses results. For instance, soil-structure interaction for a pile foundation does not just occur between the soil and the raft. SSI shall also be considered between surrounding soil and the pile (Wolf and Von Arx, 1978).

The kinematic interaction may be simply defined as the alteration of seismic ground motion nearby the foundation by means of the back and forth reflected ways by the foundation. Measured earthquake motion under the foundation has different characteristics than free field ground motion. Kinematic interaction briefly consists of the base slab averaging, embedment effect and wave scattering effect. In practice, the kinematic interaction in a rigid raft foundation can be taken into account by means of transfer functions. However, such a rigorous solution for pile groups are not yet available. The finite element method is necessary to use in order to obtain precise determination of the kinematic interaction where the resulting modified earthquake motion is called as "foundation input motion" (FIM). The analyses are carried out in the time domain and FIM records are used as the ground motions for the superstructure. This type of interaction is not considered in this thesis.

1.2 Organization of the Thesis

In the second chapter, site specific geotechnical investigations and 1D nonlinear site response analysis methodology are explained. The criteria applied to the selection of the earthquake records and their scaling are presented. The soil material model determination has a direct effect on 1D site response analysis results.

Therefore, detailed steps are explained in this chapter to obtain accurate soil G/G_{max} reduction and damping curves.

In the third chapter, soil-structure interaction analyses methodology of the subsystem approach was introduced. The raft-soil interaction and pile-soil-pile interaction principals are given according to various methods and approaches. An algorithm that was developed for the inertial interaction analysis of a pile group is defined. A brief explanation of the kinematic interaction analysis is provided in this chapter for the sake of the integrity of overall text. The transfer functions as suggested in NEHRP guidelines, are given for the raft foundation-soil interface.

In the fourth chapter, the structure subject to soil-structure interaction analyses, is described. Besides, the idealized soil profile and shear wave velocity profile for the site where the building is considered to be located are introduced in the same chapter. Details of the methods and parameters that are required for soil structure interaction analyses are presented. The selection and scaling procedure of the earthquake records to be used in soil structure interaction analysis is also given. Two different approaches for the consideration of rock level where transfer of the ground motion to the foundation level commences are described.

In the fifth chapter, the results of site response and structural analyses are given. The results obtained using two different sets of ground motions are discussed in this section of the thesis.

In the final chapter, this thesis study is concluded based on the achieved results. Some key findings and recommendations for future studies are presented in this chapter.

CHAPTER TWO
SITE-SPECIFIC GEOTECHNICAL INVESTIGATIONS AND DYNAMIC SITE RESPONSE ANALYSES

2.1 Introduction

In General, The Response Spectrum Method is used to determine the dynamic behavior of the structures which have less number of stories. However, the time history analysis is preferred for high-risk structures or structures have a large number of stories. For the weak soil conditions, Site Response Analysis is required and recommended in many international earthquake code. Material model based on the soil dynamic properties must be determined realistically in order to Site Response Analysis to give accurate results. Since, Foundation Input Motion will be obtained from this analysis directly affects the design of the superstructure elements.

Today, many test methods are effectively used and the field tests are the portion of these methods. Laboratory experiments constitute the other part of the test methods. These experiments are required for the determination of variable parameters of commonly used material models.

2.2 Measurement of Dynamic Soil Properties

The measurement of dynamic soil properties is a critical task for the solution of Geotechnical Earthquake Engineering problems. Various field and laboratory testing techniques are available. Each has different advantages and limitations According to different problems. Some of these are used to determine the dynamic properties at low-strain and the others are used to determine the dynamic characteristics of high-strain levels. The choice of testing techniques for the measurement of dynamic soil properties requires careful consideration and a good understanding of the problem at hand.

2.2.1 Multichannel Analysis of Surface Waves (MASW)

MASW technique is often used to determine the soil dynamic properties of low-strain level in Geotechnical Engineering, site response study and soil profiling. MASW not required to intervene on the ground in particular (drilling, excavations, sampling, etc.), and the method is advantageous because it takes less time. Another advantage is the ability to determine the layer transition and boundaries. For the shallow depth (up to approximately 30~50 meters) is a convenient method. It also enables the creation of ground shear wave velocity profiles in 2D and 3D.

2.2.2 Down-Hole Test

The purpose of the seismic down-hole test is to measure P and S waves travel time at the energy source to the receiver. This test can be performed in a single borehole. A test borehole is drilled to the required depth and the vibration source is used to determine the shear wave velocity. The generated waves travel downward through the soil layers. In the down-hole test vibration source is located close to the borehole on the ground surface. A constant multiple receivers can be placed at known different depths in the borehole or a single receiver is carried through the depths in testing progresses. This test, which the results are obtained directly in the soil media, is assumed that better reflect the reality.

For the sensitivity of data:

- It is necessary to avoid filling boreholes with water.
- If there is space between the hole wall and the casing, it must be filled by injection.

2.2.3 SPAC (Spatial Auto-Correlation) Method

There may be some restrictions on the use of seismic refraction method in the creation of Vs profile. Depth of bedrock increases the required energy of vibration source. But the limited signal source used in applications in the residential area of seismic refraction and reflection studies.

In these circumstances, surface wave analysis methods are used in the field studies. If the bedrock is too depth, the passive method uses the soil as a source of natural vibration. The passive method which is called SPAC (Spatial Auto Correlation) can be used for the obtaining deeper Vs profiles.

2.2.4 Laboratory Methods

Low strain level dynamic properties of the soil material can be determined by the limited number of laboratory tests. Some of these; resonance column test, ultrasonic pulse testing and piezoelectric element bending test.

At higher shear strain levels, soil generally tends to exhibit the change in volume. Under drained loading conditions, this trend will allow to show itself in the form of volumetric strain, but is in undrained conditions cause changes in pore water pressure. All methods should allow controlling the drainage of water from the soil sample and should have the capability to accurately measure of volume change, pore water pressure.

Some of these types of tests are; cyclic triaxial test, cyclic direct simple shear tests, cyclic torsional shear tests.

2.3 Nonlinear Dynamic Site Response Analysis

1D nonlinear site response analyses will be conducted by DEEPSOIL v6.0 (Hashash et al. 2002) Software. DEEPSOIL is a site response analysis program that can perform 1D nonlinear analysis, 1D equivalent linear analysis and deconvolution analysis. It includes the acceleration, velocity, and displacement time histories, the response spectrum and the Fourier amplitude spectrum. This software capable to build shear modulus reduction and damping curves for different methods and it uses the latest techniques for curve fitting operation. Also, in the nonlinear analysis case, the pore water pressure generation can be calculated by the software. Users can obtain the results for any soil layer.

Nonlinear dynamic site response analysis calculation steps are as follows:

1) Modelling soil profile,

2) Selecting and scaling rock motions,

3) Baseline correction of records,

4) Conducting site response analysis and obtaining results for the required layers.

These results can be achieved the time history data, spectrum data, displacement data, velocity data or Fourier amplitude spectrum data formats. Besides, DEEPSOIL presents graphically the displacement shape of the entire soil profile for each time step.

2.3.1 Modeling Soil Profile

Previously prepared idealized soil profile data are entered into DEEPSOIL Software. When the soil layer data are entered into the software, the cut-off frequency of each layer should be considered around 30 Hz. Soil layers natural frequency can be calculated according to this $f = V_s / 4H$ equation. If this condition is not ensured, the related layer is divided into the sub-layers. This process is necessary for the convergence of the iterations.

In some special cases, even though 2D or 3D site response analysis requires, one-dimensional analysis is usually sufficient in the building type structures. DEEPSOIL software can only be used in 1D analysis technique.

As shown in Figure 2.1, the shear wave velocities of the soil layers are determined according to the field and the laboratory test data. These values are used to obtain small strain shear modulus. In addition to these values such as, the effective angle of internal friction, plasticity index, overconsolidation ratio, Poisson's ratio data must be entered into the software.

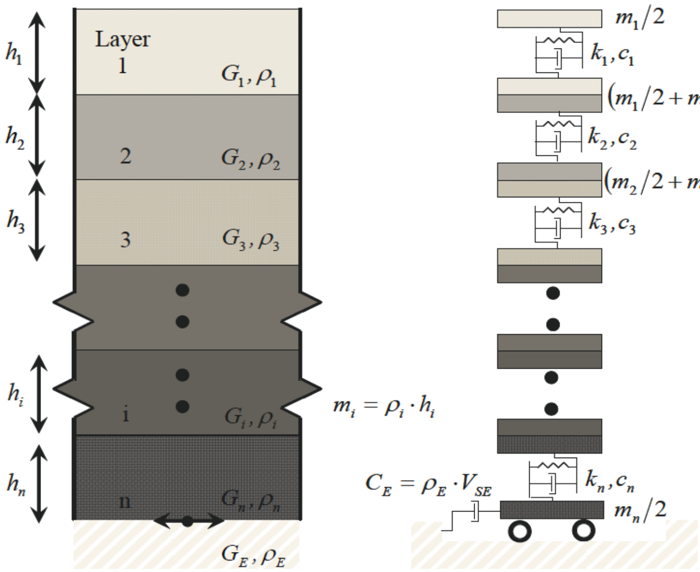

Figure 2.1 Multi-degree-of freedom lumped parameter model representation of horizontally layered soil deposit shaken at the base by a vertically propagating horizontal shear wave (Hashash et al., 2010).

2.3.2 Material Model

Modulus reduction curves, damping curves and stress-strain curves of soil material must be determined separately for each layer. Laboratory dynamic test results can be used directly in the material model. Geotechnical engineers generally prefer to empirical correlations instead of the expensive dynamic laboratory tests. The most commonly used correlations are: Seed and Idriss, 1970; Seed et al., 1986; Sun et al., 1988; Vucetic and Dobry, 1991; Electric Power Research Institute, 1993; Kramer, 1996; Darendeli, 2001.

In the Darendeli (2001)'s model:

$$\frac{G}{G_{\max}} = \frac{1}{1+\left(\dfrac{\gamma}{\gamma_r}\right)^a} \tag{2.1}$$

where;

a : Curvature coefficient and equal to 0.9190

γ : Shear strain

γ_r : Reference shear strain

Reference shear deformation, γ_r can be calculated as follows:

$$\gamma_r = \left(\frac{\sigma_0^{'}}{p_a}\right)^{0.3483} \left(0.0352 + 0.001 PI\, OCR^{0.3246}\right) \tag{2.2}$$

where;

$\sigma_0^{'}$: Average effective stress,

p_a : Atmospheric pressure,

PI : Plasticity index and

OCR : Overconsolidation ratio.

In general, the γ_r is between 0.1% - 0.3% strain levels.

The total damping ratio is obtained by summing of the minimum damping ratio (damping ratio at low strain) and Masing (1926) damping ratio (due to the behavior of Masing). It is given by:

$$D_{\min}(\%) = (\sigma_0^{'})^{-0.2889} \left(0.8005 + 0.0129 PI\, OCR^{-0.1069}\right)\left(1 + 0.2919 \ln f\right) \tag{2.3}$$

Where, f represents the excitation frequency and f is defined as 1 Hz in the site response analysis.

The Massing damping ratio can be achieved by the integration of the area under the hysteresis curve. Approximately this integration value is given by:

$$D_{\text{Masing}}(\%) = \frac{100}{\pi}\left\{4\left[\frac{\gamma - \gamma_r \ln\left(\frac{\gamma + \gamma_r}{\gamma_r}\right)}{\frac{\gamma^2}{\gamma + \gamma_r}}\right] - 2\right\} \tag{2.4}$$

The total damping ratio is calculated as follows:

$$D = b\left(\frac{G}{G_{\max}}\right)^{0.1} D_{\text{Masing}} + D_{\min} \tag{2.5}$$

In the equation (2.4) and (2.5), b value can be calculated by:

$$b = 0.6329 - 0.0057 \ln N \tag{2.6}$$

where;

G :Shear modulus

G_{max} :Low strain shear modulus (maximum shear modulus)

D :Total Damping ratio (%)

D_{Masing} :Masing damping ratio (%)

D_{min} :Minimum damping ratio (%)

N :Number of cycles (in the most site response analysis N is defined as 10)

The shear modulus reduction method, which is defined the above equation, give good results in the range of shear strains between 0.3% and 0.7%. In cases of large shear deformations, a correction should be made in the generated G/G_{max} curve (Stewart and Kwok, 2008). The Modulus reduction and damping curves, which are corrected according to the given technique in Figure 2.2, can be used directly the site response analysis. Otherwise, If the other methods shall be used, corrected reduction curves obtained from Equations 2.1~2.6 are accepted as a target curve;

$$G / G_{\max} = \frac{1}{1 + \beta(\gamma / \gamma_r)^a} \tag{2.7}$$

Giving a starting value to the curve fitting parameter "β" and "a" of the general G/G_{max} Equation 2.7 (Hardin and Drnevich, 1972). The standard error between the target curve and the general curve is estimated with the aid of Equations 2.10. The modulus reduction curve is the final curve, which is obtained from Equation 2.7, if "β" and "a" curve fitting parameters minimize the standard error. This error rate is also estimated while using a weighting function, in particular has a high accuracy range of the target curve (0.3%- 0.7%) can be considered. There are 3 different adaptation methods as follow:

a) *MR Fitting*: only applicable shear modulus reduction curves.
b) *MRD Fitting*: Applicable both shear modulus reduction curves and damping curves at the same time.
c) *DC Fitting*: Only applicable damping curves.

The Effects on the dynamic soil behavior arising from the different fitting approaches have been examined by Stewart and Kwok (2008). Only to use of the DC option is not recommended. The analyses are expected to large shear deformation, MR and MRD method is recommended for obtaining the best results.

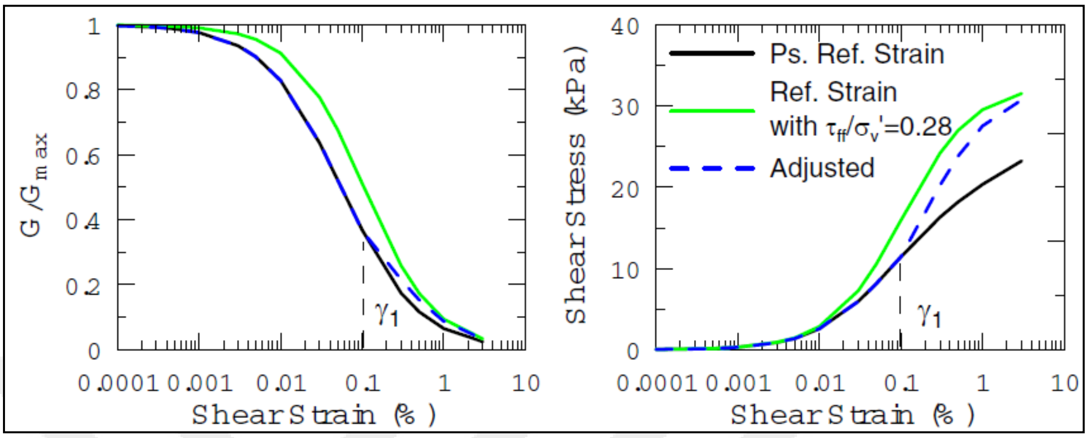

Figure 2.2 G/G_{max} and Damping curve correction method for high strain levels suggested by Stewart ve Kwok (2008)

Analogously to the methods described above, the small strain damping ratio (D_{min}) and reference shear strain can be calculated as follows;

$$\zeta = Small\ Strain\ Damping\ Ratio \left(\frac{1}{\sigma_v^{'}} \right)^d \tag{2.8}$$

and

$$\gamma_r = Reference\ Strain \left(\frac{\sigma_v^{'}}{Reference\ Stress} \right)^b \tag{2.9}$$

where;

d: is the damping curve fitting parameter

Reference Stress: In the DeepSoil software is taken as 0.18 MPa, In Darendeli's equation is taken as 0.1 MPa.

"d" is an exponential coefficient, which is used to calculate the pressure dependent small strain damping ratio. If "d" equal to zero, the small strain damping ratio is calculated as the pressure independent. Similarly, the coefficient "b" is chosen as zero, the reference strain will be a constant value.

After the curve fitting process, the standard error between the fitted curve and the target curve can be calculated by the following equations;

$$\varepsilon = \sqrt{\left(w_{G/G_{\max}} \times \bar{\varepsilon}_{G/G_{\max}}\right)^2 + \left(w_\beta \times \bar{\varepsilon}_\beta\right)^2} \tag{2.10}$$

Where $\bar{\varepsilon}_{G/G_{\max}}$ and $\bar{\varepsilon}_\beta$ are the mean error between the model and target G/G_{max} and Damping Curve. $\bar{\varepsilon}_{G/G_{\max}}$ or $\bar{\varepsilon}_\beta$ is calculated as:

$$\bar{\varepsilon}_{G/G_{\max}} = \frac{\sqrt{\sum\left(\varepsilon_{G/G_{\max}}(\gamma_i)\right)^2}}{N} \tag{2.11}$$

N is the number of strain levels, $w_{G/G_{\max}}$ and w_β are the weight factor depend on fitting approaches. These weight factors should be calculated from the Table 2.1.

Table 2.1 Weight criterion for different approaches. (Stewart and Kwok, 2008)

Fitting Approach	Weight Criterion
MR	$w_{G/Gmax}=1,\ w_\beta=0$
MRD	$(w_{G/Gmax})^2+(w_\beta)^2=1$ $\frac{w_{G/G_{\max}}}{w_\beta} = \begin{cases} 1, & \beta_{\max} > 25\% \\ 1+\frac{0.25-\beta_{\max}}{0.15}, & 10\% < \beta_{\max} < 25\% \\ 2, & \beta_{\max} < 10\% \end{cases}$
D	$w_{G/Gmax}=0,\ w_\beta=1$

2.3.3 Selecting Input Rock Motion

PEER Strong Ground Motion Database can be used for selection of the earthquake acceleration records which will be applied seismic bedrock level or engineering bedrock level. The code based response spectrums can be used as a target spectrum in the investigation site for selection the appropriate time acceleration records. Thus, the acceleration record spectrum, which gives the lowest standard error with the target spectrum can be selected. On the other hand, fault mechanism, magnitute, fault to site distances, soil $V_{s,30}$'s, record durations and record peak ground accelerations must be represented the investigation area. The suitable records in conformity with criteria are selected and scaled linearly by the scale factors. The more the scale factor can be selected smaller, the more the earthquake record stays original pattern.

2.4 Site Response Analysis

Some software which can make 1D, 2D and 3D site response analysis are presented in the Table 2.2. Exhibits the nonlinear behavior of soils, consisting of weak clay layers, nonlinear analysis is preferred. To examine the effect of liquefaction in the sandy soils, analysis methods capable taking into account the changes in pore pressure should be preferred.

Table 2.2 1D, 2D and 3D site response analysis capable softwares.

<table>
<tr><th>Dimensions</th><th>OS</th><th>Equivalent Linear</th><th>Nonlinear</th></tr>
<tr><td rowspan="2">1D</td><td>DOS</td><td>Dyneq, Shake91</td><td>AMPLE, DESRA, DMOD, FLIP, SUMDES, TESS</td></tr>
<tr><td>Windows</td><td>ShakeEdit, ProShake, Shake2000, EERA</td><td>CyberQuake, DeepSoil, NERA, FLAC, DMOD2000</td></tr>
<tr><td rowspan="2">2D / 3D</td><td>DOS</td><td>FLUSH, QUAD4/QUAD4M, TLUSH</td><td>DYNAFLOW, TARA-3, FLIP, VERSAT, DYSAC2, LIQCA, OpenSees</td></tr>
<tr><td>Windows</td><td>QUAKE/W, SASSI2000</td><td>FLAC, PLAXIS</td></tr>
</table>

CHAPTER THREE
SOIL STRUCTURE INTERACTION ANALYSIS

3.1 Introduction

In this chapter the methodology followed during Soil Structure Interaction (SSI) analyses of the thesis study is explained. The subsystem model which was recommended by Whitman, consists of two parts, including inertial and kinematic interaction. The inertial interaction between the soil is taken care of using the method stated by NEHRP provisions (NEHRP, 2012) and Novak's improved method. Although DYNAN software that employs Novak's Method was used in the analyses, the analytical method of Gazetas & Makris (1992, 1993) was also utilized in the thesis. A computer code that runs Gazetas and Makris approach was developed for this purpose. The results of this code, which has a graphical user interface enabling fast data input, were compared with those of the DYNAN to show that dynamic stiffness matrices computed according to both methods are in good agreement.

3.2 Inertial Interaction

In simple terms, vibration waves during on earthquake, travel in the soil media and arrive at the structure's foundation. These waves cause vibrations in the structure due to its mass. The foundation emits the waves back to the soil media and acts as a vibration source. These emitted waves are different from incoming waves. Since, the structure and the soil have different stiffness values. Oscillations in the structure cause deformations in the soil because of the elastic properties of the soil material and alter the wave form. This effect in the soil structure interaction is named as the inertial interaction.

Mostly, the soil shows elastic behavior under lower stress levels. When exposed to high stress, it shifts into the nonlinear region. Beyond this region, the strength of the soil is completely lost for practical purposes. The soil springs were used for theoretical modelling of the soil-structure interaction. The impedance function of the soil spring is determined as linear, nonlinear or frequency depended according to the type of problem. Apart from these modeling techniques, the soil media can be modeled entirely with the prismatic finite element. In practical engineering, soil spring is preferred instead of the finite element modeling. Since, the soil media must be divided into too many finite elements. Thus, it is increased the computers effort and solution time.

3.2.1 Factors Affecting Inertial Interaction

Inertial interaction reduces or increases depending on the building period, dynamic and mechanical properties of the soil, structure height, foundation size and depth as well as foundation rigidity (Veletsos and Nair, 1975 and Bielak, 1975).

h/V_sT, h/B, B/L, $m/\rho_s 4BLh$, υ parameters control period lengthening.

where:

h: height to the center of mass of the first mode shape (approximately two-thirds of the structure height),

B and *L*: the half-width and half-length of the foundation,

*m:*effective modal mass,

ρ_s: soil mass density,

υ: Poisson’s ratio of the soil.

The structure height to foundation width ratio, h/B, and foundation width to length ratio, B/L are aspect ratios describing the geometry of the soil structure system. The mass ratio, $m/\rho s4BLh$, is the ratio of structure mass to the mass of soil in a volume extending to a depth equal to the structure height, *h*, below the foundation. The mass ratio term was introduced so that period lengthening could be related to easily recognizable characteristics such as structural first mode period, *T*, and soil shear wave velocity, V_s, rather than structural stiffness, *k*, and soil shear modulus, *G*. The effect of mass ratio is modest, and it is commonly taken as 0.15 (Veletsos and Meek, 1974). The Poisson’s ratio of the soil, υ, affects the stiffness and damping characteristics of the foundation.

From the foregoing expression h/V_sT refers to structure-to-soil stiffness ratio. This value is smaller than 0.1 meaning that negligible inertial interaction occurs. (Stewart et al., 1999b).

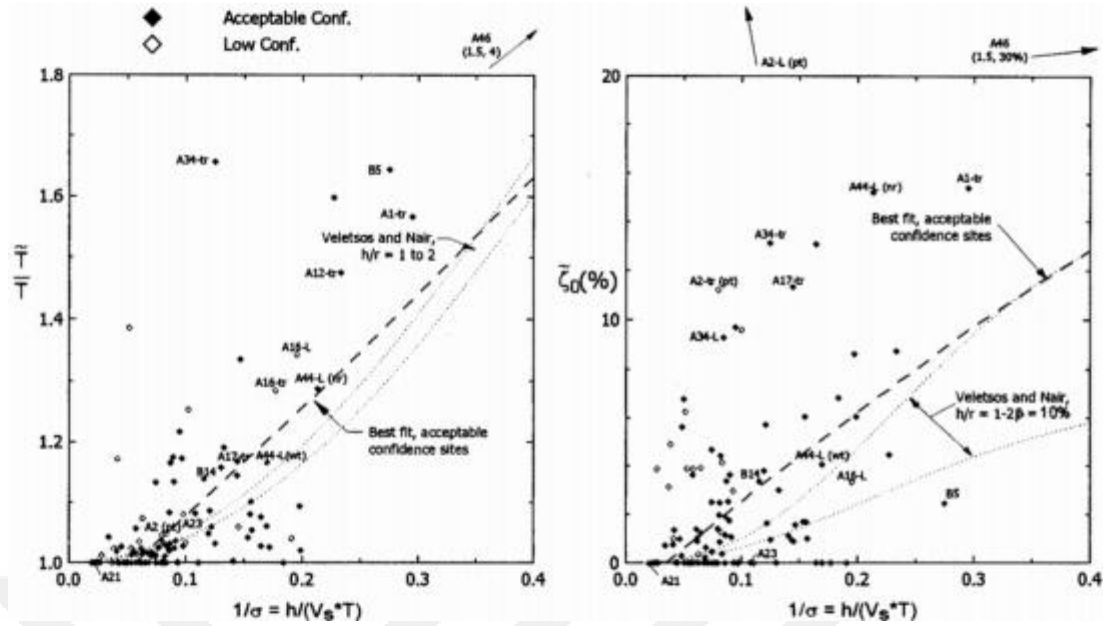

Figure 3.1 Period Lengthening Ratio and Foundation Damping Factor for Sites Sorted by Confidence Level and Analytical Results from Veletsos and Nair (1975). Where: $\tilde{T}$: Lengthened structural period, ξ_0 : foundation damping factor with hysteretic and radiation components, σ: ratio of the soil to structure stiffness (Stewart, 1999)

Figure 3.1 shows that period lengthening increases markedly with structure-to-soil stiffness ratio, which is the most important parameter controlling inertial SSI effects.

Dynamic impedance function, which depends on the frequency, has been explained previously. Generally, the normalized dimensionless frequency ($a_0 = \omega B / V_s$) is used instead of frequency, f, in the literature. Where $\omega = 2\pi / T$, T is the flexible base period of structure and obtained from first dominate period. The effect of higher mode contribution on the period lengthening is negligible for tall buildings (T> 2 sec.) (Stewart et al., 1999). Therefore, it is adequate to consider the dominant period of the structure.

3.2.2 Impedance Function of the Foundation-Soil Interface

Detailed data obtained from site and laboratory tests must be used while determining the impedance function of the spring, which represents the foundation-soil intersection.

The most important geometric and material factors affecting the dynamic impedance of a foundation are:

(1) The foundation shape (circular, strip, rectangular, arbitrary),

(2) The type of soil profile (deep uniform or multi-layer deposit, shallow stratum on rock),

(3) The embedment depth (surface foundation, embedded foundation, pile foundation).

The dynamic impedance function of the foundation-soil spring is depends on the vibration frequency and damping characteristics of the soil-foundation interface. Hence, impedance function is represented as the complex valued and can be written as (Luco and Westman, 1971; Veletsos and Wei, 1971):

$$\bar{k}_j = k_j + i\omega c_j \tag{3.1}$$

where;

$\bar{k}_j$: complex-valued impedance function

j : an index denoting degree of freedom

k_j *and* c_j :frequency-dependent foundation stiffness and dashpot coefficients, respectively.

ω : circular frequency (rad/s).

The dashpot coefficient, c represents the effects of damping about soil-foundation interaction.

The equation 3.1 can be also written as;

$$\bar{k}_j = k_j(1+2i\beta_j) \tag{3.2}$$

where:

$$\beta_j = \frac{\omega c_j}{2k} \ (defined\ \ for\ k_j > 0) \tag{3.3}$$

In the Equation 3.3, β_j is the damping ratio and the imaginary part of Equation 3.1 represents a phase difference between the exication and response at a given frequency. The phase difference, ϕ_j, between the exication force and lagged displacement is as follows (Clough and Penzien 1993; Wolf 1985):

$$\phi_j = \tan^{-1}\left(2\beta_j\right) \tag{3.4}$$

3.2.3 Elastic Solution of the Foundation Dynamic Stiffness

Analytical solution of the impedance function for rigid circular and rectangular foundation is studied by various investigators (Kausel and Pais, 1988, Mylonakis et al., 2006) to obtain formulations for practical engineering applications. In these formulations, the foundation can be considered at the ground surface or at a specific embedment depth. In addition, the soil media are considered as uniform, elastic or visco-elastic half-space in these formulations.

$$k_j = K_j \times \alpha_j \times \eta_j \tag{3.5}$$

$$K_j = GB^m f\left(B/L, \upsilon\right), \quad \alpha_j = f\left(B/L, a_0\right) \tag{3.6}$$

$$\eta_j = f\left(B/L, D/B, d_w/B, A_w/BL\right) \tag{3.7}$$

where:

K_j: Static foundation stiffness at zero frequency for mode j,

α_j: Dynamic stiffness modifier,

η_j: Embedment modifier,

G: Shear modulus of soil,

υ: Poisson's Ratio of soil,

B: Foundation half-width (small plan dimension),

L: Foundation half-length (large plan dimension),

m: An exponent, m=1 for translation, m=3 for rotation,

d_w: Height of effective side wall contact,

A_w: Sidewall-solid contact area,

a_0: Dimensionless frequency,

$$a_0 = \omega B / V_s \tag{3.8}$$

and V_s is the shear wave velocity.

Some important parameters are introduced in Figure 3.2, and foundation dynamic stiffness formulas are given in Table 3.1~3.4.

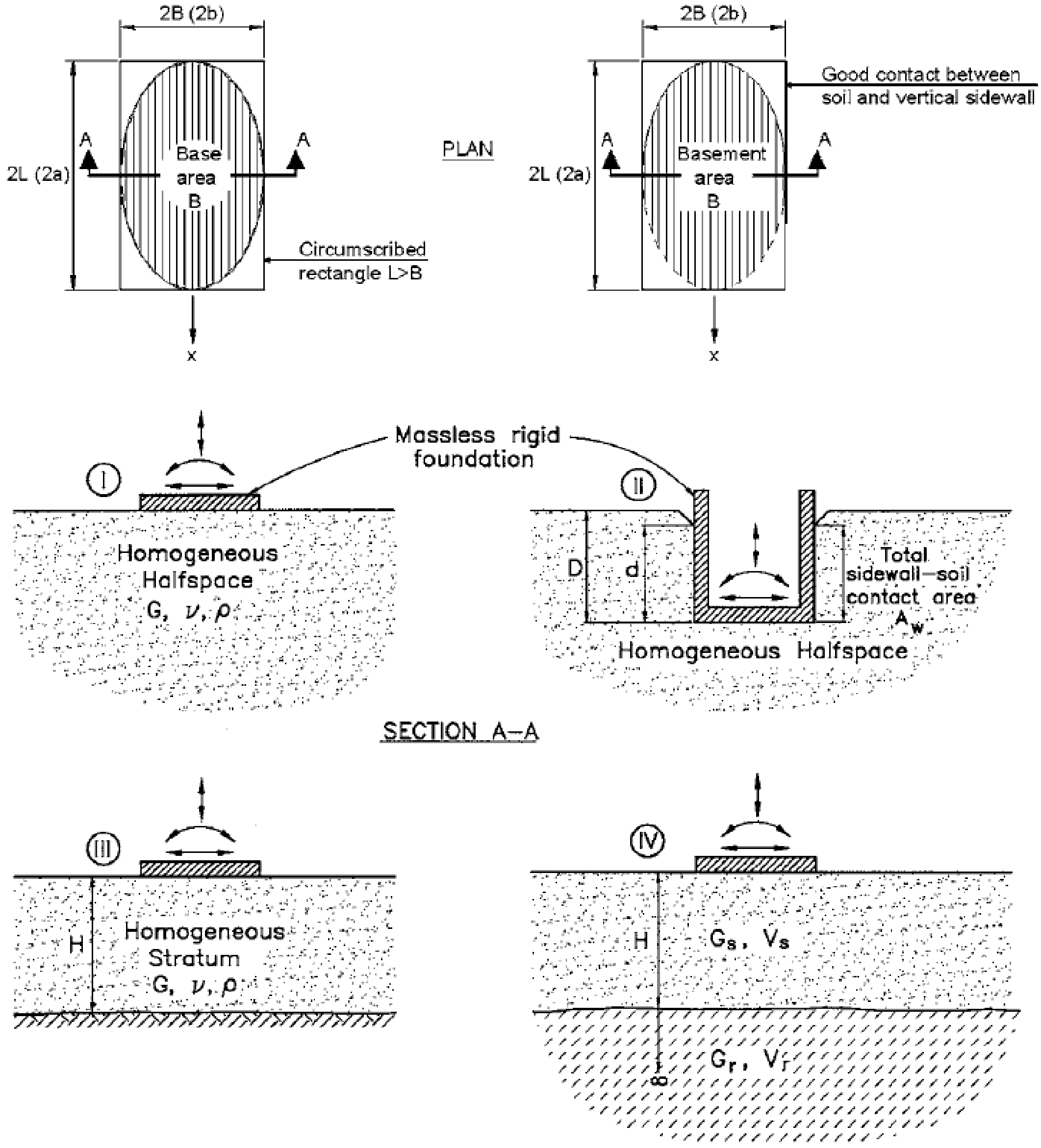

Figure 3.2 The four foundation–soil systems whose impedances are given in tabular form. (No. I–IV refer to corresponding tables, Mylonakis et al., 2006)

Table 3.1 Elastic solutions for static stiffness of rigid footings at the ground surface (NEHRP, 2012)

Degree of Freedom	Pais and Kausel (1988)	Gazetas (1991); Mylonakis et al. (2006)
Translation along z-axis	$K_{z,\,sur} = \frac{GB}{1-\nu}\left[3.1\left(\frac{L}{B}\right)^{0.75} + 1.6\right]$	$K_{z,\,sur} = \frac{2GL}{1-\nu}\left[0.73 + 1.54\left(\frac{B}{L}\right)^{0.75}\right]$
Translation along y-axis	$K_{y,\,sur} = \frac{GB}{2-\nu}\left[6.8\left(\frac{L}{B}\right)^{0.65} + 0.8\left(\frac{L}{B}\right) + 1.6\right]$	$K_{y,\,sur} = \frac{2GL}{2-\nu}\left[2 + 2.5\left(\frac{B}{L}\right)^{0.85}\right]$
Translation along x-axis	$K_{x,\,sur} = \frac{GB}{2-\nu}\left[6.8\left(\frac{L}{B}\right)^{0.65} + 2.4\right]$	$K_{x,\,sur} = K_{y,\,sur} - \frac{0.2}{0.75-\nu}GL\left(1 - \frac{B}{L}\right)$
Torsion about z-axis	$K_{zz,\,sur} = GB^3\left[4.25\left(\frac{L}{B}\right)^{2.45} + 4.06\right]$	$K_{zz,\,sur} = GJ_t^{0.75}\left[4 + 11\left(1 - \frac{B}{L}\right)^{10}\right]$
Rocking about y-axis	$K_{yy,\,sur} = \frac{GB^3}{1-\nu}\left[3.73\left(\frac{L}{B}\right)^{2.4} + 0.27\right]$	$K_{yy,\,sur} = \frac{G}{1-\nu}(I_y)^{0.75}\left[3\left(\frac{L}{B}\right)^{0.15}\right]$
Rocking about x-axis	$K_{xx,\,sur} = \frac{GB^3}{1-\nu}\left[3.2\left(\frac{L}{B}\right) + 0.8\right]$	$K_{xx,\,sur} = \frac{G}{1-\nu}(I_x)^{0.75}\left(\frac{L}{B}\right)^{0.25}\left[2.4 + 0.5\left(\frac{B}{L}\right)\right]$

Notes:

Axes should be oriented such that $L \geq B$.

I_i = area moment of inertia of soil-foundation contact, i denotes which axis to take the surface around.

$J_t = I_x + I_y$ polar moment of inertia of soil-foundation contact surface.

G = shear modulus (reduced for large strain effects, e.g., Table 2-1).

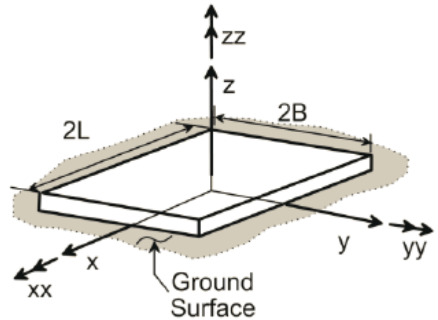

Table 3.2 Embedment correction factors for static stiffness of rigid footings (NEHRP, 2012)

Degree of Freedom	Pais and Kausel (1988)	Gazetas (1991); Mylonakis et al. (2006)
Translation along z-axis	$\eta_z = \left[1.0+\left(0.25+\frac{0.25}{L/B}\right)\left(\frac{D}{B}\right)^{0.8}\right]$	$\eta_z = \left[1+\frac{D}{21B}\left(1+1.3\frac{B}{L}\right)\right]\left[1+0.2\left(\frac{A_w}{4BL}\right)^{2/3}\right]$
Translation along y-axis	$\eta_y = \left[1.0+\left(0.33+\frac{1.34}{1+L/B}\right)\left(\frac{D}{B}\right)^{0.8}\right]$	$\eta_y = \left(1+0.15\sqrt{\frac{D}{B}}\right)\left[1+0.52\left(\frac{z_w A_w}{BL^2}\right)^{0.4}\right]$
Translation along x-axis	$\eta_x \approx \eta_y$	Same equation as for η_y, but A_w term changes for $B \neq L$
Torsion about z-axis	$\eta_{zz} = \left[1+\left(1.3+\frac{1.32}{L/B}\right)\left(\frac{D}{B}\right)^{0.9}\right]$	$\eta_{zz} = 1+1.4\left(1+\frac{B}{L}\right)\left(\frac{d_w}{B}\right)^{0.9}$
Rocking about y-axis	$\eta_{yy} = \left[1.0+\frac{D}{B}+\left(\frac{1.6}{0.35+(L/B)^4}\right)\left(\frac{D}{B}\right)^2\right]$	$\eta_{yy} = 1+0.92\left(\frac{d_w}{B}\right)^{0.6}\left[1.5+\left(\frac{d_w}{D}\right)^{1.9}\left(\frac{B}{L}\right)^{-0.6}\right]$
Rocking about x-axis	$\eta_{xx} = \left[1.0+\frac{D}{B}+\left(\frac{1.6}{0.35+L/B}\right)\left(\frac{D}{B}\right)^2\right]$	$\eta_{xx} = 1+1.26\frac{d_w}{B}\left[1+\frac{d_w}{B}\left(\frac{d_w}{D}\right)^{-0.2}\sqrt{\frac{B}{L}}\right]$

Notes:

d_w = height of effective side wall contact (may be less than total foundation height)

z_w = depth to centroid of effective sidewall contact

A_w = sidewall-solid contact area, for constant effective contact height, d_w, along perimeter.

For each degree of freedom, calculate $K_{emb} = \eta K_{sur}$

Coupling Terms: $K_{emb,rx} = \left(\frac{D}{3}\right)K_{emb,x}$

$K_{emb,ry} = \left(\frac{D}{3}\right)K_{emb,y}$

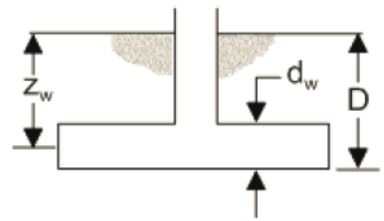

Table 3.3 Dynamic stiffness modifiers and radiation damping ratios for rigid footings (adapted from Pais and Kausel, 1988, NEHRP, 2012)

Degree of Freedom	Surface Stiffness Modifiers	Radiation Damping
Translation along z-axis	$\alpha_z = 1.0 - \left[\dfrac{\left(0.4+\dfrac{0.2}{L/B}\right)a_0^2}{\left(\dfrac{10}{1+3(L/B-1)}\right)+a_0^2}\right]$	$\beta_z = \left[\dfrac{4\psi(L/B)}{(K_{z,sur}/GB)}\right]\left[\dfrac{a_0}{2\alpha_z}\right]$
Translation along y-axis	$\alpha_y = 1.0$	$\beta_y = \left[\dfrac{4(L/B)}{(K_{y,sur}/GB)}\right]\left[\dfrac{a_0}{2\alpha_y}\right]$
Translation along x-axis	$\alpha_x = 1.0$	$\beta_x = \left[\dfrac{4(L/B)}{(K_{x,sur}/GB)}\right]\left[\dfrac{a_0}{2\alpha_x}\right]$
Torsion about z-axis	$\alpha_{zz} = 1.0 - \left[\dfrac{\left(0.33-0.03\sqrt{L/B-1}\right)a_0^2}{\left(\dfrac{0.8}{1+0.33(L/B-1)}\right)+a_0^2}\right]$	$\beta_{zz} = \left[\dfrac{(4/3)\left[(L/B)^3+(L/B)\right]a_0^2}{\left(K_{zz,sur}/GB^3\right)\left[\left(\dfrac{1.4}{1+3(L/B-1)^{0.7}}\right)+a_0^2\right]}\right]\left[\dfrac{a_0}{2\alpha_{zz}}\right]$
Rocking about y-axis	$\alpha_{yy} = 1.0 - \left[\dfrac{0.55a_0^2}{\left(0.6+\dfrac{1.4}{(L/B)^3}\right)+a_0^2}\right]$	$\beta_{yy} = \left[\dfrac{(4\psi/3)(L/B)^3 a_0^2}{\left(\dfrac{K_{yy,sur}}{GB^3}\right)\left[\left(\dfrac{1.8}{1+1.75(L/B-1)}\right)+a_0^2\right]}\right]\left[\dfrac{a_0}{2\alpha_{yy}}\right]$
Rocking about x-axis	$\alpha_{xx} = 1.0 - \left[\dfrac{\left(0.55+0.01\sqrt{L/B-1}\right)a_0^2}{\left(2.4-\dfrac{0.4}{(L/B)^3}\right)+a_0^2}\right]$	$\beta_{xx} = \left[\dfrac{(4\psi/3)(L/B)a_0^2}{\left(K_{xx,sur}/GB^3\right)\left[\left(2.2-\dfrac{0.4}{(L/B)^3}\right)+a_0^2\right]}\right]\left[\dfrac{a_0}{2\alpha_{xx}}\right]$
Notes:	Orient axes such that $L \geq B$. Soil hysteretic damping, β_s, is additive to foundation radiation damping, β. $a_0 = \omega B / V_s$; $\psi = \sqrt{2(1-\nu)/(1-2\nu)}$; $\psi \leq 2.5$	

Table 3.4 Dynamic stiffness modifiers and radiation damping ratios for embedded footings (adapted from Pais and Kausel, 1988, NEHRP, 2012)

Degree of Freedom	Radiation Damping
Translation along z-axis	$\beta_z = \left[\dfrac{4\left[\psi(L/B)+(D/B)(1+L/B)\right]}{\left(K_{z,emb}/GB\right)}\right]\left[\dfrac{a_0}{2\alpha_z}\right]$
Translation along y-axis	$\beta_y = \left[\dfrac{4\left[L/B+(D/B)(1+\psi L/B)\right]}{\left(K_{y,emb}/GB\right)}\right]\left[\dfrac{a_0}{2\alpha_y}\right]$
Translation along x-axis	$\beta_x = \left[\dfrac{4\left[L/B+(D/B)(\psi+L/B)\right]}{\left(K_{x,emb}/GB\right)}\right]\left[\dfrac{a_0}{2\alpha_x}\right]$
Torsion about z-axis	$\beta_{zz} = \left[\dfrac{(4/3)\left[3(L/B)(D/B)+\psi(L/B)^3(D/B)+3(L/B)^2(D/B)+\psi(D/B)+(L/B)^3+(L/B)\right]a_0^2}{\left(\dfrac{K_{zz,emb}}{GB^3}\right)\left[\left(\dfrac{1.4}{1+3(L/B-1)^{0.7}}\right)+a_0^2\right]}\right]\left[\dfrac{a_0}{2\alpha_{zz}}\right]$
Rocking about y-axis	$\beta_{yy} = \left[\dfrac{(4/3)\left[\left(\dfrac{L}{B}\right)^3\left(\dfrac{D}{B}\right)+\psi\left(\dfrac{D}{B}\right)^3\left(\dfrac{L}{B}\right)+\left(\dfrac{D}{B}\right)^3+3\left(\dfrac{D}{B}\right)\left(\dfrac{L}{B}\right)^2+\psi\left(\dfrac{L}{B}\right)^3\right]a_0^2}{\left(\dfrac{K_{yy,emb}}{GB^3}\right)\left[\left(\dfrac{1.8}{1+1.75(L/B-1)}\right)+a_0^2\right]}+\dfrac{\left(\dfrac{4}{3}\right)\left(\dfrac{L}{B}+\psi\right)\left(\dfrac{D}{B}\right)^3}{\left(\dfrac{K_{yy,emb}}{GB^3}\right)}\right]\left[\dfrac{a_0}{2\alpha_{yy}}\right]$
Rocking about x-axis	$\beta_{xx} = \left[\dfrac{(4/3)\left[\left(\dfrac{D}{B}\right)+\left(\dfrac{D}{B}\right)^3+\psi\left(\dfrac{L}{B}\right)\left(\dfrac{D}{B}\right)^3+3\left(\dfrac{D}{B}\right)\left(\dfrac{L}{B}\right)+\psi\left(\dfrac{L}{B}\right)\right]a_0^2}{\left(\dfrac{K_{xx,emb}}{GB^3}\right)\left[\left(\dfrac{1.8}{1+1.75(L/B-1)}\right)+a_0^2\right]}+\dfrac{\left(\dfrac{4}{3}\right)\left(\psi\dfrac{L}{B}+1\right)\left(\dfrac{D}{B}\right)^3}{\left(\dfrac{K_{xx,emb}}{GB^3}\right)}\right]\left[\dfrac{a_0}{2\alpha_{xx}}\right]$
Notes:	Soil hysteretic damping, β_s, is additive to foundation radiation damping, β_f. $\alpha_{emb} = \alpha_{sur}$; from Table 3-2a $a_o = \omega B/V_s$; $\psi = \sqrt{2(1-\nu)/(1-2\nu)}$; $\psi \le 2.5$

3.2.4 Effect of Non-Uniform Soil Over the Foundation Dynamic Stiffness

There is an inherent difficulty in applying analytical and semi-analytical methods to problem involving inhomogeneous soil media because of the difficulties associated with the decoupling of the governing equations and solving the related differential equations with variable coefficients (Mylonakis et. al., 2005). Above given tables are for on or in homogeneous soil profiles. For the non-homogeneous soil, average parameters it is possible the use (NEHRP, 2012). Namely, the shear wave velocity usually increases with depth depending on the soil properties. This increase indicates that the dynamic properties of the soil generally increase with depth without some exceptions. In the FEM analysis, the soil layers can be taken into account separately. However, for using equations given in Table 3.1a to Table 3.2b, soil profile must be idealized.

The shear wave velocity is generally measured at the ground surface. Data is gathered through the soil profile. Measurement depth depends on the utilized thecnique and soil type. However, shear wave velocity would be different beneath the foundation due to stress increase. This aspect of foundation effect can be taken into consideration as follows:

$$V_{S,F}(z) \approx V_s(z)\left(\frac{\sigma_v^{'}(z)+\Delta\sigma_v^{'}(z)}{\sigma_v^{'}(z)}\right)^{n/2} \tag{3.9}$$

where:

$V_{s,F}$ (z) : Overburden-corrected shear wave velocity at depth z,

V_S (z) : Denotes the shear wave velocity measured in the free-field at depth z,

$\sigma_v^{'}(z)$: Effective stress of the soil at depth z, and

$\Delta\sigma_v^{'}(z)$: Increment of vertical stress due to the weight of the structure at depth z.

n: An exponential constant (varies from approximately 0.5 for granular soils (Hardin and Black, 1968; Marcuson and Wahls, 1972) to 1.0 for cohesive soils with plasticity index (PI) greater than 6.5 (Yamada et al., 2008).

The overburden correction in Equation 3.9 is typically significant only at shallow depths (i.e., 50% to 100% of the foundation dimension).

While calculating a profile consisting of layers, V_s is found by taking the weighted average of the effective profile depth (Luco and Wong, 1985).

The profile is discretized into layers having thickness Δzi and velocity $V_{s,F}$ $(z)_i$. Designated as $V_{s,\,avg}$, the average effective profile velocity should be calculated as the ratio of the profile depth, z_p, to the summation of shear wave travel time through each depth interval (Equation 3.10). The depth interval, z_p is given:

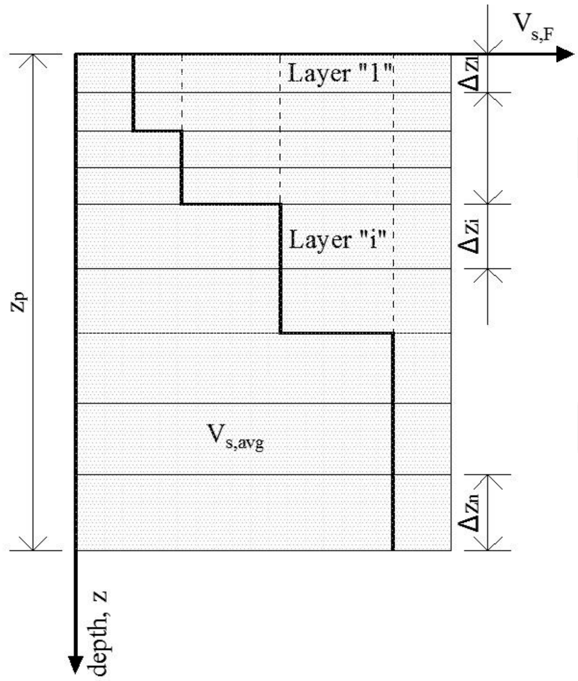

Figure 3.3 Representing overburden corrected Vs calculation.

$$V_{s,avg} = \frac{z_p}{\sum_{i=1}^{n} \left(\Delta z_i \big/ (V_{s,F}(z))_i \right)} \tag{3.10}$$

$$Horizontal\ (x\ and\ y): \quad z_p = B_e^A, \quad B_e^A = \sqrt{A/4} = \sqrt{BL} \tag{3.11}$$

$$Rocking(xx): \quad z_p \approx B_e^I, \quad B_e^I = \sqrt[4]{0.75 I_x} = \sqrt[4]{B^3 L} \tag{3.12}$$

$$Rocking(yy): \quad z_p \approx B_e^I, \quad B_e^I = \sqrt[4]{0.75 I_y} = \sqrt[4]{B L^3} \tag{3.13}$$

where:

B_e^A: the area of the actual foundation,

B_e^I : the moment of inertia of the actual foundation,

I_x : moment of inertia of the half dimension foundation about x-x axis,

I_y : moment of inertia of the half dimension foundation about y-y axis,

Δz_i : thickness of layer *i*.

3.2.5 Effect of Soil Nonlinearity

Soft soil sites or strong shaking acceleration levels often lead to occurrence of nonlinear behavior on the soil. Nonlinear effects are taken into consideration in the realistic models and can be examined by FEM analysis programs. However, we can consider nonlinear properties of the ground in a practical manner using equivalent linear analysis technique. The analyses according to equivalent linear method results in solutions that stay on the safe side. However, the engineer should properly use recommended reductions for various site classes:

Table 3.5 Values of shear wave velocity and shear modulus reduction for various site classes and shaking amplitudes (ASCE, 2010; FEMA, 2009)

	Reduction Factor (V_s)			Reduction Factor (G/G_0)		
	$S_{DS}/2.5$ (1)			$S_{DS}/2.5$ (1)		
Site Class	≤0.1	0.4	≥0.8	≤0.1	0.4	≥0.8
A	1.00	1.00	1.00	1.00	1.00	1.00
B	1.00	0.97	0.95	1.00	0.95	0.90
C	0.97	0.87	0.77	0.95	0.75	0.60
D	0.95	0.71	0.32	0.90	0.50	0.10
E	0.77	0.22	(2)	0.60	0.05	(2)
F	(2)	(2)	(2)	(2)	(2)	(2)

Notes: (1) S_{DS} is the short period spectral response acceleration parameter defined in ASCE/SEI 7-10; use straight line interpolation for intermediate values of $S_{DS}/2.5$.
(2) Value should be evaluated from site-specific analysis.

3.2.6 Effect of Flexible Foundation

Many researchers assumed foundation as a rigid plate to determine the impedance function. This assumption simplifies the analytical equation solution. However, the foundation systems never behave infinitely rigid. They rather act as flexible. The impedance function of the flexible circular foundation plate has been evaluated for different shear wall configurations assuming (Figure 3.4);

a) Rigid core walls (Iguchi and Luco, 1982)
b) Thin perimeter walls (Liou and Huang, 1994),
c) Rigid concentric interior and perimeter walls (Riggs and Waas, 1985).

For determining the relative rigidity of the base plate;

$$\psi = \frac{Gr_f^3}{\left(E_f t_f^3 / \left(12\left(1-\upsilon_f^2\right)\right)\right)} \tag{3.14}$$

where:

E_f : Foundation elastic modulus,

t_f : Thickness of foundation plate,

r_f : Radius of foundation

υ_f :Poisson's ratio of the foundation.

The case of $\psi = 0$ represents a fully rigid foundation.

Liou and Huang (1994) showed that, in case of a foundation consisting of flexible perimeter walls, translational stiffness and damping rates are not significantly affected.

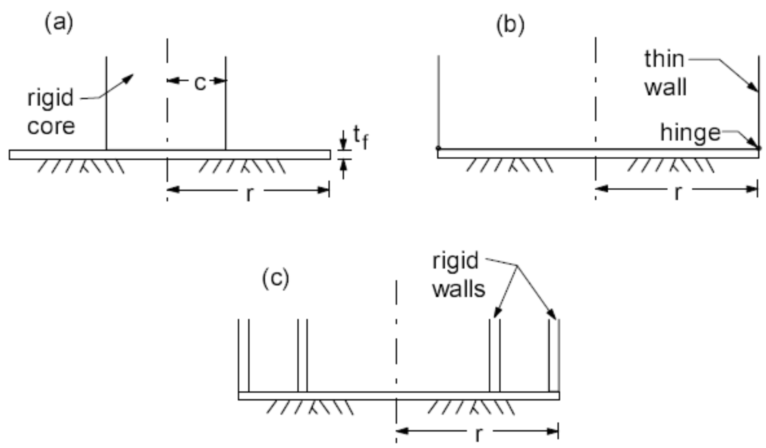

Figure 3.4 Disk foundations with (a) rigid core considered by Iguchi and Luco (1982) (b) thin perimeter walls considered by Liou and Huang (1994), and (c) rigid concentric walls considered by Riggs and Waas (1985)

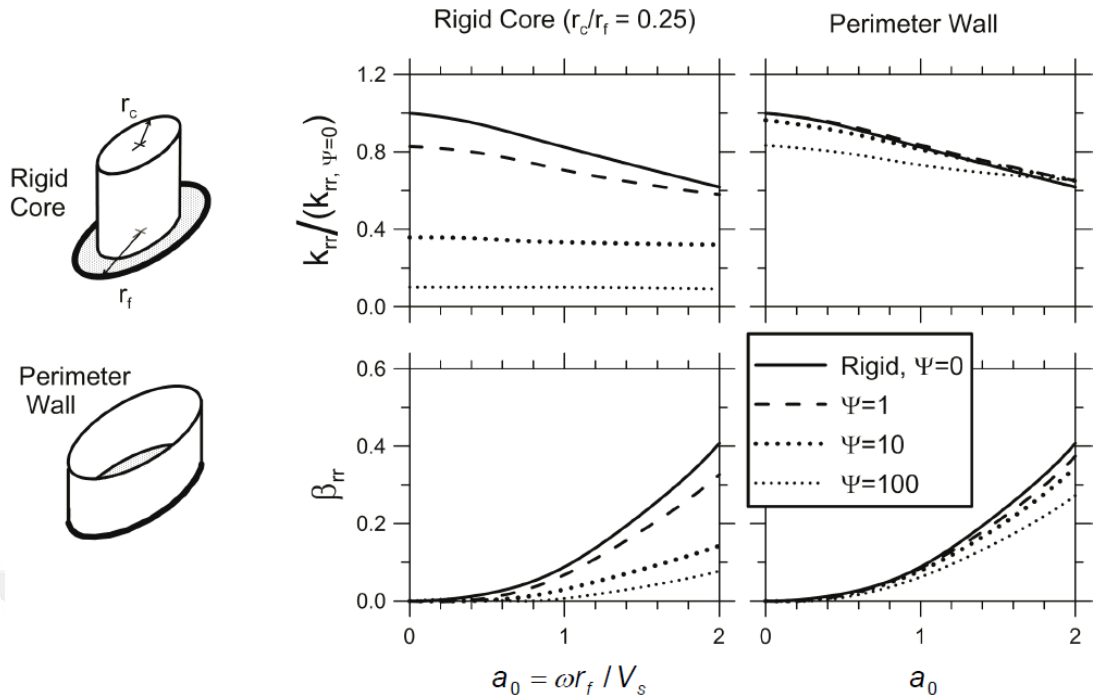

Figure 3.5 Rocking stiffness and damping factors for flexible foundations; rigid core cases (Iguchi and Luco, 1982) and perimeter wall case (Liou and Huang, 1994)

Foundation flexibility effect on the rotation stiffness and radiation damping, is shown in Figure 3.5; In case of flexible perimeter walls it is relatively small and in the case of the rigid core it is important.

A single equivalent spring for a certain degree of freedom is often used in soil-structure interaction. Thus, total six degrees of freedom significantly reduces the solution time in solving large problems. This requires the adoption of the fully rigid base assumption if possible. Rigid central cores are used by structural engineers in some high-rise buildings. The raft thickness at the point where the base is connected to the core exhibits rigid plate behavior. The outer region of the raft demonstrates a more flexible behavior. The basement surrounded by rigid perimeter shear walls prevents flexible behavior by suppressing deformations of the shear walls. However, the foundation raft will be flexible between the core and the perimeter. Here, the foundation shape, distance between the peripheral walls and the core, and slab thickness will be decisive on the foundation flexibility.

Flexible foundation solutions are required for representing the real behavior. It is very difficult to determine the impedance function with analytical or semi-analytical methods. Instead, the foundation flexibility can be taken into consideration by the springs distributed at the foundation base as illustrated in Figure 3.6. Imposed loads transferred from the superstructure to the foundation cause the reactions on springs by means of distributed springs. These reactions are caused by out of plane deformations of the plate. For vertical springs, as described above, the obtained vertical translational impedance (also known as coefficient of subgrade reaction) is normalized by the foundation footprint to calculate the stiffness intensity, k_z^i with dimensions of force per cubic length:

$$k_z^i = \frac{k_z}{4BL} \tag{3.15}$$

Where; B, L are the foundation half-widths.
A dashpot intensity can be similarly calculated as:

$$c_z^i = \frac{c_z}{4BL} \tag{3.16}$$

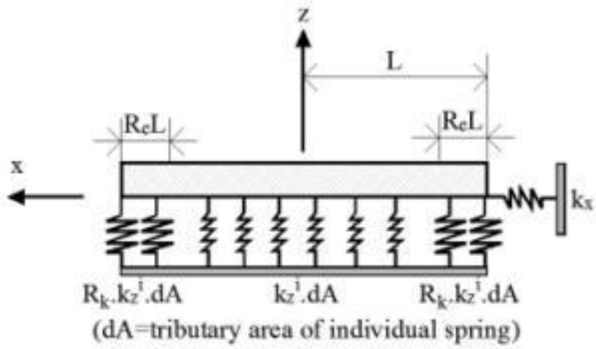

Figure 3.6 Vertical spring distribution used to reproduce total rotational stiffness k_{yy}. A comparable geometry can be shown in the y-z plane (using foundation dimension 2B) to reproduce k_{xx} (NEHRP, 2012)

Stiffness intensity values expressed by Equation (3.15) and (3.16), are not applied uniformly in the complete foundation base area. The vertical ground reaction due to the rocking effect will be greater than the center of the foundation. The ratio of the length of this edge region and the total length of the foundation are named End Length Ratio, R_e has been explained by Harden and Hutchinson (2009) as shown in Figure 3.6.

The End Length Ratio is a function of L/B that usually varies between 0.3 and 0.5 and is used for correction of the spring stiffness in the foundation edge strip. Similarly the foundation damping ratio is calculated oversize at the rocking components. The reason is the emergence of a significant radiation damping in the translational components. Therefore, this should be corrected by a reduction factor.

More generally, the increase in spring stiffness, R_k, can be calculated as a function of foundation end length ratio, R_e, as:

$$Rocking(yy): \quad R_{k,yy} = \frac{\left(\dfrac{3k_{yy}}{4k_z^i BL^3}\right) - \left(1-R_e\right)^3}{1-\left(1-R_e\right)^3} \tag{3.17}$$

$$Rocking(xx): \quad R_{k,xx} = \frac{\left(\dfrac{3k_{xx}}{4k_z^i B^3 L}\right) - \left(1-R_e\right)^3}{1-\left(1-R_e\right)^3} \tag{3.18}$$

Equation 3.17 and 3.18 are obtained by matching the moment produced by the springs under the unit rotation of foundation with the rotational stiffness k_{xx} or k_{yy}. Dashpot intensity over the entire length and width of foundation reduced by R_c factor. R_c is given by;

$$Rocking(yy): \quad R_{c,yy} = \frac{\dfrac{3c_{yy}}{4c_z^i BL^3}}{R_{k,yy}(1-(1-R_e)^3)+(1-R_e)^3} \tag{3.19}$$

$$Rocking(xx): \quad R_{c,xx} = \frac{\dfrac{3c_{xx}}{4c_z^i B^3 L}}{R_{k,xx}(1-(1-R_e)^3)+(1-R_e)^3} \tag{3.20}$$

In the horizontal direction, the use of a vertical distribution of horizontal springs depends on 2D or 3D analyses and foundation embedment depth.

Current recommendations are as follows:

If the foundation is located on the ground surface, the horizontal spring stiffness is directly applied to the foundation (no distributed springs.) for 2D analysis.

2D analysis case of an embedded foundation,

1. When the embedded side soils perfectly bonded to the foundation side walls

   In this case, two horizontal stiffness are calculated:

a) According to the soil dynamic properties of foundation embedment level and removing side soil condition as shown in Figure 3.7-II,
b) According to the presence of side soil condition as shownd in Figure 3.7-I.

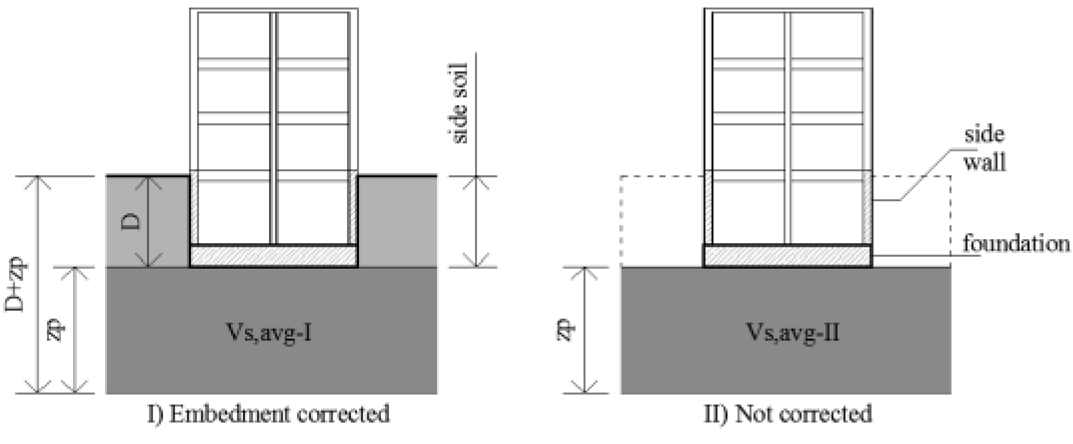

Figure 3.7 Horizontal dynamic stiffness of the side-walls (embedment effect)

The difference between the above explained two cases gives the sum of the spring stiffness the corresponding direction which can be used for horizontal spring stiffness distribution.

2. If the fill between the soil and the basement wall is not guaranteed, side wall contribution should be neglected. The contact area between the sidewalls of an embedded foundation and the surrounding soil tends to increase the stiffness (spring constant) and damping (dashpot constant). The actual sidewall area that is in ‘‘good’’ contact with the surrounding soil is usually smaller than the nominal contact area. (Gazetas, 1991)

For 3D analysis, springs are distributed uniformly around the perimeter of the foundation. The sum of the spring stiffnesses in a given direction should match the total stiffness of the impedance function.

3.2.7 Pile Group Dynamic Stiffness

Single pile dynamic behavior can be obtained analytically according to Beam on Dynamic Winkler Foundation (BDWF) method. However, the dynamic behavior of pile groups cannot be obtained simply by multiplying one pile dynamic stiffness with the total number of piles in the group. Because piles under dynamic loads are interacting with each other depending on the distance between piles, the frequency of vibration, pile length, pile stiffness, pile diameter, soil dynamic properties.

The vertical pile which radially radiates waves outwards in all directions can act as a source of vibration in the soil media. These radiated waves hit the adjacent pile and cause deformation therein. The ratio of the deformation function of the adjacent pile and the original pile gives the attenuation function as shown in Figure 3.8. The interaction between the two piles can be obtained from solution of governing differential equations (Makris and Gazetas 1992). So, the interaction ratio between the any two piles in the group can be easily calculated. In this way, entire pile-to-pile interaction factors are calculated in the group and sum of them yields group interaction factor. This technique is named as Superposition Technique and developed by Poulos (1968).

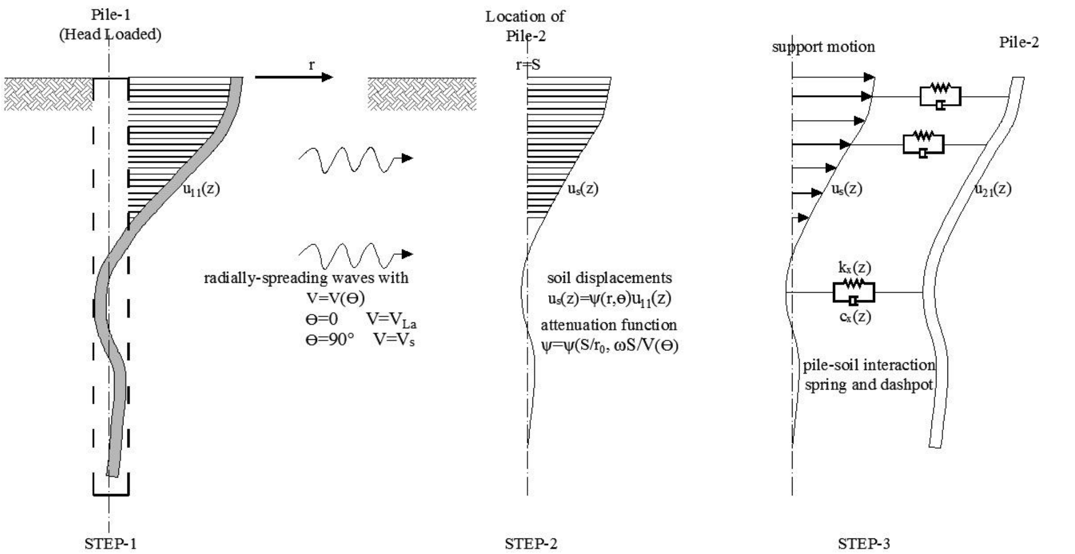

Figure 3.8 Schematic illustration of the developed 3-step procedure for computing the influence of Pile-1, deforming under harmonic lateral head loading, upon the adjacent Pile-2 (Makris and Gazetas, 1992)

Pile groups are generally connected to each other through the raft foundation of the superstructure. The distance between piles greatly affect the behavior of the group. For greater range, piles do not affect each other and the group dynamic stiffness are calculated as the sum of the individual pile contributions separately. However, as the piles get close to each other, they interact with one another and cause a significant effect on the stiffness of the pile group and damping.

3.2.7.1 Lateral Dynamic Stiffness of a Single Pile

Pile-soil interaction is realistically modelled by means of dynamic Winkler springs which are frequency dependent ($k_x(\omega)$, and dashpot, $c_x(\omega)$). The dynamic solution can be written for the single pile and the group stiffness are obtained from pile-to-pile interaction formulation which has been suggested by Makris and Gazetas (1992, 1993).

$$K_x^1(\omega) = K_{1x}^1(w) + iK_{2x}^1(w) = \frac{E_p I_p R^3 (r_1^2 + r_2^2)}{r_1 - ir_2} \tag{3.21}$$

where:

$E_p I_p$: is the flexural rigidity of the pile,
$K_{1x}^1(w)$: is the real part of the lateral dynamic stiffness of single pile,
$K_{2x}^1(w)$: is the imaginary part of the lateral dynamic stiffness of single pile.

$$\begin{aligned} r_1 &= -a^3 - b^3 + 3a^2 b + 3ab^2 \\ r_2 &= a^3 - b^3 + 3a^2 b - 3ab^2 \end{aligned} \tag{3.22}$$

If the excitation frequency ω is less than the characteristic frequency of the pile-soil system $\omega < \varpi = (k_x(\omega)/m)^{1/2}$ (m is the pile mass per length), the values of R, a, and b are :

$$\left.\begin{aligned} R &= \left(\frac{(k_x(\omega) - m\omega^2)^2 + (\omega c_x(\omega))^2}{(4I_p E_p)^2} \right)^{1/8} \\ a &= \cos\frac{\theta}{4} + \sin\frac{\theta}{4}, \quad b = \cos\frac{\theta}{4} - \sin\frac{\theta}{4} \\ \theta &= \tan^{-1}\left(\frac{\omega c_x(\omega)}{k_x(\omega) - m\omega^2} \right), \quad 0 < \theta < \frac{\pi}{2} \end{aligned}\right\} \tag{3.23}$$

And for values of $\omega > v = (k_x(\omega)/m)^{1/2}$, the values of R, a, and b are:

$$\left.\begin{aligned} R &= \left(\frac{(k_x(\omega) - m\omega^2)^2 + (\omega c_x(\omega))^2}{(E_p I_p)^2} \right)^{1/8} \\ a &= cos\frac{\theta}{4}, \qquad b = -sin\frac{\theta}{4} \\ \theta &= tan^{-1}\left(\frac{-\omega c_x(\omega)}{-k_x(\omega) + m\omega^2} \right), \quad -\frac{\pi}{2} < \theta < 0 \end{aligned}\right\} \tag{3.24}$$

$$\left.\begin{aligned} k_x &\approx 1.2E_s \\ c_x &= (c_x)_{rad} + (c_x)_{hyst} \approx 2d\rho_s V_s \left[1 + \left(\frac{V_{La}}{V_s} \right) \right] a_0^{-0.25} + \eta \frac{k_x}{\omega} \end{aligned}\right\} \tag{3.25}$$

where:

η : Hysteretic damping coefficient of the soil defined in Equation 2.5,

ρ_s : Mass density,

E_s : Young's modulus,

V_s : Shear-wave velocity of the soil,

$a_0 = \omega d / V_s$: Dimensionless exication frequency,

V_{La} : An apparent velocity of the compression-extension waves, called "Lysmer's analogue" velocity as shown in Figure 3.9 (Gazetas and Dobry 1984a; 1984b).

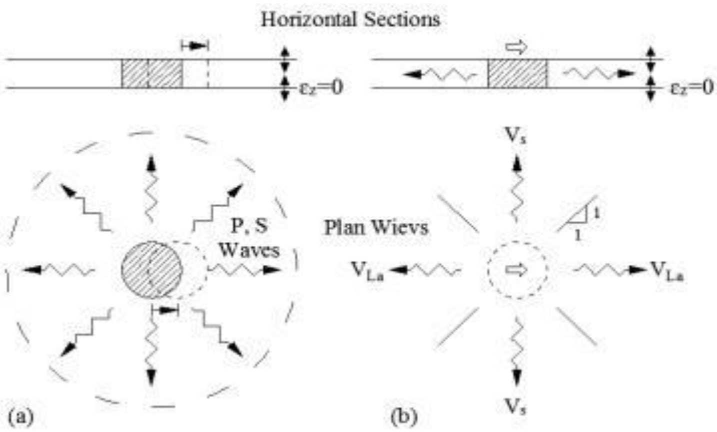

Figure 3.9 Schematic representation of 2D radiation model: (a) 'rigorous' plane-strain model of Novak et al. (1978), (b) simplified plane-strain model of Gazetas and Dobry (Gazetas and Dobry, 1984a; 1984b).

$$V_{La} = \frac{3.4}{\pi(1-\upsilon)} V_s \tag{3.26}$$

where:

υ: Poisson's ratio of the soil.

3.2.7.2 Vertical and Rocking Dynamic Stiffnesses of a Single Pile

In the low frequency range (a_0 <1), the single pile vertical stiffness for a homogeneous soil conditions is given as:

$$\left.\begin{aligned} k_z(\omega) &\approx 0.6E_s\left(1+\frac{1}{2}\sqrt{a_0}\right) \\ c_z(\omega) &= (c_z)_{rad} + (c_z)_{hyst} \approx 1.2a_0^{-0.25}\pi d\rho_s V_s + \eta\frac{k_z(\omega)}{\omega} \end{aligned}\right\} \tag{3.27}$$

A long pile can be represented as a vertical thin rod in the soil media. Distributed Winkler springs, $k_z(\omega)$ and dashpots, $c_z(\omega)$ in the vertical direction connect the pile to the surrounding soil.

Vertical dynamic stiffness of a single pile including pile-soil-pile interaction is given as follows:

$$For\ \omega < \bar{\omega}_z = \sqrt{\frac{k_z(\omega)}{m}},\quad K_z^{[1]} = K_{1z}^{[1]}(\omega) + iK_{2z}^{[1]}(\omega) = \frac{RE_pA_p}{\cos\frac{\theta}{2} - i\sin\frac{\theta}{2}} \tag{3.28}$$

In Equation 3.28;

E_pA_p: is the axial stiffness of the pile.

$$R = \left(\frac{(k_z(\omega)-m\omega^2)^2 + (\omega c_z(\omega))^2}{(A_pE_p)^2}\right)^{1/4} \tag{3.29}$$

and

$$\theta = \tan^{-1}\left(\frac{\omega c_z(\omega)}{k_z(\omega)-m\omega^2}\right), 0 < \theta < \frac{\pi}{2} \tag{3.30}$$

For $\omega > \bar{\omega}_z = \sqrt{\frac{k_z(\omega)}{m}}$ the vertical dynamic stiffness of the single pile is:

$$K_z^{[1]} = K_{1z}^{[1]}(\omega) + iK_{2z}^{[1]}(\omega) = \frac{-RE_pA_p}{\sin\frac{\theta}{2} + i\cos\frac{\theta}{2}} \tag{3.31}$$

$$\theta = \tan^{-1}\left(\frac{\omega c_z(\omega)}{k_z(\omega) - m\omega^2}\right), -\frac{\pi}{2} < \theta < 0 \tag{3.32}$$

3.2.7.3 Lateral Dynamic Stiffness of Pile Group

The horizontal dynamic interaction factor between two piles in a homogeneous half space takes the form:

$$\alpha_x(S,\theta) = \alpha_x(S,0)\cos^2\theta + \alpha_x(S,\frac{\pi}{2})\sin^2\theta \tag{3.33}$$

where:

θ: Angle between the unit harmonic load direction and the line connecting the center of the two piles as shown in Figure 3.10,

$$\alpha_x(S,0) = \frac{3}{4}\psi(S,0)\frac{k_x + i\omega c_x}{k_x - m\omega^2 + i\omega c_x} \tag{3.34}$$

$$\alpha_x(S,\frac{\pi}{2}) = \frac{3}{4}\psi(S,\frac{\pi}{2})\frac{k_z + i\omega c_z}{k_z - m\omega^2 + i\omega c_z} \tag{3.35}$$

where:

$\psi(r,\theta)$: An approximate attenuation function:

$$\psi(S,0) = \left(\frac{d}{2S}\right)^{\frac{1}{2}} \exp\left[-(\beta_s + i)\frac{\omega\left(S - \frac{d}{2}\right)}{V_{La}}\right] \tag{3.36}$$

$$\psi(S,\frac{\pi}{2}) = \left(\frac{d}{2S}\right)^{\frac{1}{2}} \exp\left[-(\beta_s + i)\frac{\omega\left(S - \frac{d}{2}\right)}{V_s}\right] \tag{3.37}$$

where:

S: Distance between two interacting piles as shown in Figure 3.10,

$i : \sqrt{-1}$,

d: Pile diameter

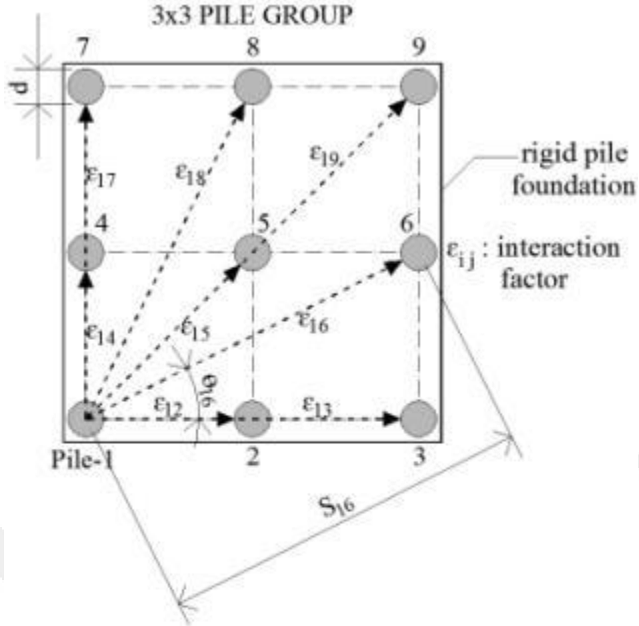

Figure 3.10 Illustration of superposition thechnique for pile to pile interaction.

Let's say that the i'th pile horizontal displacement is y_i. Superposition of displacement can be written for vibrating pile:

$$y_i = \sum_{j=1}^{N} \alpha(i, j) y_j \tag{3.38}$$

$$y_j = \frac{F_j}{K_x^{[1]}} \tag{3.39}$$

$K_x^{[1]}$ is the horizontal dynamic stiffness of the one pile, F_j is the force of the jth pile, N is the number of piles in the group. Substitution of (3.39) into (3.38) gives:

$$y_i K_x^{[1]} = \sum_{j=1}^{N} \alpha(i, j) F_j \tag{3.40}$$

If all piles are connected with a rigid plate:

The displacement of the pile group, $y^{[G]} = y_i$ and (3.40) can be written:

$$y^G K_x^{[1]} = \sum_{j=1}^{N} \alpha(i, j) F_j \tag{3.41}$$

If Equation 3.41 written for each pile, pile group can be expressed in the matrix form:

$$\begin{bmatrix} 1 & \alpha_x(1,2) & \dots & \alpha_x(1,N) \\ \alpha_x(2,1) & 1 & \dots & \alpha_x(2,N) \\ : & : & : & : \\ \alpha_x(N,1) & \alpha_x(N,2) & \alpha_x(N,3) & 1 \end{bmatrix} \begin{bmatrix} F_1 \\ F_2 \\ : \\ F_N \end{bmatrix} = y^{[G]} K_x^{[1]} \begin{bmatrix} 1 \\ 1 \\ : \\ 1 \end{bmatrix} \tag{3.42}$$

if $i=j$, $\alpha_x(i,j)=1$ and the $\alpha_x(i,j)$ matrix can be called as “interaction matrix”.

(3.42) can be solved for force vector:

$$\begin{bmatrix} F_1 \\ F_2 \\ : \\ F_N \end{bmatrix} = \begin{bmatrix} \varepsilon_x(1,1) & \varepsilon_x(1,2) & \dots & \varepsilon_x(1,N) \\ \varepsilon_x(2,1) & \varepsilon_x(2,2) & \dots & \varepsilon_x(2,N) \\ : & : & : & : \\ \varepsilon_x(N,1) & \varepsilon_x(N,2) & \dots & \varepsilon_x(N,N) \end{bmatrix} y^{[G]} K_x^{[1]} \begin{bmatrix} 1 \\ 1 \\ : \\ 1 \end{bmatrix} \tag{3.43}$$

where $\varepsilon_x(i,j)$ is the term of the inverse matrix of the interaction matrix (Figure 3.10). Equation 3.43 can be written as follows:

$$\sum_{j=1}^{N} F_j = y^G K_x^{[1]} \sum_{i=1}^{N} \sum_{j=1}^{N} \varepsilon_x(i,j) \tag{3.44}$$

$$\sum_{j=1}^{N} F_j = K^{[G]} y^{[G]} \tag{3.45}$$

Substitution of (3.45) into (3.44) gives lateral dynamic stiffness of pile group:

$$K_x^{[G]} = K_x^{[1]} \sum_{i=1}^{N} \sum_{j=1}^{N} \varepsilon_x(i,j) \tag{3.46}$$

3.2.7.4 Vertical and Rocking Dynamic Stiffness of Pile Group

Interaction between the two vertically vibrating piles is given by the following equations:

$$\alpha_z = \left(\frac{d}{2S}\right)^{1/2} \exp\left[-(\beta_s + i)\frac{\omega\left(S - \frac{d}{2}\right)}{V_s}\right] \tag{3.47}$$

The vertical dynamic stiffness of the pile group:

$$K_z^{[G]} = K_z^{[1]} \sum_{i=1}^{N} \sum_{j=1}^{N} \varepsilon_z(i, j) \tag{3.48}$$

And rocking dynamic stiffness of the pile group:

$$K_r^{[G]} = K_z^{[1]} \sum_{i=1}^{N} x_i \sum_{j=1}^{N} x_j \varepsilon_z(i, j) \tag{3.49}$$

Where:

x_i : is the distance of the i'th pile from the axis of rotation.

3.3 Calculation Foundation Dynamic Stiffness by means of a Computer Algorithm

The analytical solution suggested by Makris and Gazetas has been transformed into a simple software for rapid analysis of the SPSI (Soil Pile Soil Interaction). Hence, it is aimed to evaluate effect of the different soil or pile properties which are pile spacing, pile diameter and material information. This software is employed to achieve the dynamic impedance function of the raft foundation using the Pais-Kausel and Mylonakis-Gazetas formulas.

Detailed descriptions of these formulations were given above and Figure 3.11 shows the flowchart of the program. User can easily input the relevant data with the aid of the graphical user interface. In addition, dynamic foundation stiffness, pile interaction factor, the pile group dynamic stiffness value can be calculated in a particular frequency range and frequency-dependent charts can be created. The program has an interface for all step-by-step data entry (Appendix-A). Some important data and significant results obtained from the calculation are shown in this interface. Detailed information were given in Appendix-A for using the developed software.

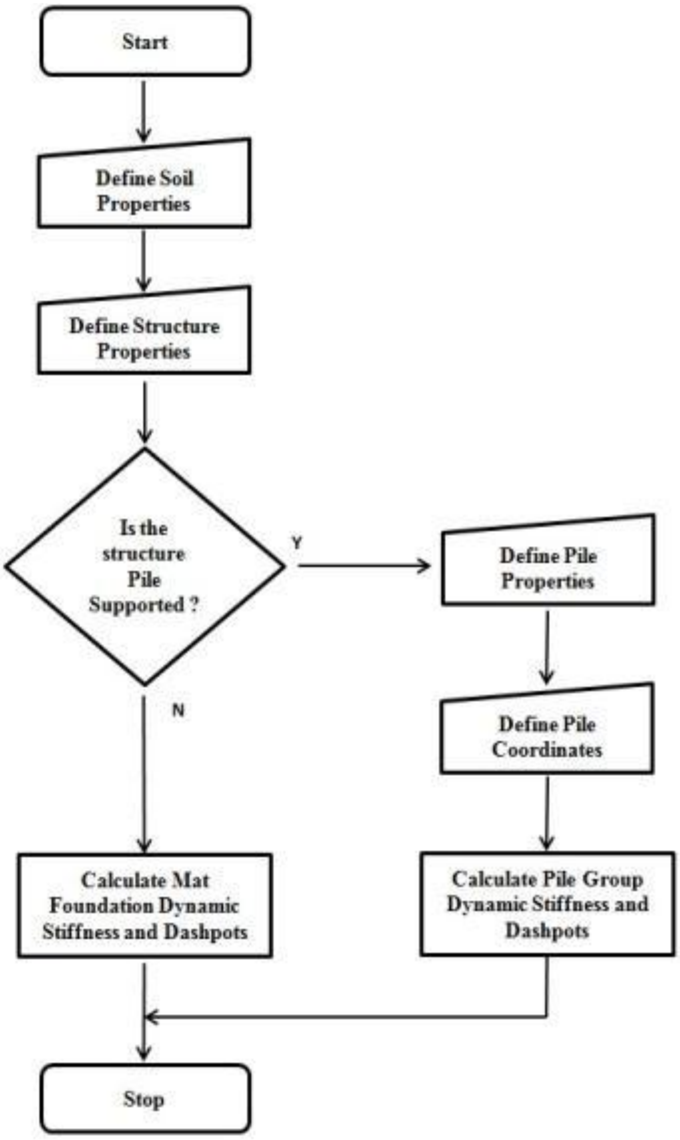

Figure 3.11 Flowchart of the algorithm

3.4 Kinematic Interaction

Spreading waves in the soil media experience a change when they encounter different soil types, layers or obstacles (such as different density, shear modulus, Poisson's ratio, existing foundations, boulders). This variation of the seismic waves in the soil media is called as the kinematic interaction (Figure 3.12). This interaction can occur between the layers in the soil medium or between the foundation and the soil (comprising different densities and different stiffness). In the absence of any structure, the time-dependent motion, reaching the free soil surface while undergoing changes in soil media, is called Free Field Motion (FFM). If there is an existing structure on the ground surface, engineers interest to foundation level ground motion. This is called the Foundation Input Motion (FIM) and pile foundations, embedded foundation, surface foundation FIM's are different from the FFM. So the FIM depends on foundation shape, embedment depth, the basic geometry of the composition of free-field incident waves and the angle of incidence of these waves (Villaverde, 2009).

Kinematic interaction can be neglected in the absence of foundation embedment for a structure excited by vertically propagating shear waves. Since, surface foundations are generally affected by laterally spreading surface waves (e.g. Rayleigh waves).

The presence of an embedded or rigid foundation on the ground surface deviates the free field motion. The main reasons of deviation are as follows:

a) Base slab averaging: Free field ground motions averaged by the raft foundation plate due to the its rigidity.
b) Embedment effects: Free field ground motions decrease with depth. In the presence of a pile foundation, interaction occurs between the incident waves and piles, so it changes the foundation base motion (Stewart, 2003).
c) Wave scattering: Reduces amplitude of high frequency components.

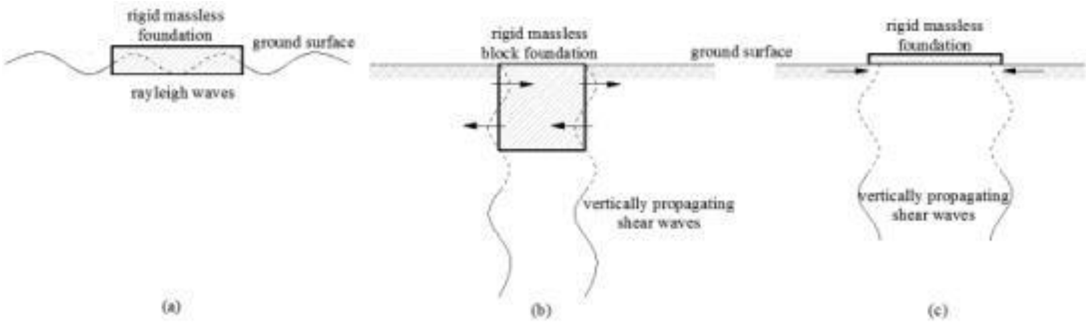

Figure 3.12 Kinematic interaction with free-field motions indicated by dashed lines: (a) flexural stiffness of surface foundation prevents it from following vertical component of free-field displacement; (b) rigidity of block foundation prevents it from following horizontal component of free-field displacement; (c) axial stiffness of surface foundation prevents immediately underlying soil from deforming incoherently (Kramer, 1996).

Kinematic interaction is expressed as the ratio of FIM / FFM depending on the frequency of the Fourier amplitudes (In other words, the transfer function) as shown in Figure 3.13. If we accept massless foundation and basement walls, FIM is the theoretical motion at the foundation base, and it is used for seismic response analysis in the substructure approach.

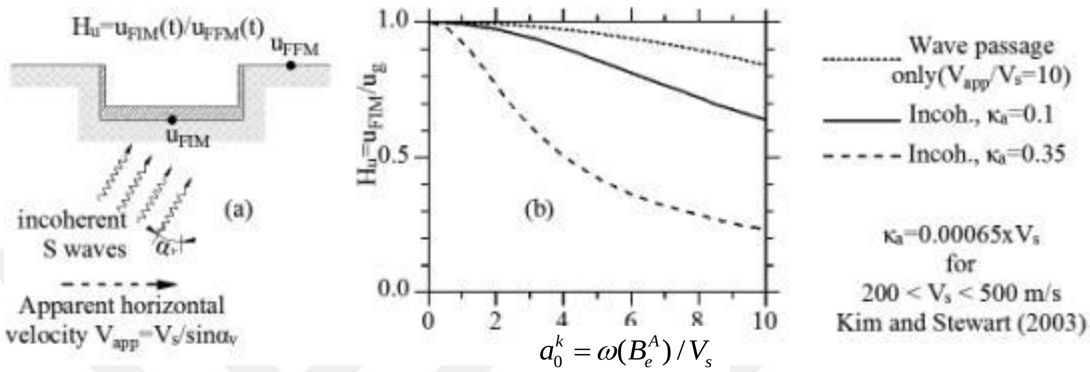

Figure 3.13 Illustration of foundation subjected to inclined shear waves: (a) schematic geometry; (b)transfer functions between FIM and free-field motion for wave passage using a semi-empirical model for incoherent waves (NEHRP, 2012).

3.4.1 Shallow Foundations at the Ground Surface

The translational components of the motions are more efficient for the structures which have less number of stories and shallow foundation on the ground surface (Figure 3.14). Many researches show that the rocking components of the motion are negligible for this kind of structures which have small embedded foundation (in order to stay on the safe side). However, the rocking effect cannot be neglected for high buildings. Emitted waves as a result of earthquake ground motion have an incoherent characteristic due to the wavefront effect, soil layers, inhomogeneity of soil media, human-made structures, etc. Geometric characteristics of the foundation (e.g. the foundation length to be smaller or larger from the wavelength of incoming shear waves), the angle between the vertical axis and incoming waves, the wave passage effect and many others play an important role in behavior. Figure 3.13(a) shows passage effect of the incoming waves. The wave-passage effect due to the non-vertical wave propagation depends on the apparent velocity (V_{app}) along the horizontal axis. Due to this effect, wave arrival times to the different points on the foundation plate are different. This causes time shifts in the time histories.

For shallow foundations, the transfer function that is defined as the ratio between the FIM and FFM given by Mylonakis et al. (2006) is as follows:

$$\left.\begin{array}{l} u_{FIM} = H_u u_g \\ H_u = \dfrac{\sin\left(a_0^k\left(\dfrac{V_s}{V_{app}}\right)\right)}{a_0^k\left(\dfrac{V_s}{V_{app}}\right)}, \quad a_0^k \le \dfrac{\pi}{2}\dfrac{V_{app}}{V_s} \\ H_u = \dfrac{2}{\pi}, \quad a_0^k > \dfrac{\pi}{2}\dfrac{V_{app}}{V_s} \end{array}\right\} \tag{3.50}$$

where:

Dimensionless frequency $a_0^k = \omega(B_e^A)/V_s$ and actual foundation area $B_e^A = \sqrt{BL}$.

If a_0^k is taken 0 in the above equation, it is seen that the transfer function is equal to 1 (static condition). In this equation, the apparent velocity, V_{app} is usually between the 2.0 km/h and 3.5 km/sec (Abrahamson, 1992b). In addition, V_{app}/V_s ratio is taken approximately 10 with a realistic estimate.

3.4.2 Embedded Shallow Foundations

FIM is lower than the surface motion for structures including basements. Since the amplitude of the seismic waves decreases with depth (Kausel et al., 1978). On the other hand, rocking behavior of the embedded foundations are at non-negligible degree as compared to shallow foundation.

For rectangular foundation shapes, transfer function is given by:

$$\left.\begin{aligned}
&H_u = \frac{u_{FIM}}{u_g} = \cos\left(\frac{D}{B_e} a_0^k\right) = \cos\left(\frac{D\omega}{V_s}\right), \quad \frac{D\omega}{V_s} < 1.1 \\
&H_u = 0.45, \quad \frac{D\omega}{V_s} > 1.1 \\
&H_{yy}(\omega) = \frac{\theta L}{u_g} = 0.26\left[1 - \cos\left(\frac{D\omega}{V_s}\right)\right], \quad \frac{D\omega}{V_s} < \frac{\pi}{2} \\
&H_{yy}(\omega) = 0.26, \quad \frac{D\omega}{V_s} > \frac{\pi}{2}
\end{aligned}\right\} \tag{3.51}$$

Where D is the embedment depth.

Equations for rocking component is written as in Equation 3.51 about x axis. The transfer function is given in the form:

$$H_{xx} = \frac{\theta B}{u_g} \tag{3.52}$$

Overburden corrected shear wave velocity, $V_{s,avg}$ is used for above equations instead of, V_s.

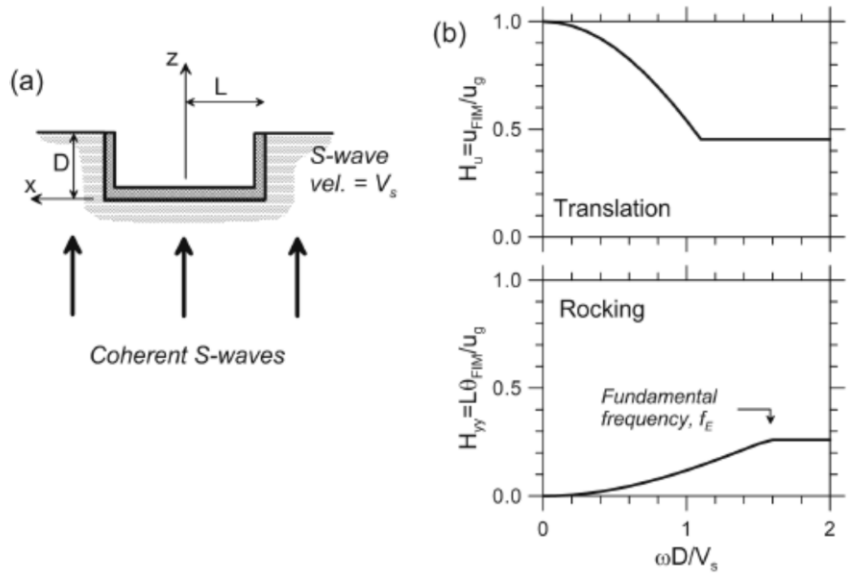

Figure 3.14 Illustration of a foundation subjected to vertically incident shear waves: (a) schematic geometry; and (b) transfer functions for horizontal foundation translation and rocking (NEHRP, 2012).

The rocking and translational components of the transfer function are given as in Figure 3.14b. Figure 3.14b shows that the translational component of the transfer function reduces nearly parabolic up to a_0 = 1, after this point, it is takes 0.45 constant value due to the Equation 3.51. It can be seen that the rocking component of the transfer function attains maximum value about a_0=1.6. The value is the fundamental frequency of the soil column, which is located between the free field surface and foundation base. Here, base slab averaging clearly showed a dominant behavior at the a_0 <1 region (low frequency), otherwise, embedment effect is more efficient in the a_0 >1 region (high frequency region).

3.4.3 Pile Foundations

Determination of transfer function to account for kinematic interaction effects for pile foundations is a complex task. Factors that influence this task may be listed as follows:

a) Gaps may occur between the pile and the soil due to cyclic load in the clayey soils.
b) In the conducted works in the literature, coherent seismic waves have generally been used for kinematic interaction of pile system. But in reality, seismic waves are incoherent.
c) In case of the presence of friction piles and highly flexible piles, pile deformation can follow the ground deformation. But rigid piles do not follow the ground deformation, unlike it shows a resistance. This causes a change in the FIM (Fan et al., 1991).

Current available methods cannot be safely used in practice, since they cannot be generalized because solutions are highly dependent on different ground conditions, structure-pile-foundation dynamics and geometric features. Works on this issue is still ongoing.

3.4.4 Application of Transfer Functions

Design-based response spectra are generally applicable to the free ground surface conditions. In addition, time domain acceleration records are developed when time history analyses will be performed. This section discusses how a transfer function obtained from the kinematic interaction analyses should be used to modify acceleration-time records or response spectrum.

Acceleration histories representing the FIM can be modified from free-field motions using the following procedure:

1. Calculate the Fourier transforms of acceleration time records at the free soil surface, u_g
2. Multiply the amplitude of u_g by the transfer function, Hu.
3. Perform a reverse Fourier transform to estimate foundation input motion, $u_{FIM}(t)$.

This simplified procedure can be used in practical applications. For more detailed analyses, finite element methods may be used.

CHAPTER FOUR
CASE STUDY: 14 STORY REINFORCED CONCRETE BUILDING SSI ANALYSIS

4.1 Introduction

In this section, the proposed simplified analytical methods by Makris & Gazetas and DYNAN Software were used to obtain impedance function of the foundation-soil interface and these two methods were compared. In this comparison, reduced soil shear modulus is used to account for the nonlinear behavior of the soil. Thus, approximate nonlinear behavior of soil is represented.

4.2 Technical Advisories for Tall Buildings in the İzmir New Town Center

For the geotechnical analyses of the structures that wold be constructed in the New Town Center of İzmir, imperative rules were given as follows:

- Drilling depth cannot be less than 100 m under any circumstances in order to obtain the parameters of the soil model, which will be used for dynamic soil analysis.
- Relevant laboratory tests will be carried out on the disturbed and undisturbed soil samples.
- If the shear wave velocity happens to be 760 m/s at a certain depth, this level will be assumed as the engineering rock level in the soil profile.
- All measured shear wave velocities must be greater than 760 m/s below the engineering rock level until 250m.
- Shear wave velocities shall not be determined using the correlative relationships.
- Shear wave velocity profile which shall be used in design is obtained from deep geophysical site investigations.
- If the engineering rock level cannot be achieved in the first 250m of the soil profile, the level where $V_s \geq 760$m/s is measured after 250m depth shall be assumed as the engineering bedrock level.

- Selected records for the site response analyses are to be compatible with the design spectrum of B type soil, where D1, D2, D3 earthquake intensity level records are assigned to the model.
- The magnitude of the selected earthquakes will be between 6 and 7 (M_w = 6~7).
- The earthquake records will be selected for both close and far distance stations located around the faults.

In this study, data were collected according to the rules given in the technical advisories. The earthquake motions were selected according to the shear wave velocity represented by the site class B and A. So that, engineering bedrock level motions were represented with the site class B earthquake records and seismic rock motions were also represented with the site class A records for using in the defined Method-I and Method-II (Figure 4.8).

4.3 Site Soil and Structure Definition

The study area is located at latitude 38.4347, longitude 27.1635 coordinates (Figure 4.1). The site surface is generally straight. However, the elevations differ by about 1.5 m because of the already made site scraping. The conducted geophysical studies in this site are as follows:

a) Downhole test (80 m depth),
b) MASW (Multichannel Analysis of Surface Waves) tests (50 m depth),
c) SPAC (Spatial Auto-Correlation) test (290 m depth).

Shear wave velocities (V_s) of the soil layers were obtained with these test methods. P wave velocities (V_p) were determined from SPAC measurements. P and S wave variations with depth were obtained from SPAC measurement using a circular array at the site (3 measurements were completed through different radius circular layouts).

The average depth of groundwater level was observed as 1.9 m. 22 boreholes (including 240 m deep drill hole) were drilled in the scope of field studies. MASW measurements were performed on a total of 11 profiles.

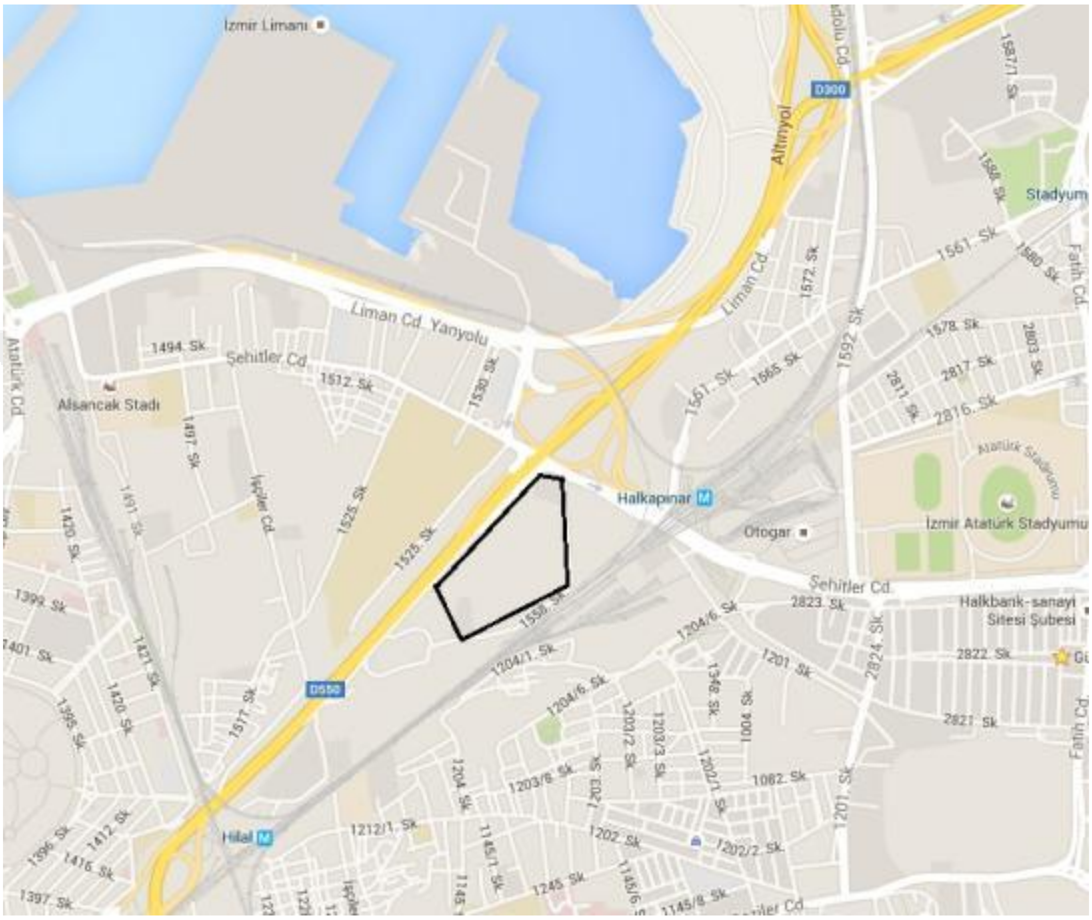

Figure 4.1 Satellite view of the study area.

Figure 4.1 shows the satellite view of the construction site. This area, which is only 2 m above the sea level, is situated 600 m away from Izmir Bay and 350 m west of Meles River. Hence, alluvial deposits of the Meles delta are observed in the study area. This alluvial strata mostly contain clayey and silty sands and bands of gravelly levels. The alluvial strata exist until the seismic rock level, which is located at 1100 m deep.

The structure consists of one basement and 14 stories (Figure 4.2). The basement story of the structure is embedded into the ground 4.5 meters averagely. The bearing system of the structure consists of high ductile columns, beams and shear walls. The structural loads are transferred to the ground through a piled raft foundation. The building height is 47.40 m from the foundation base level. The foundation dimensions of the structure are 14.4 m (X axis direction) and 15.25 m (Y-axis direction). The story heights until 4th story are 3.2 m and the rest are 3.0 m (Figure 4.2).

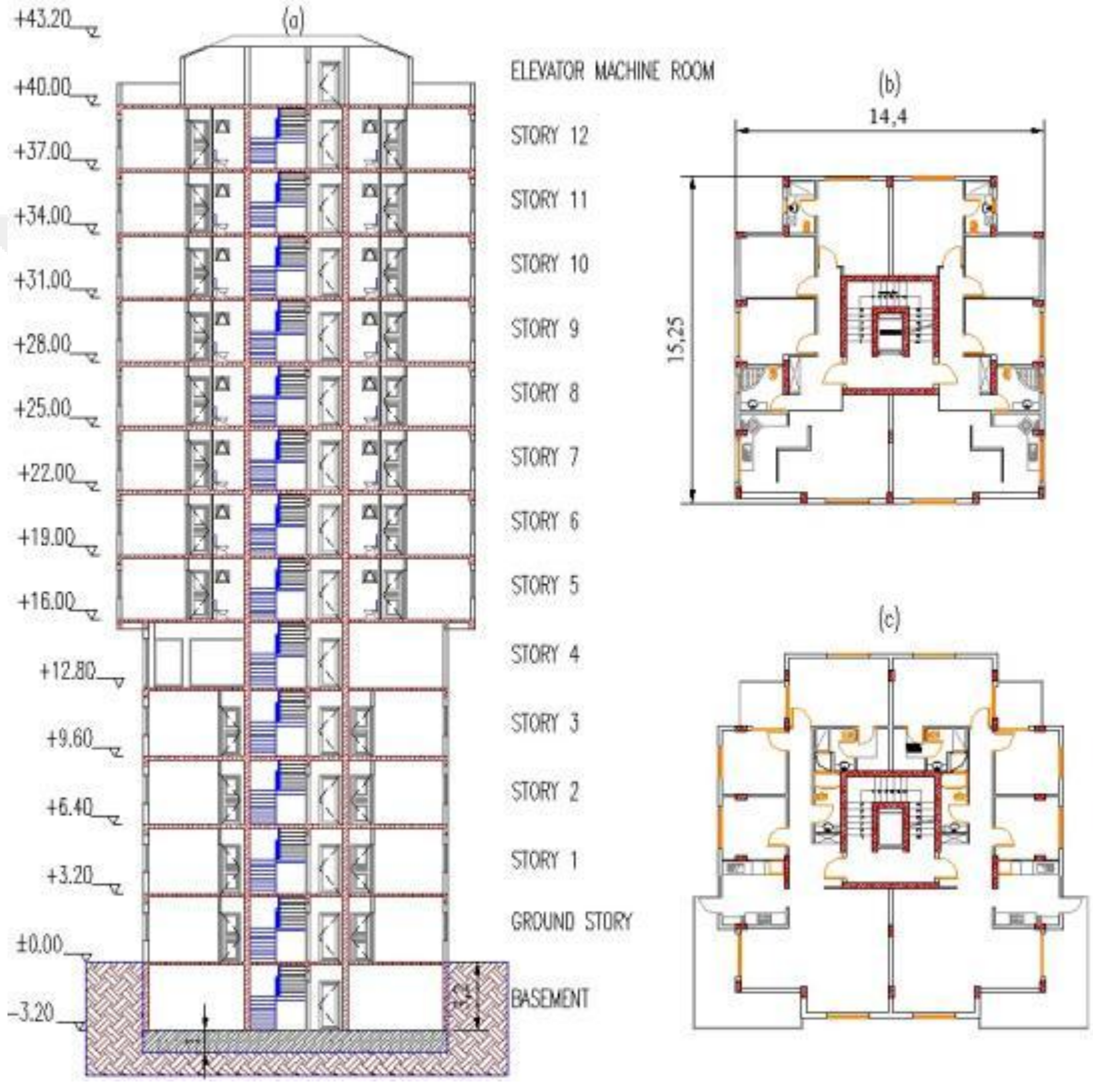

Figure 4.2 a) Structure section view, b) Architectural plan up to 4th story, c) Architectural plan up to 12th story

The upper stories have some cantilever extensions as shown in Figure 4.2 (c). The stair and elevator shaft are located in the central core shear walls. This core carries the seismic forces that act along x and y axes. Thus the perimeter columns were designed predominantly for vertical forces (such as: dead load, live load, etc.).

The piled foundation plan and its section view are shown in Figure 4.3. The pile spacing in the X axis direction is 3.35 m, whereas it is 3.56 m in the Y axis direction. The diameter of the piles is 0.6 m. The pile cap (raft foundation) thickness is 1 m as shown in Figure 4.3.

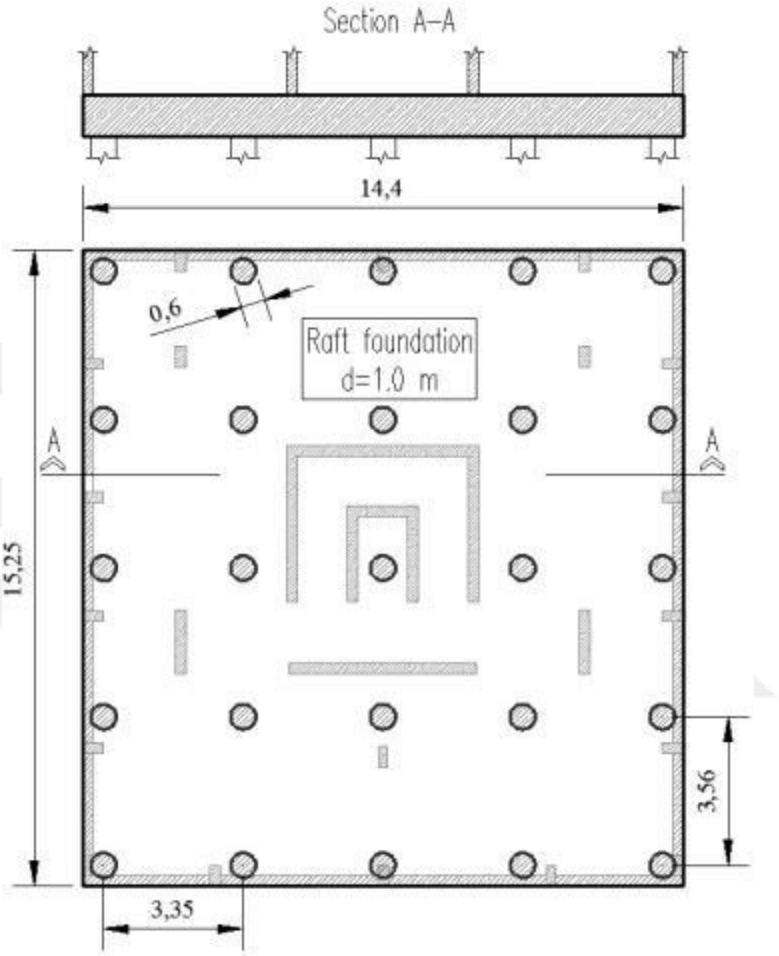

Figure 4.3 Piled raft foundation plan and section view.

4.4 Idealized Soil Profile

The soil consists of predominantly clay layers which contain sand, gravel and silt. Thin sand and gravel bands are available between the thick clay layers. Weaker clay layers are located within the first 50 m depth. Shear wave velocities of these weaker layers were measured between 150 m/s and 250 m/s (Figure 4.4). The fill is not evenly distributed over the site and its thickness also varies. CPT, SPT and MASW test results were used in order to create first 50 m of the idealized soil profile. 100 m deep drilling data were used for the creation of idealized profile between 50 m and

100 m. The rest of the soil profile was obtained through the data from 240 m deep drilling. The dynamic soil properties of deeper rock strata were obtained from microgravity studies (conducted studies for İzmir Bay in the past years) and deep geophysical explorations (explosives were used).

For creating the diagram of shear wave velocity with depth, MASW, downhole, SPAC seismic tests were used for 0-30 m, 30-80 m, >80 m depths respectively. The shear wave velocity profile obtained in this manner is shown in Figure 4.4.

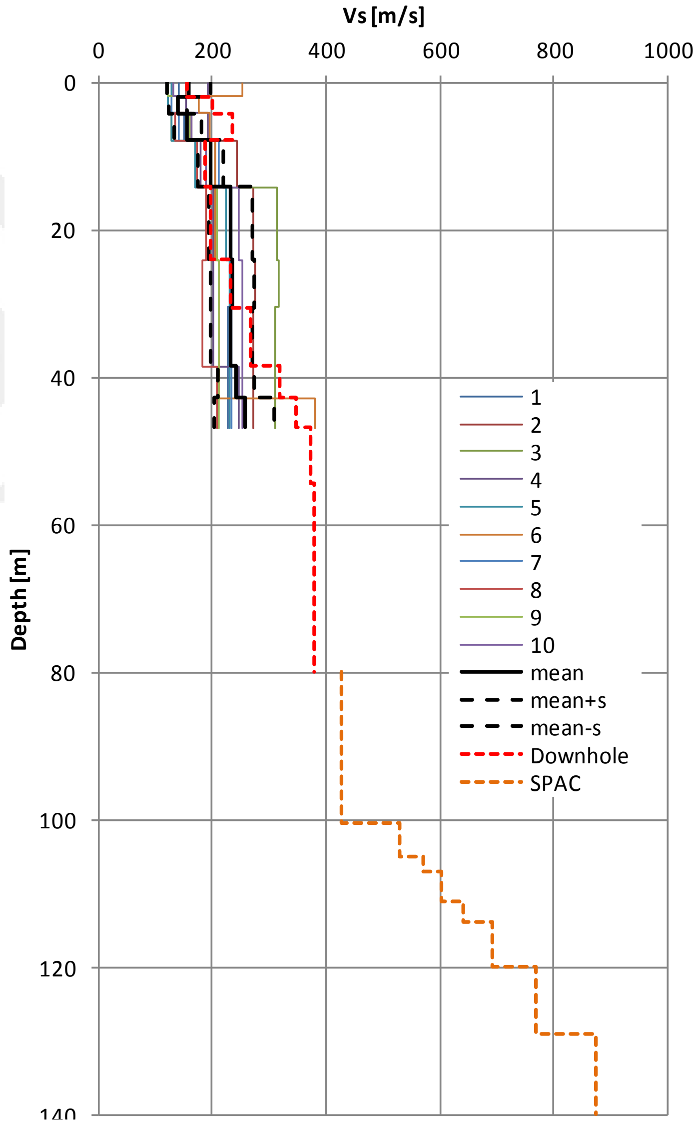

Figure 4.4 Shear wave velocity variation with depth (according to the MASW, Downhole and SPAC tests)

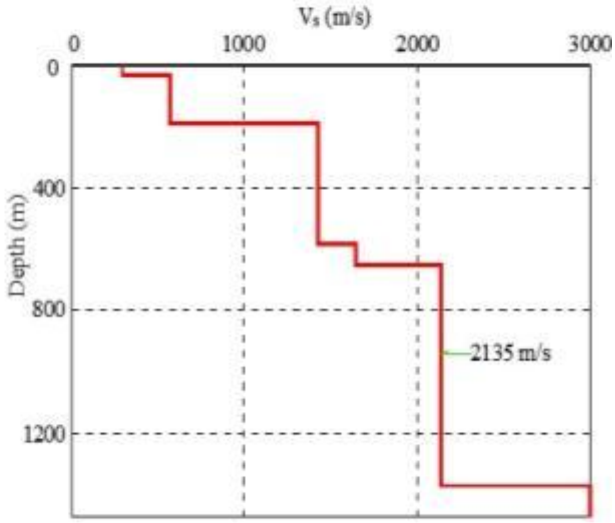

Figure 4.5 Averaged shear wave velocity profiles until 1400 m depth (Akgün et al., 2013)

V_s profile in Figure 4.5 was obtained from previously conducted site investigations. For the soil profile deeper than 140 m, this averaged shear wave velocity data were used in the site response analyses. Dynamic soil properties, which is for soils deeper than 140 m, were obtained from Figure 4.5 and soil unit weights were obtained from Figure 4.6.

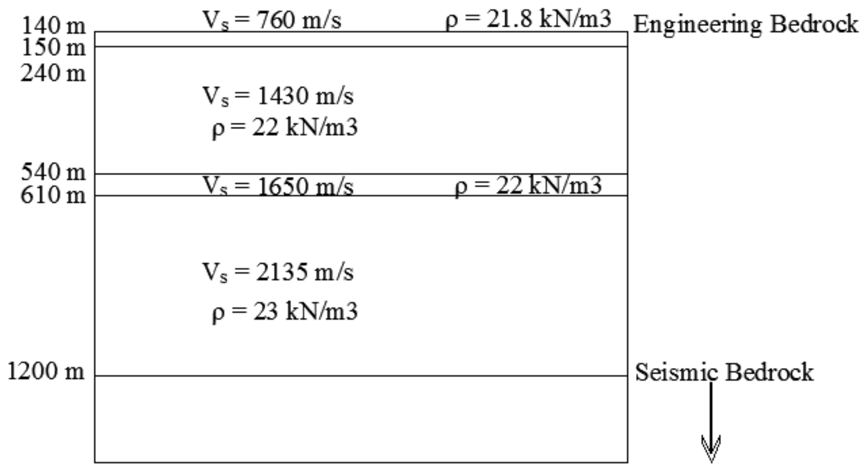

Figure 4.6 Soil dynamic properties after 140 m depth.

Depth [m]	Thickness							
0								
	1.9	γ_n=18 kN/m^3		**FILL**		υ=0.44	V_s=155 m/s	V_p=468
1.9		ρ=1.83 kN.s^2/m		G.W.T			σ'_v=	17.1
		γ_n=18.1 kN/m^3		**CL**		υ=0.44	V_s=155 m/s	V_p=468
	2.3	ρ=1.85 kN.s^2/m	ϕ'=21.4°	c_u=27 kPa	N_{60}=6 N_{1-60}=5		-No.200=82	
4.2		G_{max}=44 MPa	w_n=26.5 w_{LL}=42 w_{PL}=22 I_P=20 I_L=0.23				σ'_v=	43.515
		γ_n=18.2 kN/m^3		**GM-GC**		υ=0.44	V_s=155 m/s	V_p=475
	3.6	ρ=1.86 kN.s^2/m	ϕ'=34°		N_{60}=17 N_{1-60}=14		-No.200=8	
7.8		G_{max}=44.6 MPa					σ'_v=	67.59
		γ_n=19 kN/m^3		**CL**		υ=0.41	V_s=195 m/s	V_p=506
	6.4	ρ=1.94 kN.s^2/m	ϕ'=21.7°	c_u=48 kPa	N_{60}=8 N_{1-60}=5		-No.200=84	
14.2		G_{max}=73.8 MPa	w_n=21 w_{LL}=38 w_{PL}=19 I_P=19 I_L=0.11				σ'_v=	111.15
		γ_n=19.7 kN/m^3		**CL**		υ=0.4	V_s=230 m/s	V_p=565
	9.8	ρ=2.01 kN.s^2/m	ϕ'=22.1°	c_u=94 kPa	N_{60}=11 N_{1-60}=7		-No.200=68	
24		G_{max}=106.3 MPa	w_n=21 w_{LL}=37 w_{PL}=19 I_P=18 I_L=0.11				σ'_v=	187.48
		γ_n=19.4 kN/m^3		**GC**		υ=0.42	V_s=235 m/s	V_p=622
	6.5	ρ=1.98 kN.s^2/m	ϕ'=36°		N_{60}=34 N_{1-60}=20		-No.200=54	υ=
30.5		G_{max}=109.3 MPa	w_n=18.6 w_{LL}=38 w_{PL}=19 I_P=19 I_L=-0.02				σ'_v=	265.56
		γ_n=19.7 kN/m^3		**CH**		υ=0.41	V_s=268 m/s	V_p=698
	8	ρ=2.01 kN.s^2/m	ϕ'=17.4°	c_u=72 kPa	N_{60}=16 N_{1-60}=7		-No.200=90	
38.5		G_{max}=144.4 MPa	w_n=27.5 w_{LL}=57 w_{PL}=25 I_P=32 I_L=0.08				σ'_v=	334.91
		γ_n=19.9 kN/m^3	ϕ'=34°	**SM-SP**	υ=0.4	-No.200=38	V_s=318 m/s	V_p=780
42.8		ρ=2.03 kN.s^2/m	w_n=15.2	G_{max}=205 MPa	N_{60}=29 N_{1-60}=12		σ'_v=	395
		γ_n=20 kN/m^3		**CH**		υ=0.4	V_s=346 m/s	V_p=836
		ρ=2.04 kN.s^2/m	ϕ'=18.2°	c_u=95 kPa	N_{60}=20 N_{1-60}=10		-No.200=94	
46.8		G_{max}=244 MPa	w_n=27.5 w_{LL}=51 w_{PL}=22 I_P=29 I_L=0.19				σ'_v=	436.28
		γ_n=20.3 kN/m^3		**CL**		υ=0.4	V_s=372 m/s	V_p=916
		ρ=2.07 kN.s^2/m	ϕ'=20.1°	c_u=106 kPa	N_{60}=27 N_{1-60}=16		-No.200=77	
54.4		G_{max}=286 MPa	w_n=23.8 w_{LL}=42 w_{PL}=19 I_P=23 I_L=0.21				σ'_v=	495.42
		γ_n=20.5 kN/m^3		**CL**		υ=0.42	V_s=380 m/s	V_p=1009
		ρ=2.09 kN.s^2/m	ϕ'=20.1°	c_u=113 kPa	N_{60}=43 N_{1-60}=12		-No.200=94	
60.4		G_{max}=301 MPa	w_n=20.5 w_{LL}=41 w_{PL}=18 I_P=23 I_L=0.39				σ'_v=	566.06
		γ_n=20.6 kN/m^3		**CL**		υ=0.44	V_s=380 m/s	V_p=1178
		ρ=2.10 kN.s^2/m	ϕ'=22.1°	c_u=140 kPa			-No.200=91	
80.4		G_{max}=303 MPa	w_n=24 w_{LL}=39 w_{PL}=21 I_P=18 I_L=0.17				σ'_v=	703.56
		γ_n=20.8 kN/m^3		**CL**		υ=0.44	V_s=426 m/s	
		ρ=2.12 kN.s^2/m	ϕ'=22.1°	c_u=183 kPa			-No.200=92	
100.6		G_{max}=347 MPa	w_n=24 w_{LL}=39 w_{PL}=21 I_P=18 I_L=0.17				σ'_v=	918.64
		γ_n=21.1 kN/m^3		**CL**			V_s=528 m/s	
		ρ=2.15 kN.s^2/m						
105		G_{max}=499 MPa					σ'_v=	1052.14
		γ_n=20.6 kN/m^3		**GC**			V_s=603 m/s	
107		ρ=2.01 kN.s^2/m	G_{max}=494 MPa				σ'_v=	1087.16
		γ_n=21.1 kN/m^3		**CL**			V_s=639 m/s	
111		ρ=2.15 kN.s^2/m	G_{max}=626 MPa				σ'_v=	1119.96
		γ_n=20.6 kN/m^3		**GC**			V_s=691 m/s	
114		ρ=2.01 kN.s^2/m	G_{max}=723 MPa				σ'_v=	1158.06
		γ_n=21.8 kN/m^3		**CL**			V_s=778 m/s	
140		ρ=2.22 kN.s^2/m	G_{max}=1282 MPa					1327.36

Figure 4.7 Idealized soil profile.

4.5 Site Response Analysis

Site response analysis was conducted for two different depths of soil profiles in this study. The first is the soil profile between the ground surface and the engineering bedrock level, which has been specified in the İzmir Technical Advistories of the Tall Buildings. In this local code, it is stated that the shear wave velocity of the engineering bedrock level shall be equal to or greater than 760 m/s. The second soil profile is between the foundation base level of the structure and seismic rock level, which is located at approximately 1200 m below the ground level.

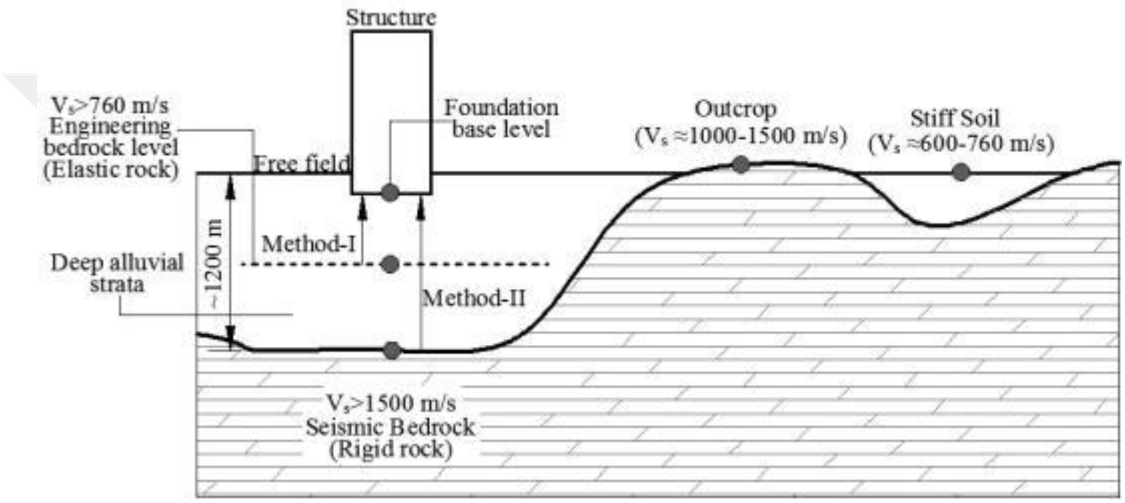

Figure 4.8 Explanation of the analysis methods. Method-I represents the engineering bedrock assumption and Method-II considers the total alluvial profile including sedimentary rock units.

4.5.1 Material Model

In major projects, site-specific modulus reduction curves can be determined by laboratory experiments. However, these tests are expensive and it is difficult to take appropriate samples from each soil layer. As mentioned in the second section of this thesis, empirical formulas can be used for determination of the modulus reduction curves. Darendeli (2001) empirical formulations were used in this study.

According to the soil profile given in Figure 4.7 and the parametric formulation (Equation 2.1~2.6) proposed by Darendeli (2001), target modulus reduction curves were formed for each layer.

For sandy soils, K_0 (coefficient of earth pressure at-rest, in terms of effective stress) is given by;

$$K_0=1-\sin\phi' \tag{4.1}$$

Where ϕ' is the effective internal friction angle. Equation 4.1 is valid for normally consolidated soils. Another important parameter N is the cycle number and generally is assumed as 10. The excitation frequency (f) is defined as 1 Hz in the formulations.

The curve defined by Equation 2.7 varies depending on "a" and "β" parameter. The curve, which is obtained from the initial values of "β" and "a" parameters, and the target curve are compared. Standard error is determined between these two curves according to Equation 2.10, 2.11, and Table 2.2. If the error is not acceptable, this process is repeated with new "a" and "β" values. This cycle is continued until the minimum error is obtained. This process is called “curve fitting” and there are three types such as MR, MRD and D. In this thesis, the MRD fitting method was used for obtaining shear modulus reduction curves.

The soil profile between 140 m and 240 m consists of very stiff clay, silt and sand layers. After 240 m, it comprises the claystone, sandstone and flysch units. The above formulas cannot be used for these rock-featured strata. Instead, the curve values which were given for rock in the Table 4.1 were utilized for deeper soil layers.

Table 4.1 G/G_{max} and damping curves; the table at the left side is given for rock units located up to first 120 m thickness, the table at the right side is given for after 120 m thickness (ENERCON SERVICES INC., 2010).

Strain	G/Gmax	Damping
0.0001	1	1.8
0.0002	1	1.8
0.0005	1	1.8
0.001	0.99	1.9
0.002	0.985	2
0.005	0.98	2.2
0.01	0.96	2.4
0.02	0.91	3

Strain	G/Gmax	Damping
0.0001	1	0.8
0.001	1	0.8
0.003	0.99	0.9
0.01	0.98	1.1
0.03	0.94	1.6

Corrected G/G_{max}, damping and stress-strain curve parameters used in the DeepSoil program are given in Table B.1 for each layer. The layer 69 in this table is designated as the engineering bedrock. Next 22 layers following the 69th layer represent the ongoing soil profile up to the seismic bedrock. After 240 m depth, soil layers which consist of claystone, flysch and some weathered rock units were named as D1 to D15 in the model. All of the 91 layers were considered in the site response analysis for the Method-II case as shown in Figure 4.8.

"d" values are shown in Table B.1 are an exponential factor which is used for calculation of the pressure dependent small strain damping ratio (Equation 2.8). Taking this factor zero means; the calculated small strain damping ratio is the pressure independent. In our calculations, this value was considered as zero. Similarly, the coefficient "b" was chosen as zero and the reference strain was taken as a constant value (Equation 2.9). This value was used for creating initial curve. As shown in Table B.1, the corrected values are calculated after the curve fitting procedure.

The initial values 0.3 and 0.7 were given "β" and "s" coefficients respectively. After the curve fitting procedures, "β" and "s" values which are given a minimum standard error between the calculated and target curves were obtained (Table B.1).

4.5.2 Selection and Scaling of Earthquake Records

The target rock spectra with respect to D1, D2, and D3 intensity levels for soil class B and A, were established according to DLH code (2008). Selected earthquake records were determined to show the best fit with the target spectrum. In addition, when examining faults near the construction area, it is seen that the extension of İzmir Fault and Tuzla Fault are at close proximity to the work area. Approximately the closest distance to the fault of the site is between 5 and 7 km. In addition, it is about 50 km from the Karaburun Fault and is about 40 km from the Foça Fault. When the mechanism of the faults is examined, we see that the İzmir Fault is a normal-fault and the other faults are strike-slip faults. In the light of this information, the fault properties of the selected records should be represented carefully.

The selected earthquake records from PEER Strong Motion Database according to the target DLH rock spectra were carefully examined and the appropriate 4 earthquake records were selected for each D1, D2, D3 earthquake intensity levels. Active Faults in İZMİR are shown in Figure 4.9.

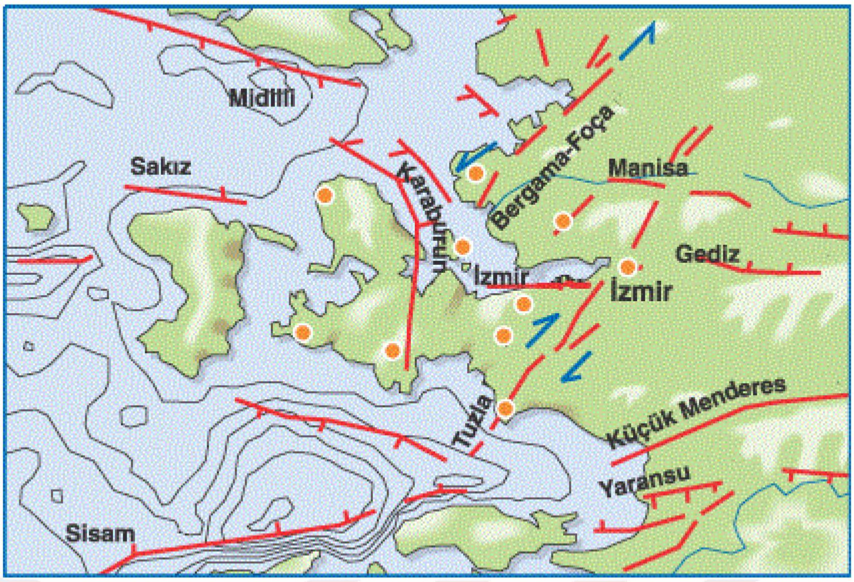

Figure 4.9 Active fault map of İzmir

In this study, the same directional components of the recordings of the different stations, which are soil class A and B, were used. The following filtering process was applied in the selection of these records:

a) The records which are most similar with DLH code target rock spectra were selected.
b) The value of the MSE (Minimum Squared Error) was noted to be as close as to zero.
c) The records obtained as the product of normal and strike-slip fault activities were chosen.
d) The records which have 1 to 17 km hypocentral distance to faults were preferred.
e) The records of the same earthquake, which were recorded in both A and B type soils, were used.

The frequency contents of the acceleration time histories were not altered. Scaling was only applied to the ordinates of the records (i.e. acceleration).

Table 4.2 D1 level selected earthquakes for Method-II.

Comp.	Record Seq. #	MSE	Scale Factor	Event	Year	Mag	Mechanism	Rjb(km)	Rrup(km)	Vs30(m/s)
H1	146	0.3	2.7134	Coyote Lake	1979	5.74	strike slip	10.21	10.67	1428.14
H1	455	0.187	3.2949	Morgan Hill	1984	6.19	strike slip	14.9	14.91	1428.14
H2	1108	0.217	0.5163	Kobe, Japan	1995	6.9	strike slip	0.9	0.92	1043
H2	4312	0.096	2.8246	Umbria-03, Italy	1984	5.6	Normal	14.67	15.72	922

Table 4.3 D2 level selected earthquakes for Method-II.

Comp.	Record Seq. #	MSE	Scale Factor	Event	Year	Mag	Mechanism	Rjb(km)	Rrup(km)	Vs30(m/s)
H1	146	0.404	6.4471	Coyote Lake	1979	5.74	strike slip	10.21	10.67	1428.14
H1	455	0.316	7.847	Morgan Hill	1984	6.19	strike slip	14.9	14.91	1428.14
H2	1108	0.131	1.5124	Kobe, Japan	1995	6.9	strike slip	0.9	0.92	1043
H2	4312	0.113	7.7052	Umbria-03, Italy	1984	5.6	Normal	14.67	15.72	922

Table 4.4 D3 level selected earthquakes for Method-II.

Comp.	Record Seq. #	MSE	Scale Factor	Event	Year	Mag	Mechanism	Rjb(km)	Rrup(km)	Vs30(m/s)
H1	146	0.529	11.634	Coyote Lake	1979	5.74	strike slip	10.21	10.67	1428.14
H1	455	0.445	14.1603	Morgan Hill	1984	6.19	strike slip	14.9	14.91	1428.14
H2	1108	0.078	2.7292	Kobe, Japan	1995	6.9	strike slip	0.9	0.92	1043
H2	4312	0.164	13.9045	Umbria-03, Italy	1984	5.6	Normal	14.67	15.72	922

Table 4.5 D1 level selected earthquakes for Method-I.

Comp.	Record Seq. #	MSE	Scale Factor	Event	Year	Mag	Mechanism	Rjb(km)	Rrup(km)	Vs30(m/s)
H2	145	0.213	1.0051	Coyote Lake	1979	5.74	strike slip	5.3	6.13	561.43
H1	454	0.207	3.8011	Morgan Hill	1984	6.19	strike slip	14.83	14.84	729.65
H2	1111	0.169	0.4614	Kobe, Japan	1995	6.9	strike slip	7.08	7.08	609
H2	4313	0.489	2.5819	Umbria-03, Italy	1984	5.6	Normal	14.47	16.76	428

Table 4.6 D2 level selected earthquakes for Method-I.

Comp.	Record Seq. #	MSE	Scale Factor	Event	Year	Mag	Mechanism	Rjb(km)	Rrup(km)	Vs30(m/s)
H2	145	0.134	2.7444	Coyote Lake	1979	5.74	strike slip	5.3	6.13	561.43
H1	454	0.328	8.9128	Morgan Hill	1984	6.19	strike slip	14.83	14.84	729.65
H2	1111	0.103	1.3236	Kobe, Japan	1995	6.9	strike slip	7.08	7.08	609
H2	4313	0.6	5.4583	Umbria-03, Italy	1984	5.6	Normal	14.47	16.76	428

Table 4.7 D3 level selected earthquakes for Method-I.

Comp.	Record Seq. #	MSE	Scale Factor	Event	Year	Mag	Mechanism	Rjb(km)	Rrup(km)	Vs30(m/s)
H2	145	0.137	4.9525	Coyote Lake	1979	5.74	strike slip	5.3	6.13	561.43
H1	454	0.45	16.0837	Morgan Hill	1984	6.19	strike slip	14.83	14.84	729.65
H2	1111	0.073	2.3885	Kobe, Japan	1995	6.9	strike slip	7.08	7.08	609
H2	4313	0.584	8.6731	Umbria-03, Italy	1984	5.6	Normal	14.47	16.76	428

Tables 4.2 to 4.7 show D1, D2 and D3 level earthquakes for representing the engineering bedrock and seismic bedrock. In the following Table 4.8, S.B. refers to the Seismic Bedrock and E.B. refers to the Engineering Bedrock. Figure 4.10 shows the parameters of Table 4.9.

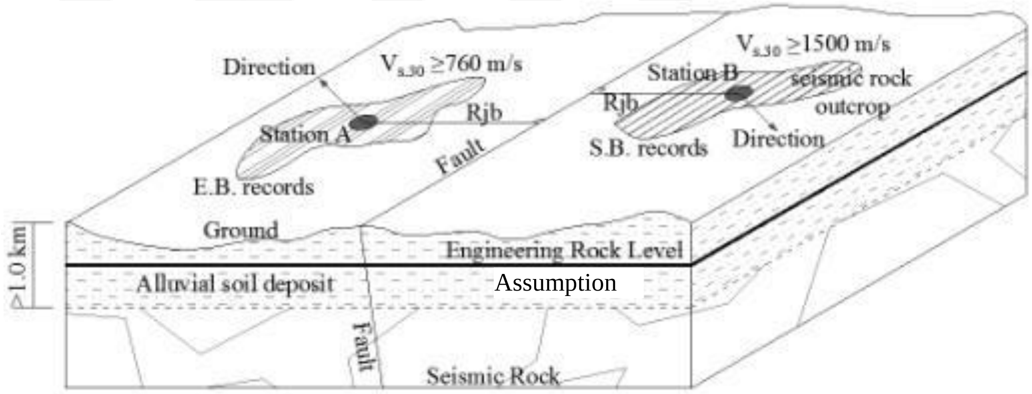

Figure 4.10 Explanation of the methods which were used for representing seismic bedrock and engineering bedrock assumptions.

In reality, earthquake record stations generally are placed on the ground surface nearby the faults. These recording stations cannot be located at seismic bedrock-soil interface or engineering bedrock level. But, seismic rock generally outcrop to the ground surface. If the station is located at the out cropping rock (V_{s30} ≥1500m/s in Figure 4.10), recorded motions have approximately same properties of seismic rock motion. Similarly, if the station is located at soil class B site (V_{s30}≥760m/s in Figure 4.10), motions can be accepted as the recorded at the engineering bedrock level. If the recording stations acquire signals from the same earthquake in the same direction, these same directional recorded motions can be compared with Method-I and Method-II in the site response analyses as explained in Figure 4.8.

Table 4.8 Directional differences and station to fault rupture distance of the selected pairs of earthquakes.

Earthquake Intensity	Comp. For S. B.	Comp. For E. B.	S.B. Record Seq. #	E.B. Record Seq. #	Rrup(km) For S.B	Rrup(km) For E.B.	Difference Rrup(km)	Direction Difference (°)
D1, D2 or D3	H1	H2	146	145	10.67	6.13	4.54	20
D1, D2 or D3	H1	H1	455	454	14.91	14.84	0.07	163
D1, D2 or D3	H2	H2	1108	1111	0.92	7.8	6.88	0
D1, D2 or D3	H2	H2	4312	4313	15.72	16.76	1.04	0

Table 4.8 shows the fairly selected records in terms of directional differences and site to fault distances. These types of records cannot be obtained easily because of the limited number of earthquake motions in the database. Therefore, some applied scale factors of the selected motions are larger (i.e. 14, 16).

In Figures 4.11 to 4.13, the spectra of the selected earthquakes and DLH target spectrum are shown together. Earthquake record sequence numbers were shown at the legends of these charts.

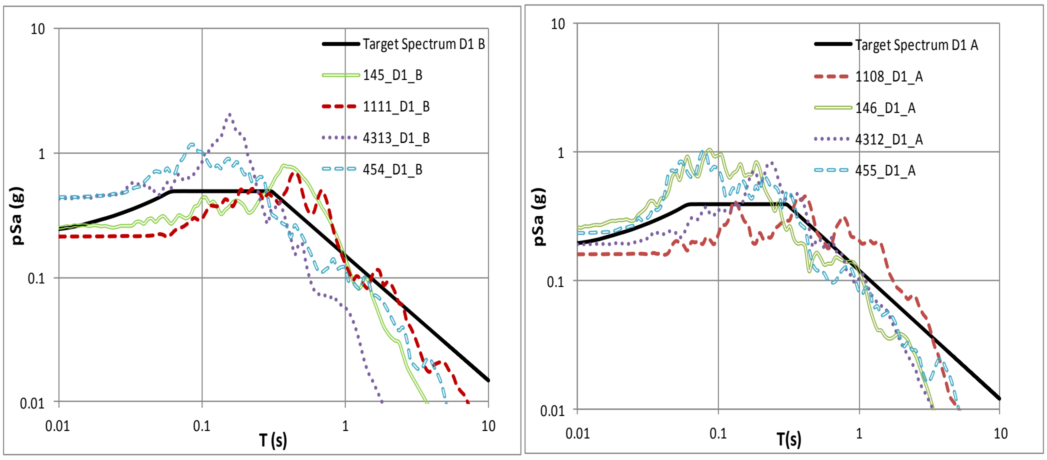

Figure 4.11 Selected earthquakes from the Peer Strong Motion Database for soil class A and B according to D1 earthquake intensity level.

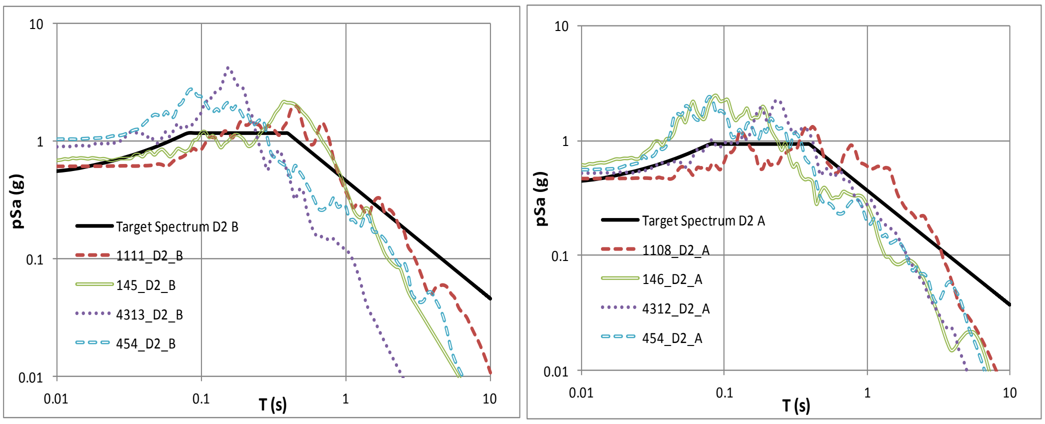

Figure 4.12 Selected earthquakes from the Peer Strong Motion Database for soil class A and B according to D2 earthquake intensity level.

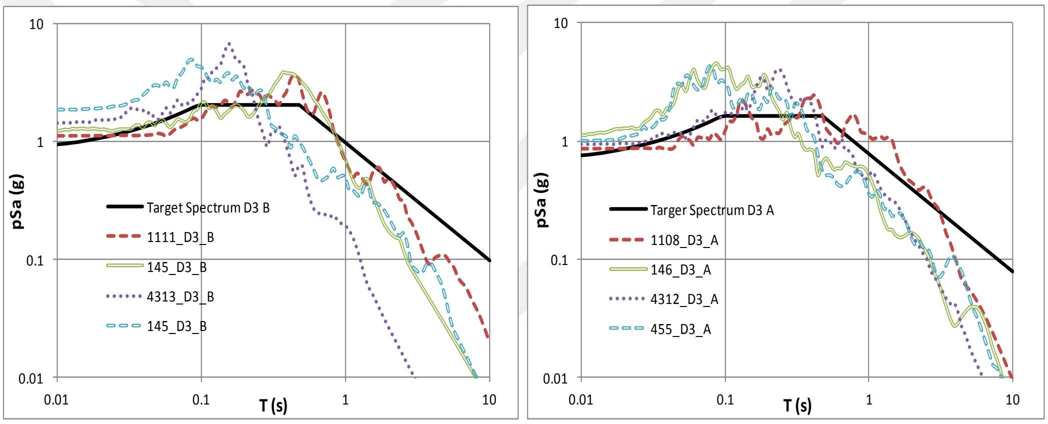

Figure 4.13 Selected earthquakes from the Peer Strong Motion Database for soil class A and B according to D3 earthquake intensity level.

4.5.3 Deconvolution Analysis

Deconvolution analysis is basically performed by applying the inverse of site response analysis. It is a linear type analysis and nonlinear type analysis is not available in the literature.

If the soil profile of the record station is available until the bedrock level, free field motion records can be used for obtaining the seismic bedrock motions with deconvolution analyses. Thus, the number of convenient earthquakes can be increased for using in the site response analyses. In this study, deconvolution analysis was not applied because of the lack of soil profile of the recording stations.

4.6 Calculating Dynamic Stiffness of the Foundation

DYNAN Software is based on the improved Novak's method where a non-reflective boundary is formed between the near field and the far field to account for the mass of soil in the boundary. It has a semi-analytical and numerical calculation algorithm. The difference from a direct equivalent linear calculation method is using a different shear modulus in the near field and far field of the region. So the nonlinear soil behavior can be modeled closer to the reality. On the other hand, the soil should be modelled by 3D solid elements for the establishment of fully nonlinear behavior. Solely, DYNAN Software is not capable of modelling the 3D finite elements. For the sake of a practical engineering approach, the equivalent linear method was used in this study.

The pile group and raft foundation dynamic stiffness calculations are explained step by step as follows:

a) The foundation and the surrounding soil is modeled in the DYNAN software and results are obtained.

b) Calculating the foundation dynamic stiffness according to the developed software code was completed.

  i) The Dynamic stiffness of the raft foundation is calculated according to proposed NEHRP method.

  ii) The Dynamic stiffness of the pile group is obtained according to analytical solutions of Makris and Gazetas.

c) The developed software results are compared with those of the DYNAN Software.

The resulting total foundation stiffness is distributed to the raft foundation which is divided into zones as shown in Figure 3.21. The R_e value (ranging from 0.3 to 0.5) is averagely taken as 0.4 in this distribution. This stiffness and damping values are distributed on each region using the link element available in the SAP2000 Software.

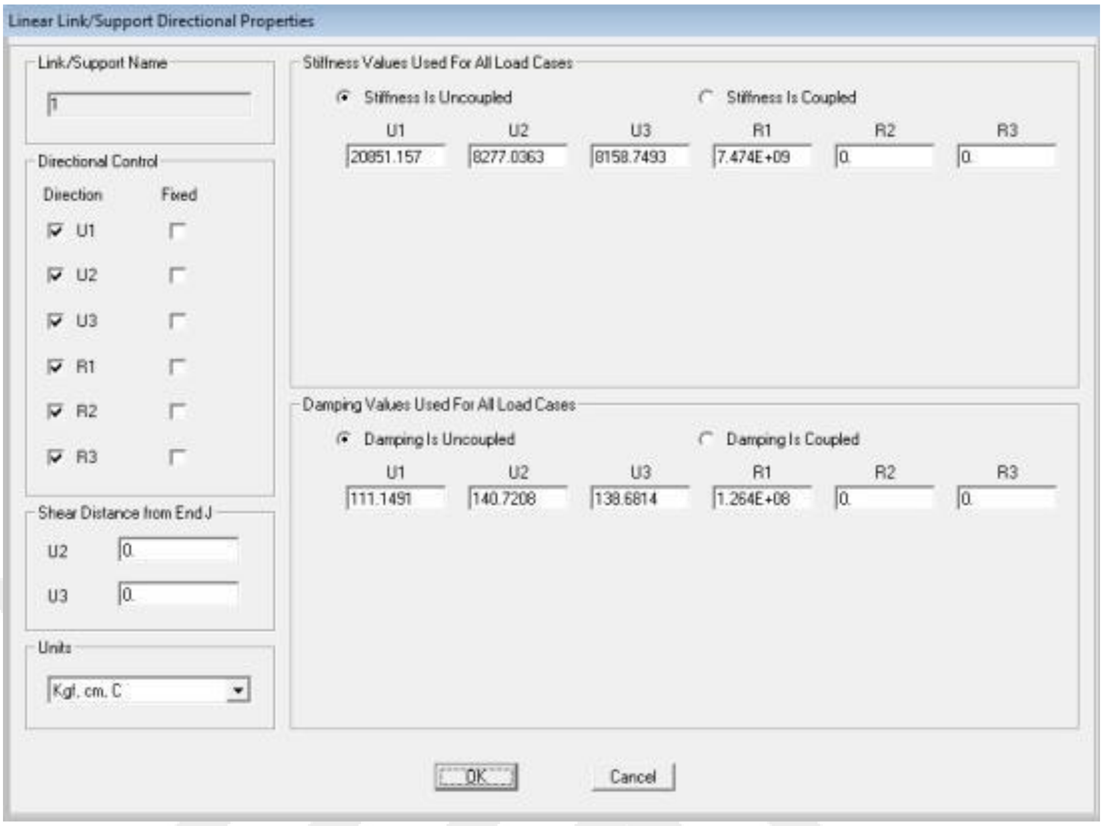

Figure 4.14 Linear link element definition in SAP2000

Figure 4.14 shows the settings of each degree of freedom, stiffness and damping properties. For distributed spring option, stiffness and damping values are chosen as uncoupled type. All degrees of freedoms are checked and only U1, U2, U3 translational stiffness and R1 vertical torsional stiffness are different from zero. R2 and R3 rotational stiffness and damping components are equal to zero because of the distribution of the stiffness under the foundation. These components are converted to vertical compression-tension actions due to the foundation geometry.

If the foundation is represented as one spring and each point on the foundation are connected to a central point on the raft with rigid bodies, coupled stiffness and damping option must be selected. Also, all translational and rotational stiffness must be entered. In this study, the distributed spring method was used.

The computation procedure can be summarized as follows:

a) Calculate dynamic stiffness of the foundation
b) Determine foundation intensity areas
c) Calculate damping and stiffness intensities with respect to Equations 3.13, 3.12
d) Calculate rocking factors using Equations 3.14~3.17
e) Calculate each stiffness and damping values of foundation intensity areas. For the corner region, take the average of the x axis rocking factor and y axis rocking factor and use the resulting value.
f) Create the foundation finite element model in the SAP2000 and generate the mesh taking the intensity areas into account.
g) Define link/support element. All degrees of freedom should be released.
h) Input the stiffness and damping values of U1, U2, U3 translational directions and input the R1 torsional stiffness and damping values.
i) Repeat the process for each intensity areas.

4.7 Structural Model

The surrounding soil around the basement story is assumed to be perfectly bonded to the shear walls. In a similar manner, soil around the pile is also perfectly bonded to the pile. In practice, the bonding between the soil and the pile is rarely perfect and slippage or separation often occurs in the contact interface. Furthermore, the soil region adjacent the pile can undergo a large degree of straining, which would cause the soil-pile system to behave in a nonlinear manner. For considering nonlinear behavior, shear modulus was reduced by a factor defined in Table 3.5.

The structure shall be examined for two cases as follows:

1- The piled raft foundation of the structure is embedded in the soil and acceleration time records that shall be used in the time history analyses, were obtained according to the Method-I (Site Response Analyses).

2- The piled raft foundation of the structure is embedded in the soil and acceleration-time records that would be used in the time history analyses, were obtained with respect to the Method-II (Site Response Analyses).

4.8 Time History Analysis

The superstructure will be analyzed in the time domain using the acceleration-time history records. These acceleration-time data used in this analyses are achieved at the foundation level according to the Method-I and Method-II site response analyses.

Some important structural data used in the interpretation of the results are listed as follows:

1. Story drift ratios
2. Peak story displacements
3. Peak story accelerations
4. Structural base shear forces

These four items are calculated for D1, D2 and D3 level earthquakes and results are compared for Method-I and Method-II.

CHAPTER FIVE
RESULTS AND DISCUSSIONS

5.1 Introduction

In this section, site response analyses were performed for Method-I and Method-II, and results were compared. As a result of those analyses, the earthquake motions at the foundation base level were obtained and they were used in the time history analyses of the superstructure. The acceleration-time records obtained either way were used in the analysis of the superstructure in time domain.

The relative storey displacements, which were obtained from time domain analyses according to the Method-I and Method-II were compared and were examined in terms of their effects on structural behavior. Contribution of the side soil around basement walls was also discussed.

5.2 Comparing Method-I and Method-II in Terms of Spectral Graphs

In the Figures 5.1~5.3, dashed lines and solid lines represent spectra of Method-I and spectra of Method-II, respectively. Also, same colored lines represent the same earthquake components which were recorded in the A and B type soil sites.

Consideration of the whole soil profile above the seismic rock (Method-II) showed a significant offset to the long period side unlike Method-I. This case affects the behavior of the superstructure since governing periods of the tall buildings generally fall into the long period side of the spectrum. Therefore, the engineering bedrock assumption, which is used in the site response analyses, in the deep alluvial soil deposits must be questioned for high-rise buildings.

On the other hand, the offsets in the computed spectra took place after $T = 0.8$ seconds (Figure 5.1~5.3). Hence, the engineering bedrock assumption can be used for structures having $T < 0.8$ s modal periods in this study area. It would be incorrect to generalize this case since the soil properties significantly affect site response analyses results.

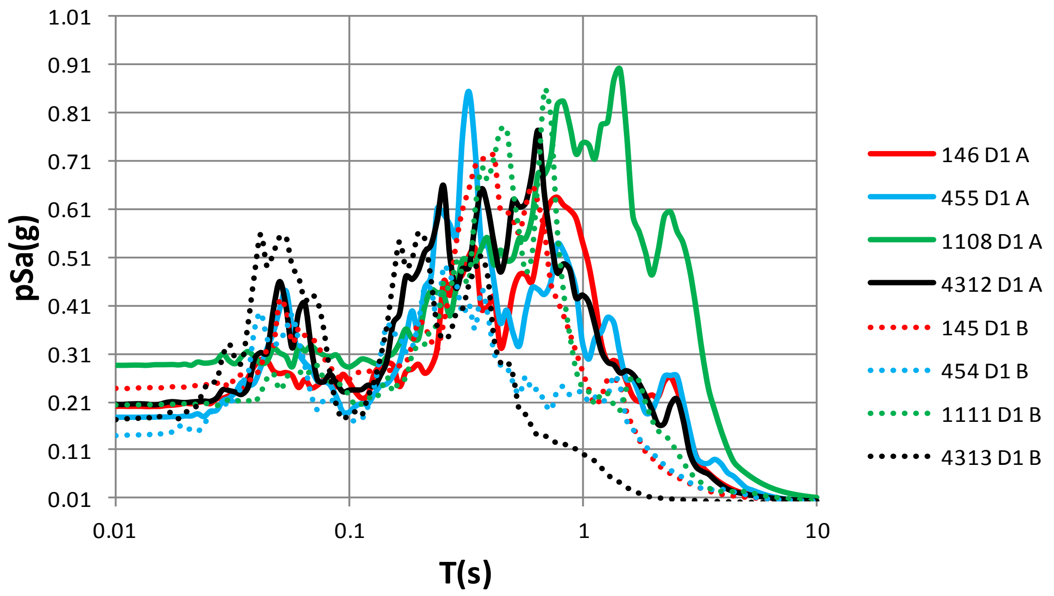

Figure 5.1 Method-I and Method-II resulting response spectra for D1 earthquake intensity level.

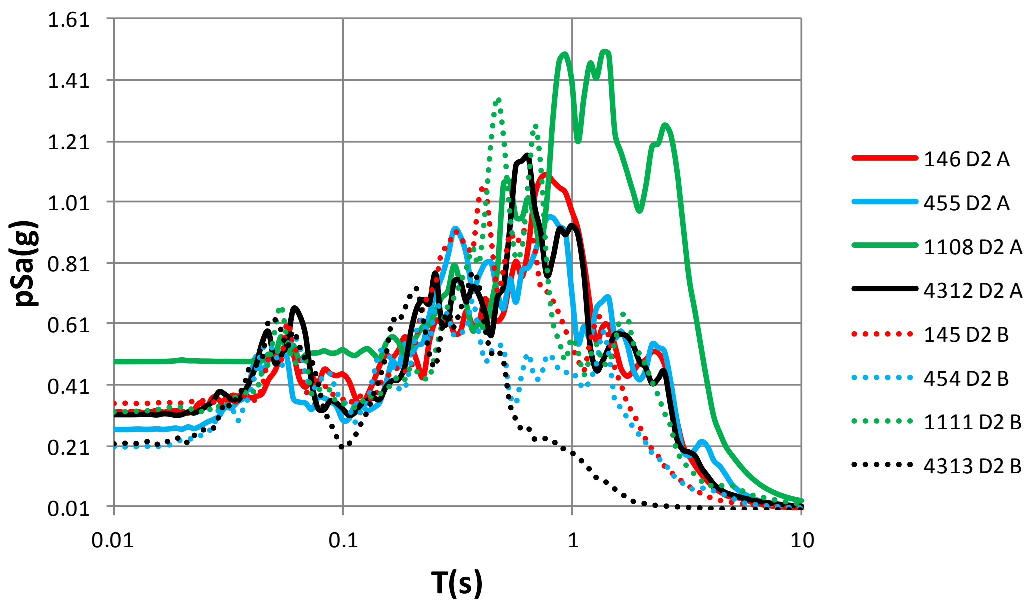

Figure 5.2 Method-I and Method-II resulting response spectra for D2 earthquake intensity level.

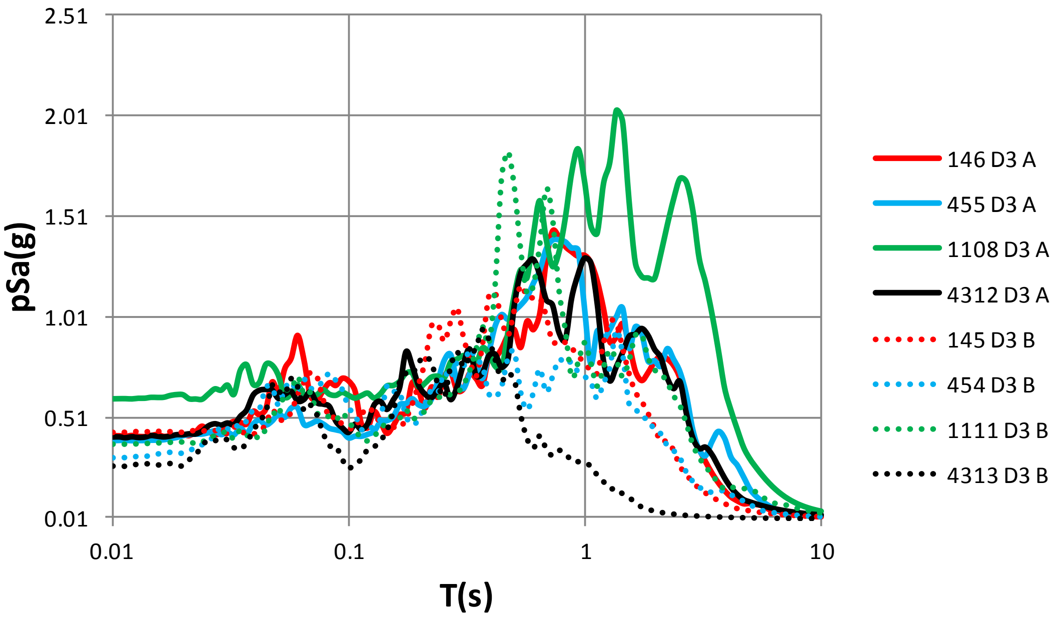

Figure 5.3 Method-I and Method-II resulting response spectra for D3 earthquake intensity level.

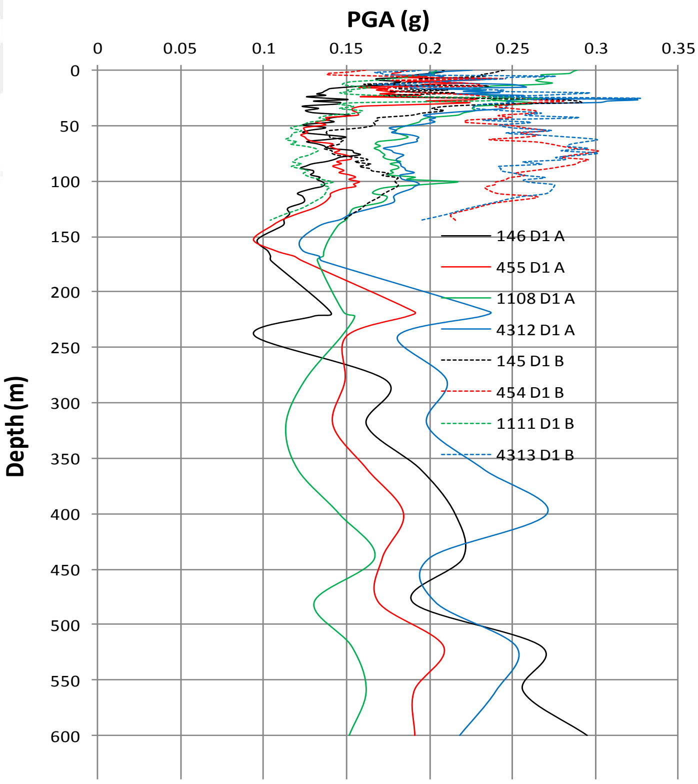

Figure 5.4 PGA values for Method-I and Method-II (D1)

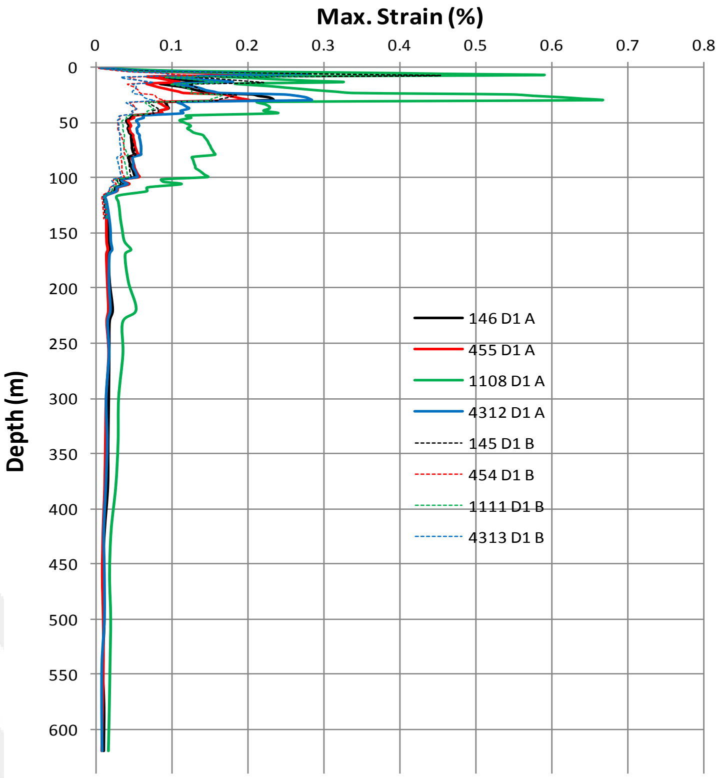

Figure 5.5 Max. strain values for Method-I and Method-II (D1)

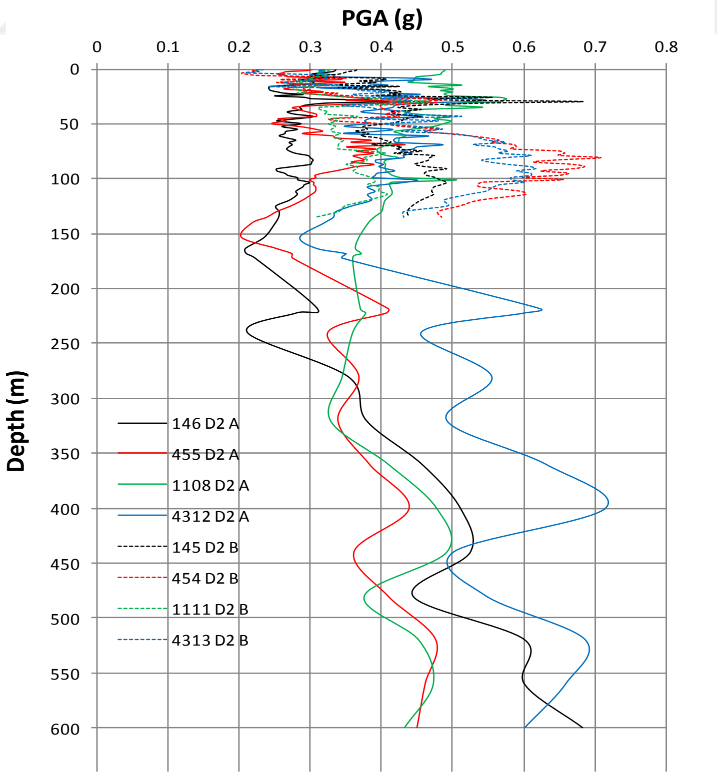

Figure 5.6 PGA values for Method-I and Method-II (D2)

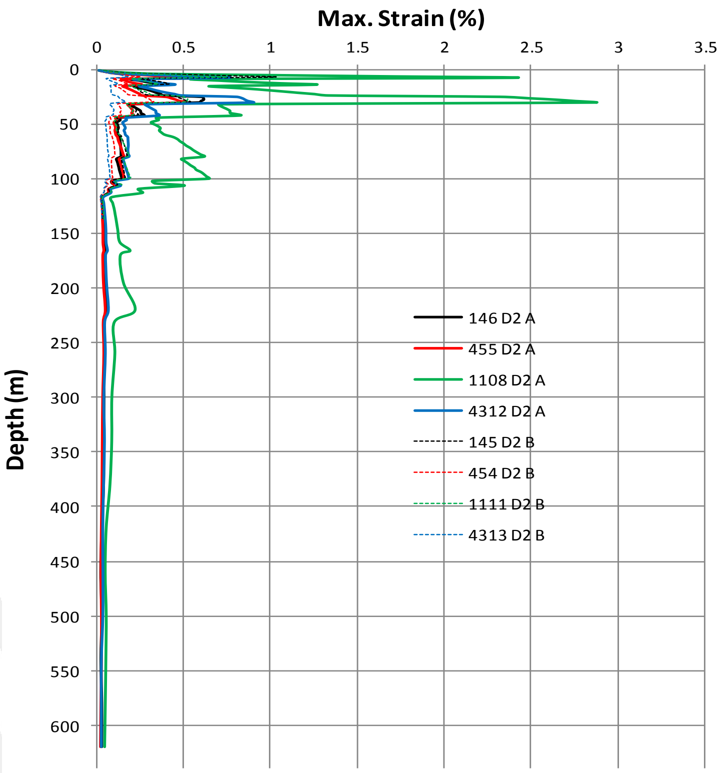

Figure 5.7 Max. strain values for Method-I and Method-II (D2)

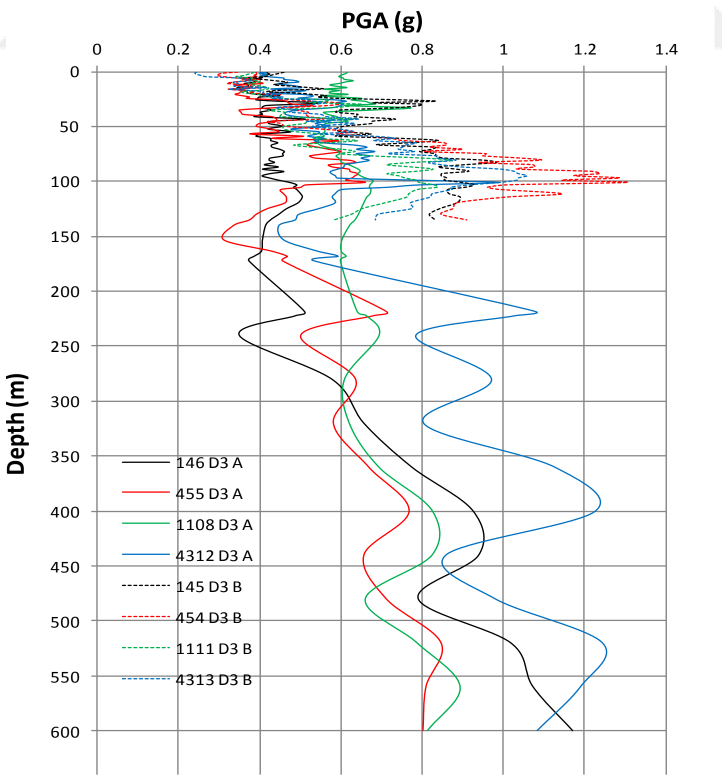

Figure 5.8 PGA values for Method-I and Method-II (D3)

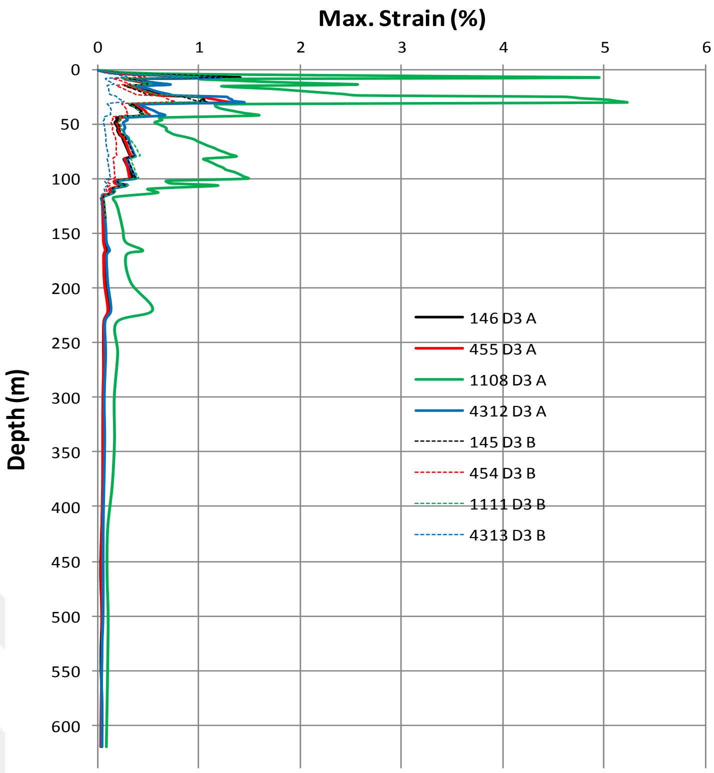

Figure 5.9 Max. strain values for Method-I and Method-II (D3)

Figures 5.4~5.9 show peak ground accelerations and maximum strain variations with depth for both Method-I and Method-II.

PGA values of the soil profile are greater when the engineering bedrock assumption is implemented. On the contrary, the Method-I gave higher soil strains than the Method-II. The soil profile between the engineering bedrock and seismic rock reduced PGA values during the Method–II site response analyses. Similarly, the strain values of the Method-II are higher than the Method-I since the deep soil profile below the engineering bedrock level (~1km thickness) caused large deformations on the soil column. Thus, this deeper soil profile gave large strain values as they reached the free soil surface.

First 50 meters of the soil column gave larger strain values due to the presence of the weak clay layers. The maximum strain values can be used in the determination of the dynamic stiffness of the foundation with equivalent linear analysis. The maximum strain and PGA values for D1, D2, D3 earthquake intensity levels are shown in Table 5.1:

Table 5.1 Max. PGA values and Max. strain of the soil profile for the Method-I and Method-II

Eq. Intensity Leve	**D1**		**D2**		**D3**	
	Method-I	**Method-II**	**Method-I**	**Method-II**	**Method-I**	**Method-II**
PGA (g)	0.327	0.324	0.708	0.715	1.31	1.24
Maximum Strain %	0.447	0.666	1.01	2.87	1.34	5.22

5.3 Calculation of the Foundation Dynamic Stiffness

5.3.1 Average Effective Velocity of the Profile

In general, soil dynamic properties vary with depth. Hence, while obtaining the dynamic stiffness and damping of the foundation according to the NEHRP method, the average dynamic properties of the soil over the effective profile depth should be considered.

The average unit weight of the soil profile was taken as 20 kN/m^3. Ground water table depth is 1.9 m. The shear modulus reduction ratio was applied as 0.5 to consider soil nonlinearity. The average Poisson ratio of the effective profile depth was selected 0.4 and soil hysteretic damping value was chosen 0.051. Average effective profile velocities for different oscillation axes are shown in Table 5.2.

Table 5.2 Effective profile depth and average shear wave velocities.

Vibration Mode	**Equations**	z_p *(m)*	**Depth Range (m)**	$V_{s,avg}$ **(m/s)**
Horizontal translation (x and y), overall	$\sqrt{BL}$	7.4	0 to 11.6	166.2
Horizontal translation (x and y), base spring	$\sqrt{BL}$	7.4	4.2 to 11.6	173.2
Vertical translation (z)	$\sqrt{BL}$	7.4	0 to 11.6	166.2
Rocking along x-axis (xx)	$\sqrt[4]{B^3L}$	7.5	0 to 11.7	166.4
Rocking along y-axis (yy)	$\sqrt[4]{BL^3}$	7.3	0 to 11.5	166

B and L are foundation half dimensions (B=7.625 m, L=7.2 m) and depth ranges can be obtained from addition of the effective profile depths (z_p) to the embedment depths.

From Table 5.2, it can be seen that each vibration modes have different depth ranges and shear wave velocities.

5.3.2 Foundation Type and Structure to Soil Stiffness Ratio

The structural weight was calculated 7038 tons. The foundation foot print area is equal to (14.4x15.25) 219.6 m^2 and embedment depth is equal to 4.2 m. Removed soil weight was calculated as (219.6x4.2x2) 1845 tons. Thus, effective load transferred to the soil was calculated as (7038-1845) 5193 tons. Uniformly distributed load over the foundation area was obtained (5193/219.6) as 23.6 t/m^2. Therefore the foundation type of the building was selected as a piled raft.

The flexible base period of the structure was found 1.66 seconds. Building total height is 46.4 m from the foundation surface and the effective building height is approximately two-third of the total height of the structure (46.4*2/3=30.93 m). Hence, the shear wave velocity value can be selected for rocking component along the Y axis. In this way, $h/(V_sT)$ ratio was calculated as (30.93/(166*1.66)) 0.112. Calculating this value greater than 0.1 means that the soil structure interaction is significant.

5.3.3 Calculation of Translational and Rotational Dynamic Stiffness and Damping

5.3.3.1 NEHRP method

The dynamic foundation stiffness values (without pile contributions) were calculated with Pais-Kausel and Mylonakis-Gazetas formulations as shown in Table 5.3~5.4. Considering the results obtained from both of the methods were proportional to each other. Pais-Kausel formulations resulted with 10% greater values than Mylonakis-Gazetas ones. It must be noted that Gazetas-Mylonakis formulations take account of the sidewall soil contact area contributions in the calculations. Users are free to choose which formulations are to be used in the developed software.

Table 5.3 Calculated values of the foundation dynamic stiffness and damping (Pais and Kausel, 1988)

Direction	Frequency	G [Mpa]	Ksur[kN/m, kN-m/rad]	Emb. Corr	Vsavg	DSM	Radiation DR	Radiation DRE	K_foundation	C_foundation
Horizontal translation (x), overall	0.602	28.16	1.20E+06	1.64	166.2	1	0.059	0.105	1.96E+06	1.62E+05
Horizontal translation (y), overall	0.602	28.16	1.20E+06	1.64	166.2	1	0.058	0.106	1.97E+06	1.64E+05
Horizontal translation (x), base spring	0.602	30.58	1.30E+06	---	173.2	1	0.056	---	1.30E+06	7.39E+04
Horizontal translation (y), base spring	0.602	30.58	1.31E+06	---	173.2	1	0.056	---	1.31E+06	7.43E+04
Vertical translation (z)	0.602	28.16	1.63E+06	1.32	166.2	1	---	0.117	2.15E+06	1.91E+05
Rocking along x-axis(xx)	0.602	28.09	7.32E+07	1.97	166	0.99	---	0.006	1.43E+08	4.35E+06
Rocking along y-axis(yy)	0.602	28.23	7.99E+07	1.92	166.4	0.99	---	0.006	1.52E+08	4.59E+06

Table 5.4 Calculated values of the foundation dynamic stiffness and damping (Gazetas, 1991; Mylonakis et al., 2006).

Direction	Frequency	G [Mpa]	Ksur[kN/m, kN-m/rad]	Emb. Corr	Vsavg	DSM	Radiation DR	Radiation DRE	K_foundation	C_foundation
Horizontal translation (x), overall	0.602	28.16	1.17E+06	1.69	166.2	1.00	0.060	0.104	1.98E+06	1.62E+05
Horizontal translation (y), overall	0.602	28.16	1.18E+06	1.68	166.2	1.00	0.060	0.106	1.97E+06	1.64E+05
Horizontal translation (x), base spring	0.602	30.58	1.27E+06	---	173.2	1.00	0.058	---	1.27E+06	7.30E+04
Horizontal translation (y), base spring	0.602	30.58	1.28E+06	---	173.2	1.00	0.057	---	1.28E+06	7.34E+04
Vertical translation (z)	0.602	28.16	1.58E+06	1.21	166.2	1.00	---	0.133	1.90E+06	1.85E+05
Rocking along x-axis(xx)	0.602	28.09	6.59E+07	2.20	166.0	0.99	---	0.006	1.44E+08	4.38E+06
Rocking along y-axis(yy)	0.602	28.23	7.50E+07	2.21	166.4	0.99	---	0.006	1.64E+08	4.91E+06

In the soil-structure analyses, foundation stiffness and damping are generally defined in terms of an “impedance function”, which is a complex valued function type. Real part of this function represents stiffness term, whereas imaginary part represents damping and phase difference. The real part of the graphical output of each translational and rotational stiffness-damping components are shown in Appendix C.

5.3.3.2 DYNAN Software

The examined dynamic foundation stiffness of the structure at 0.602 Hz (*f=1/T, 0.602=1/1.66*) are given in Table 5.5. From Tables 5.3 and 5.5, it can be seen that Pais and Kausel formulations gave similar values to the DYNAN analyses results (16% less in horizontal stiffness, 12% less in vertical and 15% less in rocking components). In order to analyze the structure in similar circumstances with the DYNAN Software, embedded foundation model in the half-space were used.

Table 5.5 Foundation stiffness calculated by DYNAN software

Raft foundation Dynamic Stiffness	Frequency	Stiffness	Damping
Component	**Hz**	**kN/m, kN-m/rad**	**kN/m/sec, kN-m/rad/sec**
Horizontal Translation, Kxx, Cxx	0.602	1.65E+06	1.24E+05
Horizontal Translation, Kyy, Cyy	0.602	1.65E+06	1.24E+05
Vertical Translation, Kww, Cww	0.602	1.90E+06	1.31E+05
Rotational, Kppx, Cppx	0.602	1.22E+08	2.75E+06
Rotational, Kppy, Cppy	0.602	1.30E+08	2.89E+06
Torsion, Kzt	6.02E-01	1.85E+08	2.80E+06

Detailed frequency – stiffness variations for all directions are given in graphical form in Appendix C.

5.3.4 Calculation of the Dynamic Stiffness and Damping of the Pile Group

5.4.3.1 Using Developed Algorithm

Dynamic Stiffness of the pile group was calculated by Makris and Gazetas analytical solution. Some important calculation parameters are shown in Figure 5.10. Pile spacing for the X axis direction is 3.35 m, whereas it is 3.56 m for the Y axis direction as previously given in Figure 4.3. Total number of piles in the group are 25.

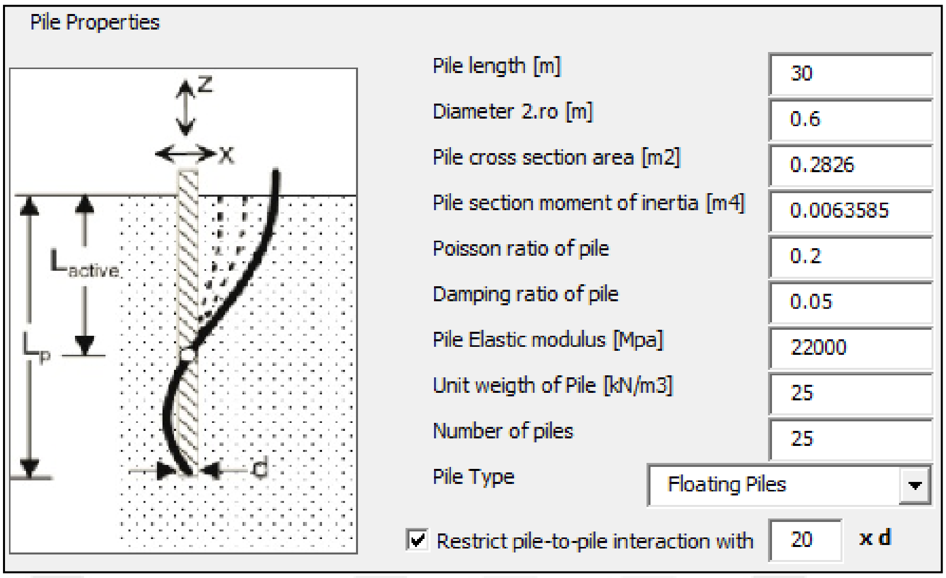

Figure 5.10 Some important properties of the concrete pile group.

- *Some important data were used in the calculation of the dynamic stiffness:*

The foundation half size in the short direction, B (m): 7.2

The foundation half size in the long direction, L (m): 7.625

The foundation embedment depth, D (m): 4.2

The active profile depth, z_p (m): Depend on the type of release

Height of the effective side wall contact, d_w (m): 3.8

Pile length, L_p (m): 30

Pile active length, L_a (m): 6.31

Pile diameter, d (m): 0.6

Dimensionless frequency, a_0 : 0.22

Flexible base period of structure, T_f (second): 1.66

The average shear wave velocity of the effective profile depth, $V_{s.avg}$ (m/s): Depend on the effective profile depth .

Shear modulus of the effective profile depth, G (MPa): Depend on the $V_{s.avg}$

Number of piles in group, n: 25

Elastic modulus of the pile material, E_{pile} (GPa): 22

Pile unit weight (kN/m^3): 25

Pile Poisson's ratio: 0.2

Soil Poisson's ratio: 0.4

Soil average unit weight (kN/m^3): 20

Elastic modulus of the soil (GPa): 81.4

- *Pile group calculation results for the horizontal X direction at 0.602 Hz:*

Real part of the interaction factor : 7.2933

Imaginary part of the interaction factor: 0.4647

Dynamic stiffness of the single pile, Re: 164 247.9 kN/m

Dynamic stiffness of the single pile, Im: 30 196.6 kN/m

Dynamic stiffness of the group for real part, K_1: 1 183 879.2 kN/m

Dynamic stiffness of the group for imaginary part, K_2: 296 565 kN/m

Static stiffness of the single pile, K_s: 163 516.2 kN/m

n * Static stiffness of the single pile: 4 087 905.1 kN/m

Group dyn. Stiff. / n * Static stiffness of the single pile, Re: 0.2896

Group dyn. Stiff. / n * Static stiffness of the single pile, Im: 0.0725

$C = K_2 / \omega$ Dashpot value: 78 320.1 kN-sec/m

Radiation damping = $C*\omega / 2*K_1$: 0.123

Pile group dynamic stiffness and damping group factor variations with frequency are shown in Figure 5.11.

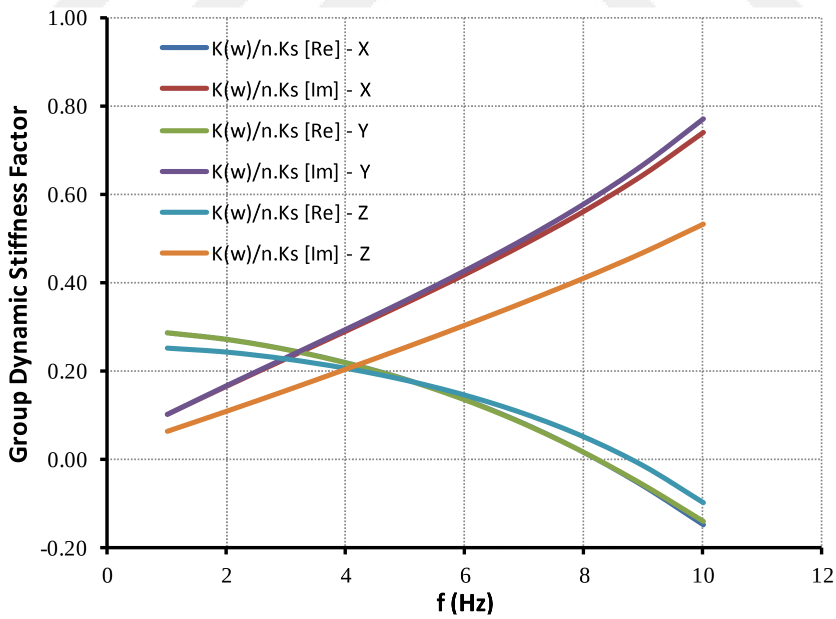

Figure 5.11 Real part and imaginary part of the group dynamic stiffness factors for the rigid capped pile group of the related structure (Developed algorithm).

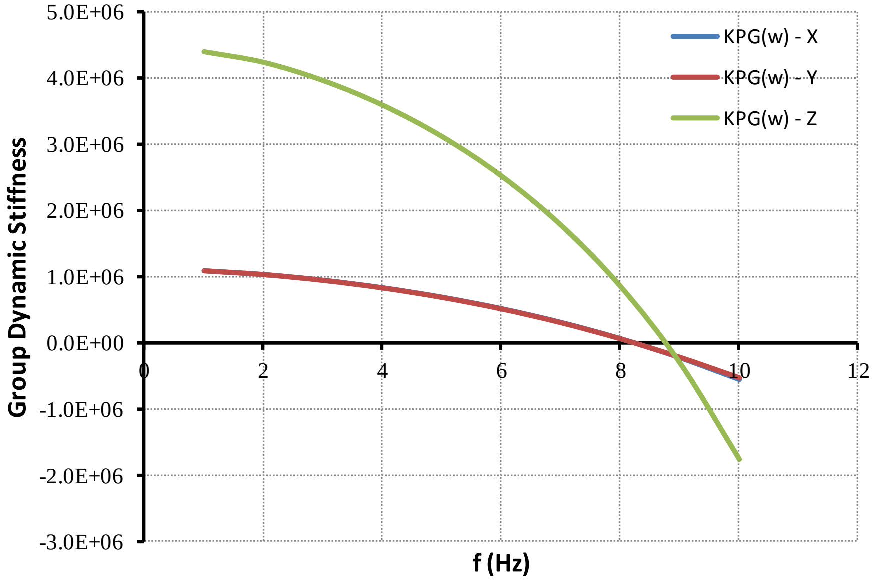

Figure 5.12 Pile group dynamic stiffness for the rigid capped pile group of the related structure in the frequency domain (Developed algorithm).

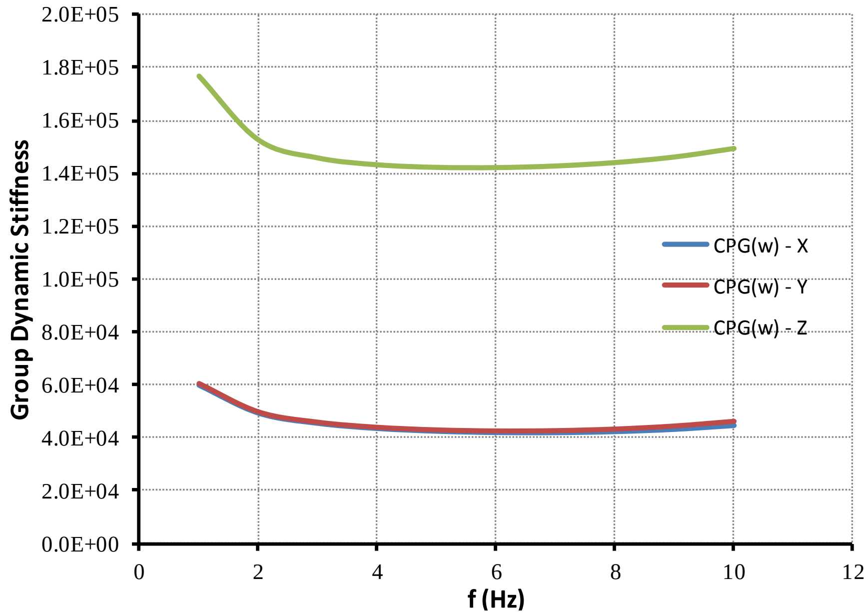

Figure 5.13 Pile group damping for the rigid capped pile group of the related structure in the frequency domain (Developed algorithm).

Figure 5.13 and 5.14 show dynamic stiffness and damping values for related frequency point. Hence, Figure 5.12 shows the group dynamic stiffness factor for both stiffness and damping that can be calculated from: [*Group dynamic stiffness*] / [*Number of piles* * *One pile static stiffness*]. Pile to pile interaction is restricted to 20 times pile diameter (Mylonakis, 2000).

For considering the nonlinear pile behavior, pile elastic modulus can be assumed as E_c=22 GPa (Markis, 2001). This value is approximately 80% of the value obtained from empirical expressions to account for the cracking that occurred during the earthquake. The unit weight of the concrete is assumed 25 kN/m^3.

Table 5.6 Pile Group dynamic stiffness and damping calculated by the developed code.

Pile Group Dynamic Stiffness $K_G=K_1+iK_2$					
Component	**f (Hz)**	**a_0**	**K1**	**K2**	**$C=K_2/\omega$**
Translational - X	0.602	1.06	1.10E+06	2.74E+05	7.25E+04
Translational - Y	0.602	1.06	1.10E+06	2.76E+05	7.29E+04
Translational - Z	0.602	1.06	4.43E+06	7.90E+05	2.09E+05

In Table 5.6, side soil contribution can be added for related directional components and the total horizontal stiffness can be obtained according to the NEHRP code. On the other hand, total vertical stiffness were only achieved from pile group stiffness since piles must be fully mobilized for the consideration of the raft foundation stiffness. Due to this reason only pile vertical stiffness were used. Table 5.7 was obtained according to this assumption.

Table 5.7 Piled raft foundation dynamic stiffness and damping calculated by the developed code.

Pile Group Dynamic Stiffness $K_G=K_1+iK_2$ (raft foundation side soil contributions were added)				
Component	**f (Hz)**	**a_0**	**K1**	**$C=K_2/\omega$**
Translational - X	0.602	1.06	1.80E+06	1.72E+05
Translational - Y	0.602	1.06	1.79E+06	1.73E+05
Translational - Z	0.602	1.06	4.43E+06	2.09E+05

5.4.3.2 Using DYNAN Software

Translational stiffness in Table 5.7 and Table 5.8 are similar apart from the vertical stiffness, which were found lower using DYNAN by 28% as compared with the NEHRP calculation. Table 5.10 was obtained from the difference between Table 5.8 and Table 5.9.

Table 5.8 Overall group dynamic stiffness and damping values calculated using DYNAN

Component	f (Hz)	Stiffness		Damping	
Horizontal Translation, Kxx, Cxx	0.602	1.52E+06	kN/m	9.09E+04	kN/m/sec
Horizontal Translation, Kyy, Cyy	0.602	1.52E+06	kN/m	9.09E+04	kN/m/sec
Vertical Translation, Kww, Cww	0.602	3.16E+06	kN/m	8.96E+04	kN/m/sec
Rotational, Kppx, Cppx	0.602	2.35E+08	kN-m/rad	4.40E+06	kN-m/rad/sec
Rotational, Kppy, Cppy	0.602	2.54E+08	kN-m/rad	4.73E+06	kN-m/rad/sec
Torsional,Kzt, Czt	0.602	1.91E+08	kN-m/rad	3.27E+06	kN-m/rad/sec

Table 5.9 Side soil removed group dynamic stiffness and damping values calculated using DYNAN

Component	f (Hz)	Stiffness		Damping	
Horizontal Translation, Kxx, Cxx	0.602	1.13E+06	kN/m	1.57E+04	kN/m/sec
Horizontal Translation, Kyy, Cyy	0.602	1.13E+06	kN/m	1.58E+04	kN/m/sec
Vertical Translation, Kww, Cww	0.602	2.93E+06	kN/m	4.33E+04	kN/m/sec
Rotational, Kppx, Cppx	0.602	2.11E+08	kN-m/rad	3.11E+06	kN-m/rad/sec
Rotational, Kppy, Cppy	0.602	2.30E+08	kN-m/rad	3.38E+06	kN-m/rad/sec
Torsional,Kzt, Czt	0.602	1.02E+08	kN-m/rad	1.42E+06	kN-m/rad/sec

Table 5.10 Only side soil dynamic stiffness and damping values calculated using DYNAN

Component	f (Hz)	Stiffness		Damping	
Horizontal Translation, Kxx, Cxx	0.602	3.85E+05	kN/m	7.51E+04	kN/m/sec
Horizontal Translation, Kyy, Cyy	0.602	3.85E+05	kN/m	7.51E+04	kN/m/sec
Vertical Translation, Kww, Cww	0.602	2.33E+05	kN/m	4.63E+04	kN/m/sec
Rotational, Kppx, Cppx	0.602	2.34E+07	kN-m/rad	1.29E+06	kN-m/rad/sec
Rotational, Kppy, Cppy	0.602	2.45E+07	kN-m/rad	1.35E+06	kN-m/rad/sec
Torsional,Kzt, Czt	0.602	8.82E+07	kN-m/rad	1.85E+06	kN-m/rad/sec

5.4 Calculation of Distributed Spring Stiffness

The DYNAN software analysis results, which is one of the three methods described above, were used for distributing the spring stiffness since the results obtained through DYNAN analysis were generally on the safe side (gives lower values from the other methods).

The foundation foot print was divided into four influence areas as shown in Figure 5.13. In the SAP2000 software, soil was modelled as linear link element which has three translational and three rotational degrees of freedom as shown in Figure 5.13. The link local axis orientations are shown in the Figure 5.14 according to the global coordinate system.

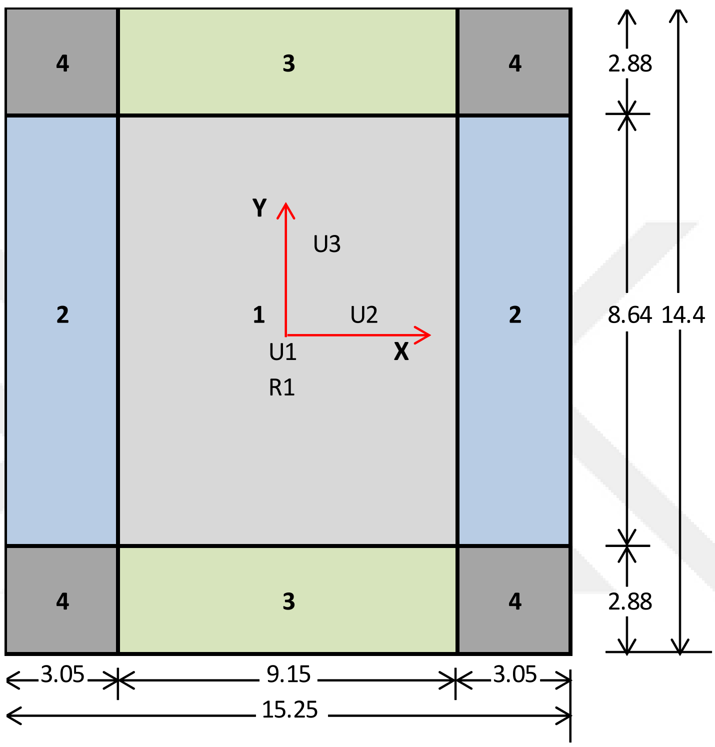

Figure 5.14 Influence area distribution of the foundation.

The influence areas can be calculated as 15.25*0.4=6.1, 6.1/2 =3.05 in the X axis direction. Similarly, they are 14.4*0.4=5.76, 5.76/2 =2.88 in the Y axis direction. Other calculations were shown in Table 5.11.

Table 5.11 Spring stiffness correction factors and resulting stiffness of 1, 2, 3, 4 regions

A_{TOTAL}=	219.6	m2
A_{CENTER}=	79.056	m2
$A_{EDGE\_LEFT\_RIGHT}$=	26.352	m2
$A_{EDGE\_TOP\_BOTTOM}$=	26.352	m2
A_{CORNER}=	8.784	m2
B=	7.2	m
L=	7.625	m
Re=	0.4	
kzi=	13339.0	kN/m / m2
czi=	197.0	kN/m/sec / m2
RKyy=	4.88255	
RKxx=	5.05169	
RCyy=	0.99695	
RCxx=	0.99669	

k_1	13339	kN/m / m2
k_2	65128	kN/m / m3
k_3	67385	kN/m / m4
k_4	66257	kN/m / m5

c_1	196	kN/m/sec / m2
c_2	959	kN/m/sec / m2
c_3	992	kN/m/sec / m2
c_4	975	kN/m/sec / m2

In the horizontal directions, dynamic stiffness and dashpots of the perimeter walls were calculated according to the effective side wall contact height as shown in Figure 5.15 and 5.16.

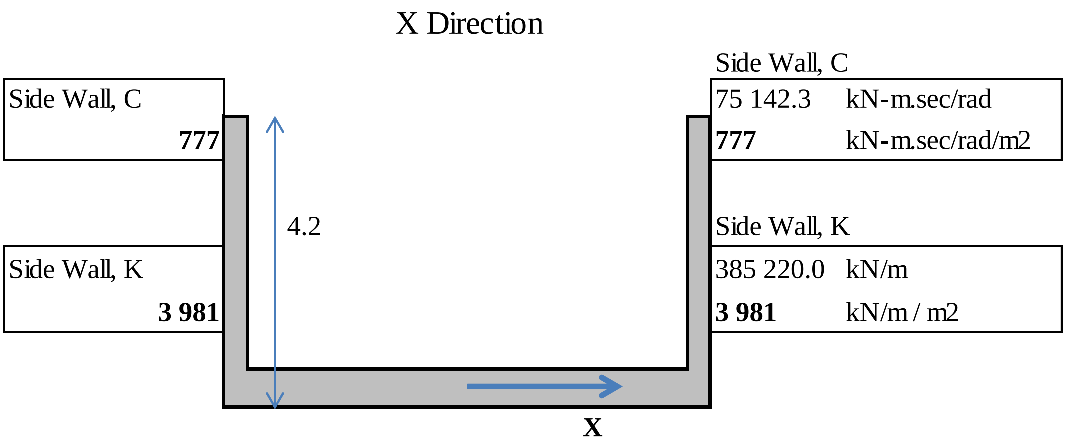

Figure 5.15 Side wall stiffness and damping contribution along the X axis direction.

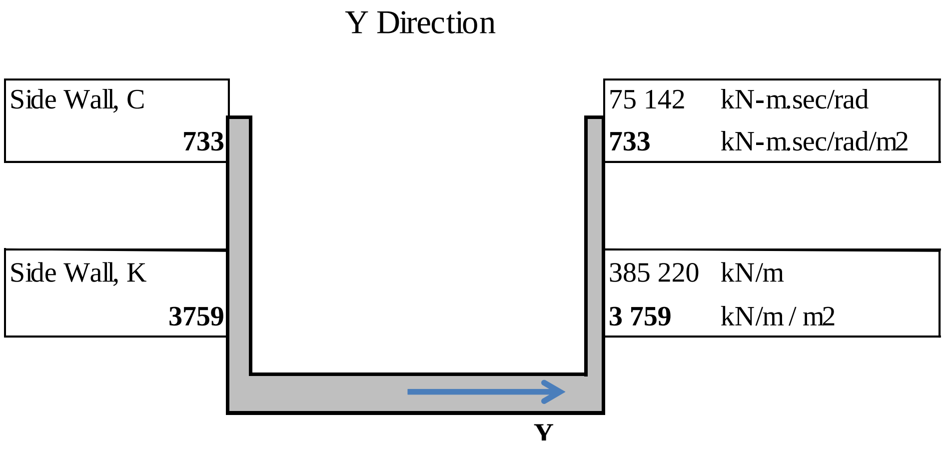

Figure 5.16 Side wall stiffness and damping contribution along the Y axis direction.

Stiffness between the embedded portion of the soil and the side wall effective contact surface can be represented by the linear link elements as they were used at the foundation base. The used link elements in the SAP2000 software for U1, U2, U3 and R1 releases were given in Table 5.12 as follows:

Table 5.12 The foundation base link stiffness and dashpots for related local axis directions

LINK PROPERTIES - K				
	U1 (Z)	**U2 (X)**	**U3 (Y)**	**R1 (Z)**
1	13339	5146	5154	466116
2	65128	5146	5154	466116
3	67385	5146	5154	466116
4	66257	5146	5154	466116

LINK PROPERTIES - C				
1	196	72	72	6458
2	959	72	72	6458
3	992	72	72	6458
4	975	72	72	6458

5.5 Time History Analyses of the Structure

Time history analyses were performed for the case, where the foundation is completely embedded into the soil (one basement story). These analyses were performed for D1, D2, D3 intensity level earthquake records which were obtained from the Method-I and Method-II site response analyses. The maxima story displacements, story drift ratios, peak story accelerations and base reaction forces of the structure were shown in graphical and tabular format in Figure 5.17~5.25 and Table 5.13~5.14. In Figure 5.17, story peak displacements of the Method-II are 1.2~2.5 times larger than the Method-I for D1 level earthquakes.

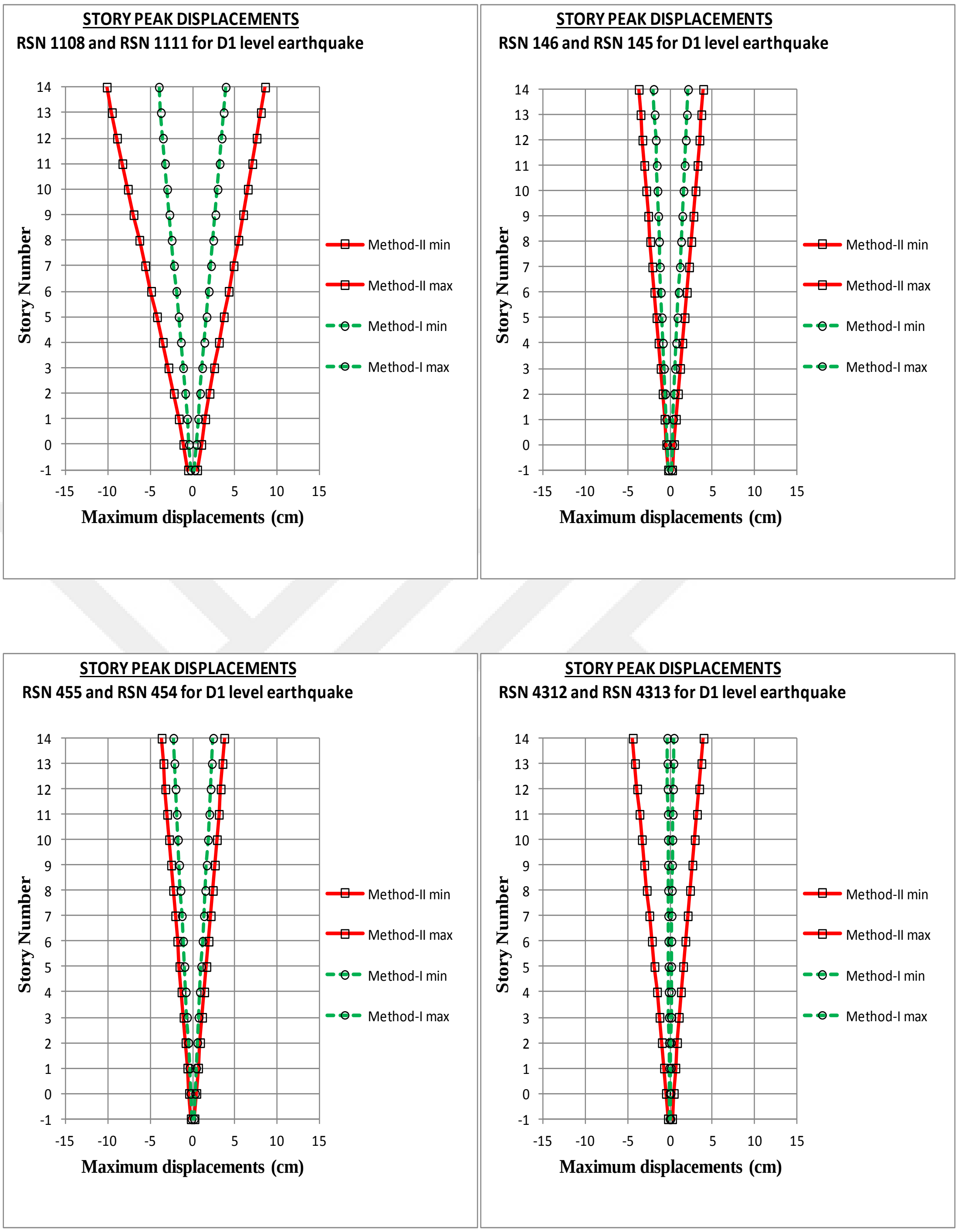

Figure 5.17 D1 level earthquake story maximum and minimum displacements for the Method-I and Method-II. (Structure behavior factor, R = 1.5, modal damping ratio constant at 0.05, RSN is the Record Sequence Number in the PEER database)

In Figure 5.17, story peak displacements of the Method-II are 1.2~2.0 times larger than the Method-I for D1 level earthquakes. On the other hand, RSN (Record Sequence Number) 4312 record showed very small displacements (Bottom right graph of the Figure 5.17). This situation occured at all earthquake intensity levels yet it is maximum in the D2 level earthquake.

Figure 5.20, 21 and 22 show the story drift ratios for each earthquake intensity levels. Method-II analysis results show significantly greater story drift ratios than the Method-I. In Figure 5.22, limit values are exceeded during the analysis under the Kobe Earthquake (RSN 1108) excitation.

Figure 5.23, 24 and 25 demonstrate story peak accelerations for D1, D2, D3 earthquake intensity levels. Differences in peak floor accelerations (Method-II and Method-I) were large up to 60% in Kobe (RSN 1108, 1111), Coyote Lake (RSN 145, 146), Morgan Hill (RSN 454, 455) and were large up to 90% in Umbria (RSN 4312, 4313) earthquakes for D1 intensity level. Similarly;

- Up to 50% in Kobe, Coyote Lake, Morgan Hill and up to 90% in Umbria earthquakes for D2 intensity level.
- Up to 50% in Kobe, Coyote Lake, Morgan Hill and up to 92% in Umbria earthquakes for D3 intensity level.

Differences in story peak accelerations were generally greater in basement levels than in the levels above grade. However, Coyote Lake Earthquakes generated story peak accelerations very close to each other at the basement level. Hence, Model-I accelerations were greater than the Model-II between the 5th and 14th stories.

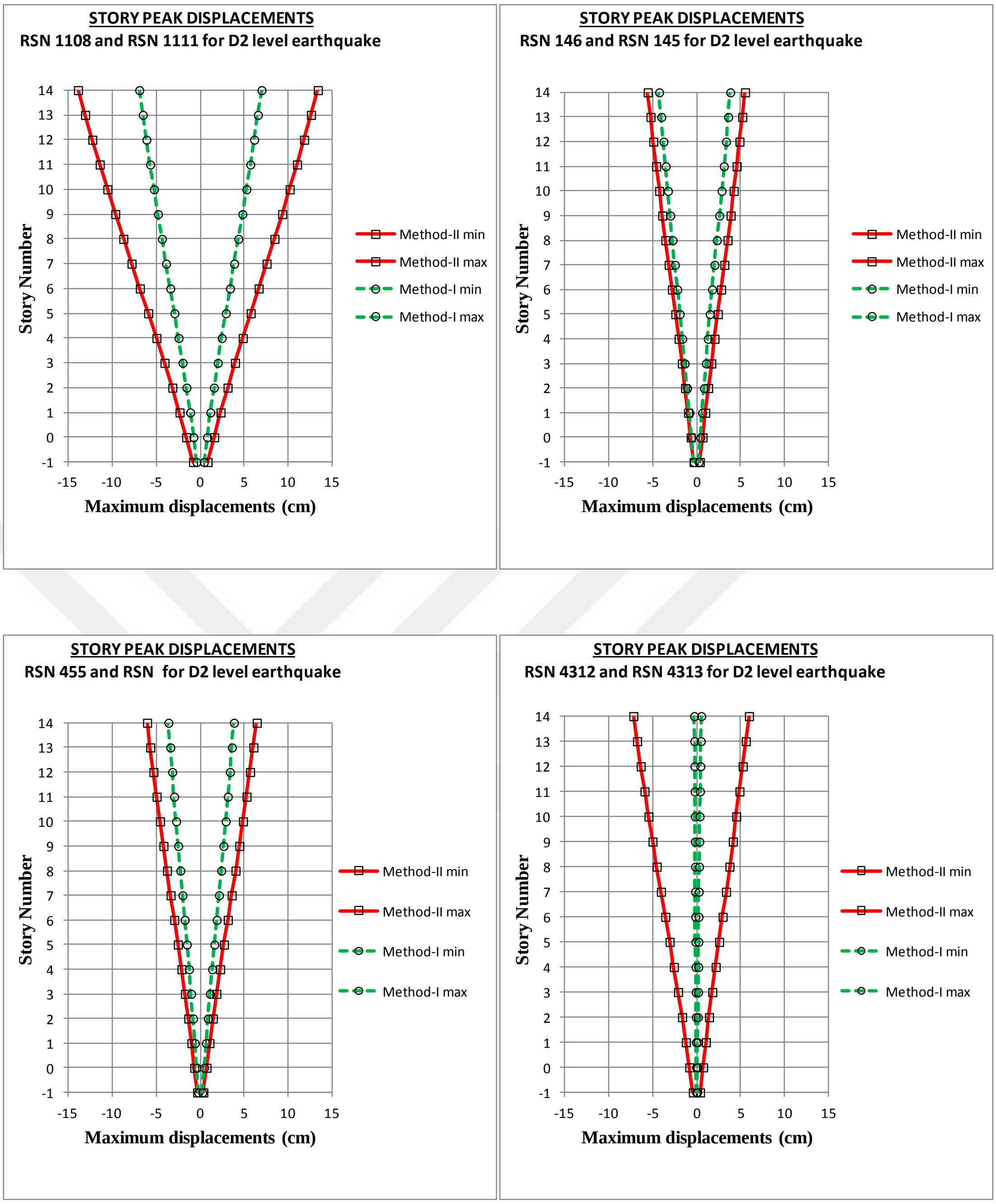

Figure 5.18 D2 level earthquake story maximum and minimum displacements for the Method-I and Method-II. (Structure behavior factor, R = 4, modal damping ratio constant at 0.05, RSN is the Record Sequence Number in the PEER Database)

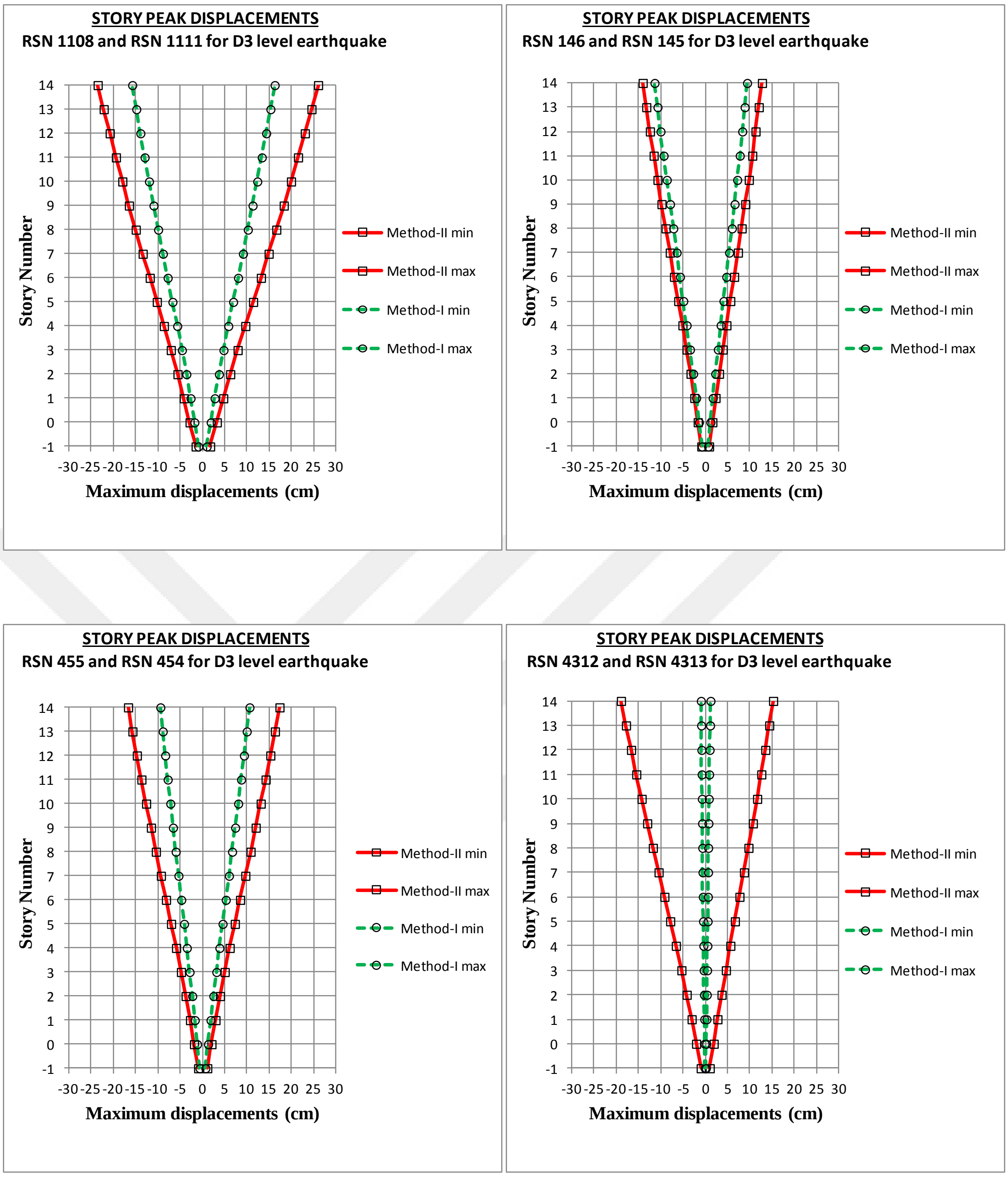

Figure 5.19 D3 level earthquake story maximum and minimum displacements for the Method-I and Method-II. (Structure behavior factor, R = 4, modal damping ratio constant at 0.05, RSN is the Record Sequence Number in the PEER database)

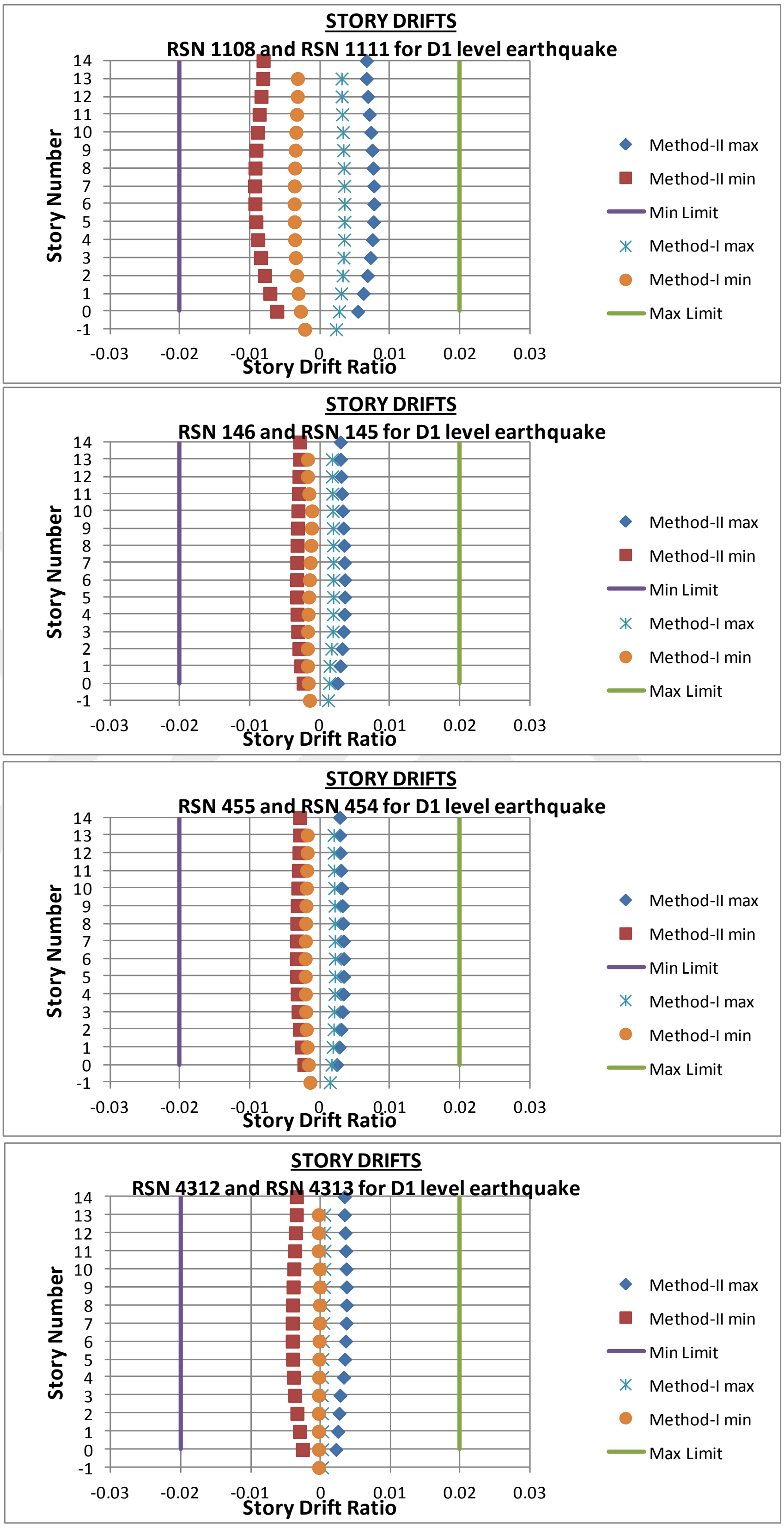

Figure 5.20 D1 level earthquake story maximum and minimum drift ratios for the Method-I and Method-II. (Max. Limit and Min. Limit represent the limit drift ratio of the stories according to Turkish Earthquake Code.)

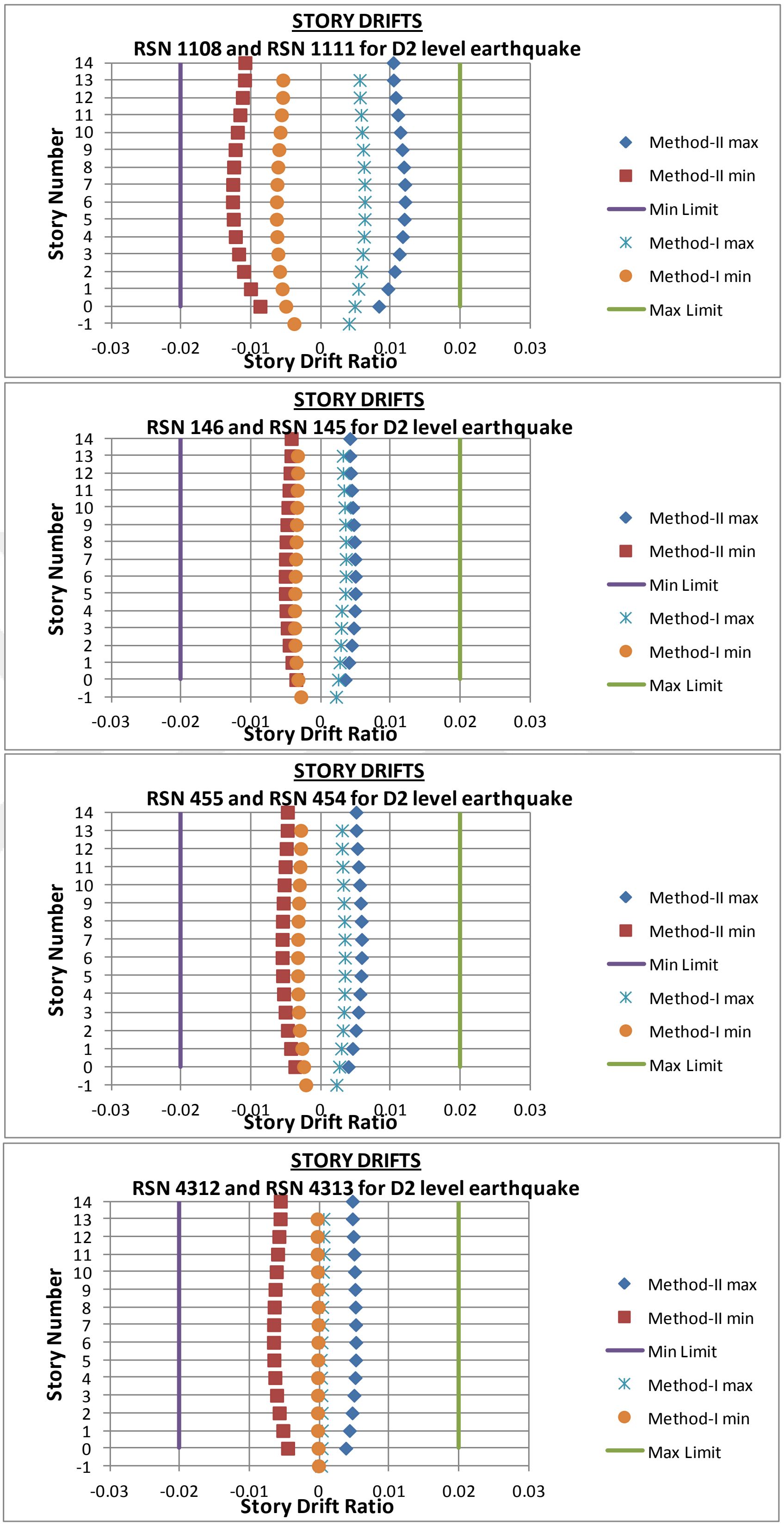

Figure 5.21 D2 level earthquake story maximum and minimum drift ratios for the Method-I and Method-II. (Max. Limit and Min. Limit represent the limit drift ratio of the stories according to Turkish Earthquake Code.)

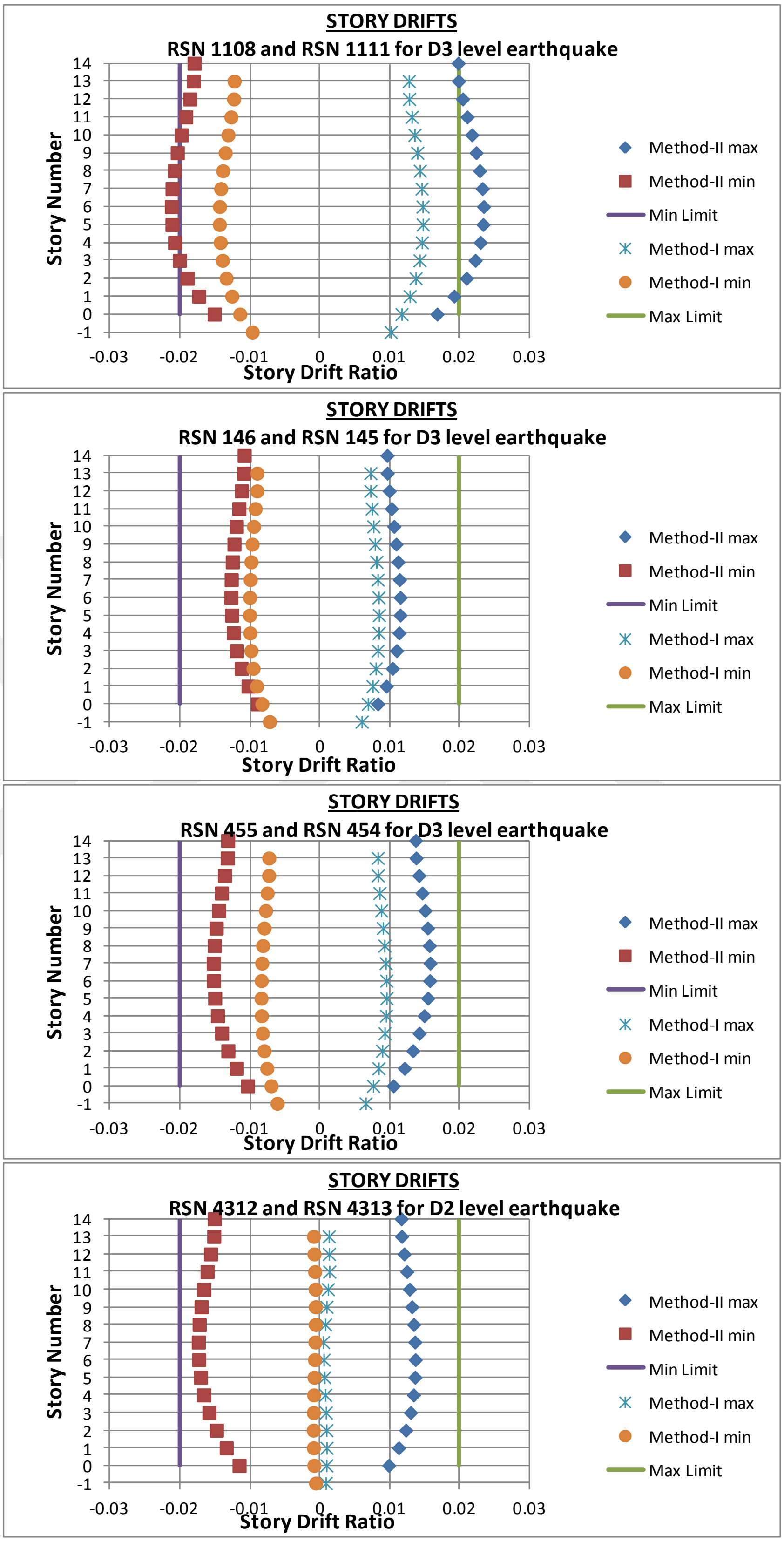

Figure 5.22 D3 level earthquake story maximum and minimum drift ratios for the Method-I and Method-II. (Max. Limit and Min. Limit represent the limit drift ratio of the stories according to Turkish Earthquake Code.)

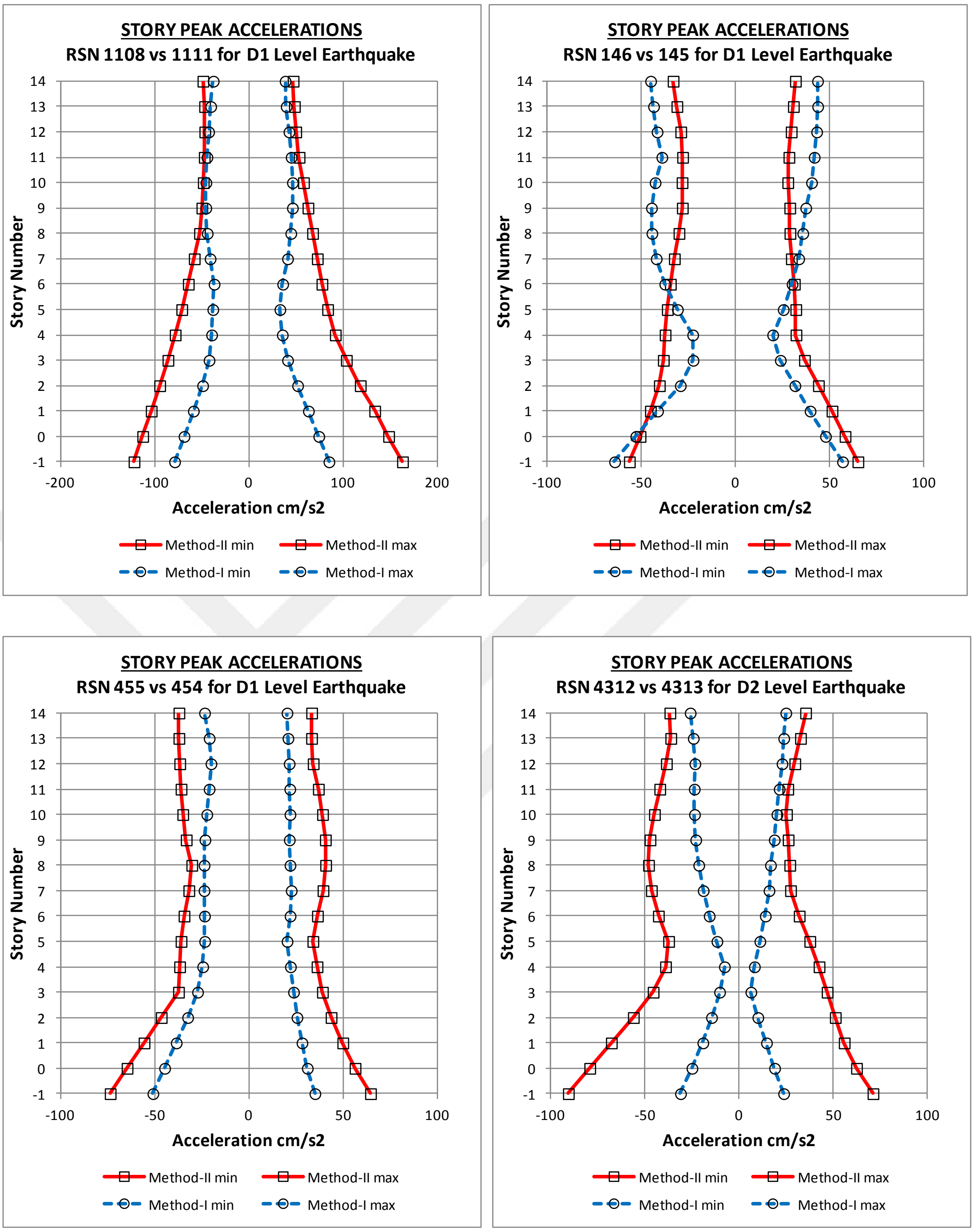

Figure 5.23 D1 level earthquake story peak accelerations for the Method-I and Method-II.

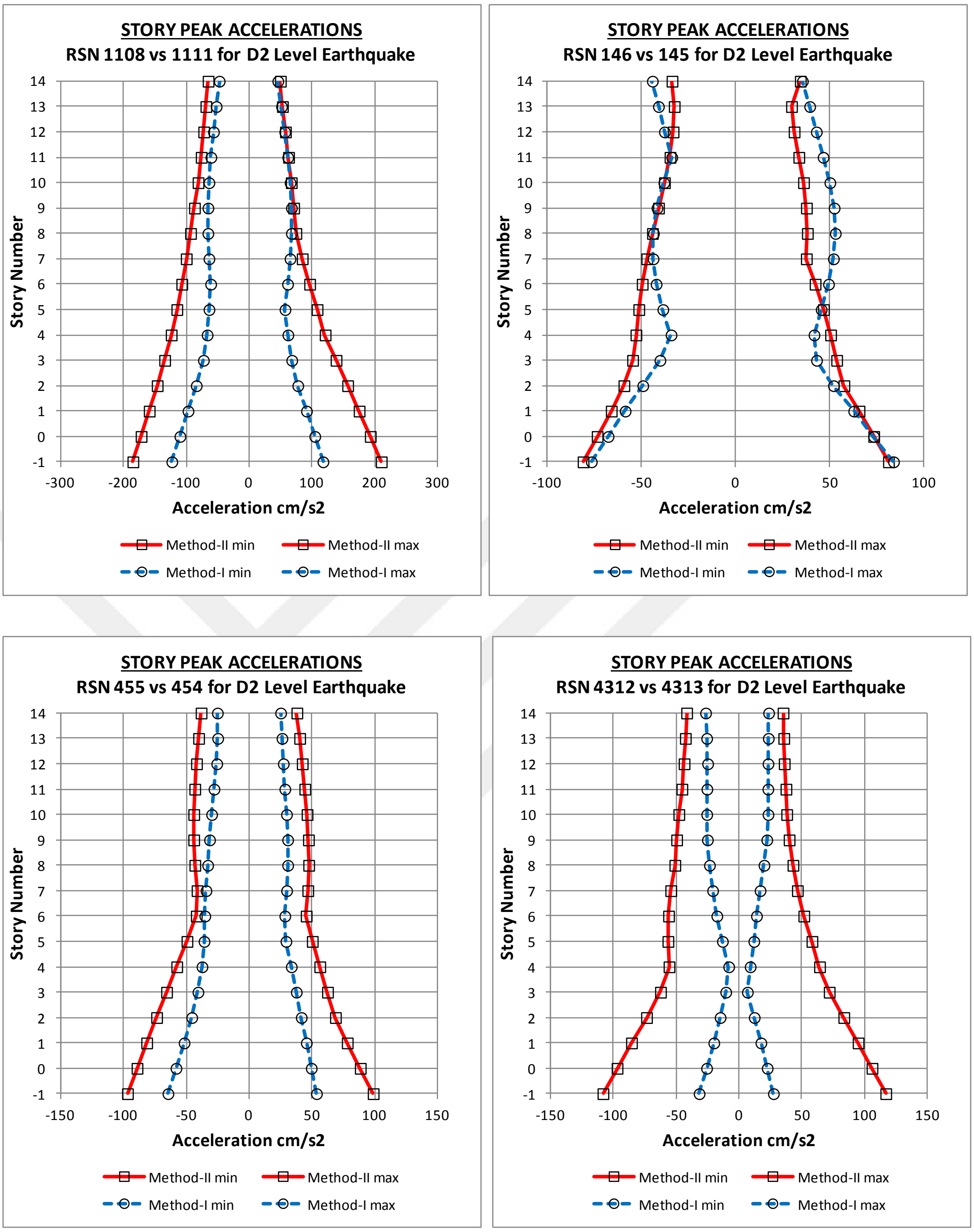

Figure 5.24 D2 level earthquake story peak accelerations for the Method-I and Method-II.

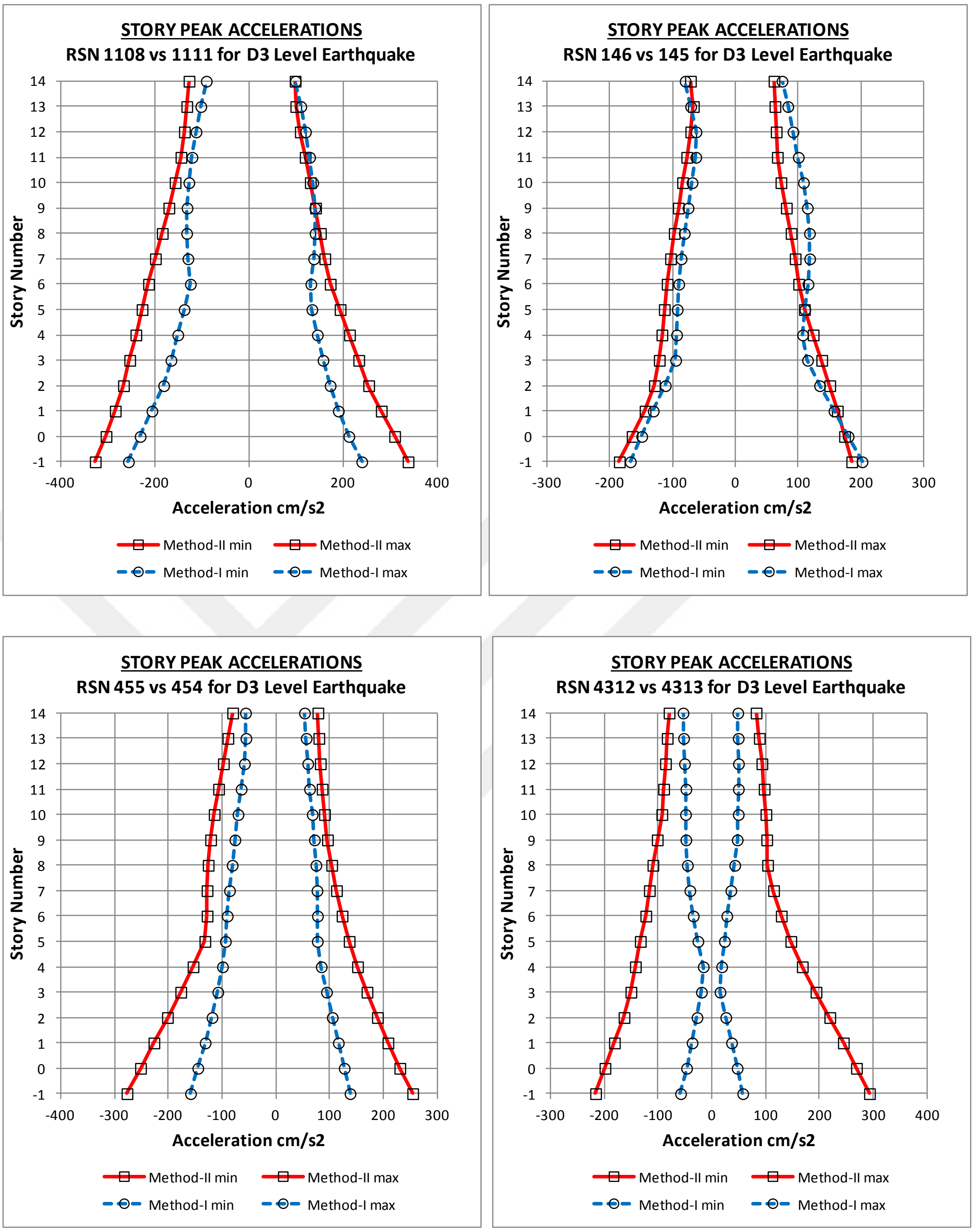

Figure 5.25 D3 level earthquake story peak accelerations for the Method-I and Method-II.

The base shear forces obtained for Method-I and Method-II are shown in Table 5.13. Differences (Method-II – Method-I) between the Kobe Earthquakes (RSN 1108, 1111) were found as high as 50%, 40% and 40% for the D1, D2, D3 intensity levels respectively. For the Coyote Lake (RSN 145, 146) Earthquakes, differences happened to be 20%, 30% and 30%. For the Morgan Hill (RSN 454, 455) Earthquakes, differences were also found as 30%, 40% and 40%. Differences between RSN4312 and RSN4313 were also calculated quite high.

Table 5.13 Comparision of base shear forces of the structures in terms of Method-I and Method-II for D1, D2, D3 earthquake intensity levels. (All values are in tonnes).

RSN #	Earthquake Intensity Level						SRA Method
	D1		D2		D3		
	Max	Min	Max	Min	Max	Min	
RSN 1108	456.6	-462.7	710.1	-733.7	1356.6	-1528.6	Method - II
RSN 1111	248.4	-252.6	422.1	-405.4	917.5	-851.9	Method - I
RSN 146	199.6	-223.6	304.3	-323.2	778.8	-762.7	Method - II
RSN 145	193.8	-170.1	312.2	-220.4	733.7	-557.9	Method - I
RSN 455	199.6	-189.2	320.0	-331.4	826.0	-996.8	Method - II
RSN 454	129.9	-144.7	225.8	-215.0	598.3	-598.1	Method - I
RSN 4312	211.0	-246.8	348.3	-340.5	838.4	-899.1	Method - II
RSN 4313	56.6	-67.6	69.1	-77.6	141.3	-158.8	Method - I

Table 5.14 shows first three modal periods of the structure for fixed base and flexible base models. First, second and third periods occured at the translational X, Y and rotational Z axis direction respectively. The flexible base model lengthened the first and second periods by 0.27 and 0.31 seconds.

Table 5.14 Fist three mode periods of the structure for fixed base and flexible base models

Mode No	Period	Frequency	CircFreq	Method
	Sec	Cyc/sec	rad/sec	
1	1.409516	0.70946	4.4577	Fixed Base
	1.679033	0.59558	3.7421	Flexible Base
2	1.291542	0.77427	4.8649	Fixed Base
	1.603128	0.62378	3.9193	Flexible Base
3	1.138632	0.87825	5.5182	Fixed Base
	1.085118	0.92156	5.7903	Flexible Base

CHAPTER SIX
CONCLUSIONS AND RECOMMENDATIONS

6.1 Conclusions

In this thesis study, soil-structure interaction analyses using substructure technique were performed according to the procedure defined for inertial interaction analysis in İzmir Local Technical Advisory for Tall Buildings. The effect of the deep soil profile on acceleration records and elastic response spectra computed at the foundation level was also investigated in detail. The side product of this thesis, however, happened to be a software developed to calculate dynamic pile group and shallow foundation stiffness of tall buildings. This software was based on the methods given in the NEHRP Standard. The pile-soil-pile interaction was handled using Makris & Gazetas approach since no clear methodology was suggested in NEHRP for this purpose. Results of this software were compared with those of a rather advanced similar program (DYNAN).

The conclusions derived from this thesis study may be summarized item by item as in the following:

- The substructure method is a simple way to perform soil structure interaction analysis.
- Nonlinear behavior of the soil can be taken into consideration by means of the equivalent linear method where shear modulus is reduced with respect to the relevant G/G_{max} ratio corresponding to the strain level for a particular earthquake intensity.
- Nonlinear behavior of piles were taken into consideration using reduced section modulus (i.e. 75% of the uncracked initial bending stiffness).
- Translational stiffness values, which were calculated with the developed algorithm and DYNAN Software were found close to each other. The vertical stiffness values calculated by the developed software were 28% higher than those of the DYNAN Software.

- The distribution of the dynamic spring stiffness over the foundation area allows consideration of flexibility of the foundation plate.
- It was observed that the DYNAN considers contribution of the raft to overall foundation stiffness. This is also the same in NEHRP. However, this assumption may only be valid for piled rafts where the number of piles is comparetively small allowing the side friction is fully mobilized and raft is in contact with the soil. Careless use of this assumption for piled foundations may result in false stiffness estimations since the raft may not be in contact with the underlying soil or its stiffness is considerably small with respect to the total stiffness of the piles. For such cases utilization of the developed software is recommended.

Two types of site response calculations, called as Method-I and Method-II in the thesis, were used to obtain time history records at the foundation level. In Method I the dynamic soil analyses commenced at the engineering bedrock level defined as the depth where shear wave velocity is either equal or greater than 760 m/s in the İzmir Local Technical Advisory. The Method II, on the other hand, considered the rock horizon (i.e. seismic rock) in the area. The thickness of the weathered rock strata down to the rock horizon is almost 1000 m. The conclusions based on the calculations with respect to both methods may be given as;

- Foundation level acceleration response spectra obtained from Method-II were significantly shifted towards the long period side (beyond T= 0.8 s) compared to Method-I.
- As a result of the time history analyses, Method-II yielded larger peak story displacements as compared with Method-I. Same conclusion is also valid for story accelerations as well. Method-II also resulted in larger shear forces.
- The above results suggest that inclusion of all layers overlying the rock horizon (i.e. seismic rock) is a necessity for site response analyses that are desired to stay on the safe side.

- Analyses for pile-soil-pile interaction showed that the interaction distance between any two piles may be safely taken as 20d. Beyond this distance interaction can be ignored.

6.2 Recommendations for Future Studies

Other aspects of the soil-structure interaction phenomenon that would be studied in future studies may be mentioned as in the following:

- The fundamental assumption regarding the nonlinear soil behavior surrounding the piles of the foundation was such that the reduction in shear modulus was obtained from dynamic site response analyses meaning that inertial interaction effect on soil behavior was not considered. Since the pile displacements due to structural loads may generate additional nonlinearity inside the soil around the piles, this aspect shall be investigated in future studies.
- The definiton method of the distributed dynamic springs in vertical and horizontal directions may be studied in the future since gap formation or tension case for spread foundations without piles may be quite influential on foundation and building response. The dynamic soil action on basement walls is an aspect of dynamic soil-structure-interaction that needs closer attention.

REFERENCES

Abrahamson, N.A., (1992). *Spatial variation of earthquake ground motion for application to soil-structure interaction*, Report: *EPRI TR-100463*, Electrical Power Research Institute, Palo Alto, California.

Akgün, M., Gönenç, T., Tunçel, A., & Pamukçu, O. (2013). A multi-approach geophysical estimation of soil dynamic properties in settlements: A case study in Güzelbahce-İzmir (western Anatolia). *Journal of Geophysics and Engineering, 10*, 12.

American Society of Civil Engineers (ASCE), (2010). *Minimum design loads for buildings and other structures* (2nd ed.) (7-10). Virginia: Reston.

Bielak, J., (1975). Dynamic behavior of structures with embedded foundations. *Earthquake Engineering and Structural Dynamics*, 3, 259-274.

Clough, R.W., & Penzien, J., (1993). Response to harmonic loading. In *Dynamics of structures*, (52-57). New York: McGraw Hill.

Darendeli, M. B. (2001). *Development of a new family of normalized modulus reduction and material damping curves.* P.hD. Thesis, The University of Texas, Austin, Texas.

Electric Power Research Institute (EPRI), (1993). *Guidelines for determining design basis ground motions*. Retrieved May 14, 2015, from http://peer2.berkeley.edu/ngaeast_wg/wp-content/uploads/2010/09/TR-102293-V2.pdf

Enercon Services Incorporation (2010). *Comanche peak nuclear power plant, nonlinear sensitivity analyses*. Retrieved May 14, 2015, from http:// pbadupws.nrc.gov / docs / ML1006 / ML100640190.pdf

Fan, K., Gazetas, G., Kaynia, A., & Kausal, E., (1991). Kinematic seismic response of single piles and pile groups. *Journal of Geotechnical Engineering*, 117, 1860-1879.

Federal Emergency Management Agency (FEMA), (2009). *NEHRP recommended seismic provisions for new buildings and other structures*. Retrieved May 20, 2015, from http://www.fema.gov/media-library-data/20130726-1730-25045-1580/femap_750.pdf

Gazetas G. & Dobry, R., (1984). Horizontal response of piles in layered soils. *Journal of Geotechnical Engineering Division American Society of Civil Engineers, 110*, 20-40.

Gazetas G. & Dobry, R., (1984). Simple radiation damping model for piles and footings. Horizontal response of piles in layered soils. *Journal of Geotechnical Engineering Division American Society of Civil Engineers, 110*, 937-956.

Gazetas, G., (1991). Foundation vibrations. In H.-Y. Fang, ed. *Foundation engineering handbook*, (2nd ed.), (Chapter 15), New York: Chapman and Hall.

Türkiye Cumhuriyeti Ulaştırma Bakanlığı, (2008). *Kıyı ve liman yapıları, demiryolları, hava meydanları inşaatlarına ilişkin deprem teknik yönetmeliği (DLH)*. Retrieved April 27, 2014, from http://www.koeri.boun.edu.tr/depremmuh/eski/DLH-2008-Revizyon.pdf

Harden, C.W., & Hutchinson, T.C., (2009). Beam-on-nonlinear-Winkler-foundation modeling of shallow, rocking-dominated footings. *Earthquake Spectra*, *25*, 277-300.

Hardin, B.O., & Black, W.L., (1968). Vibration modulus of normally consolidated clay. *Journal of the Soil Mechanics and Foundation Division*, *94*, (2), 353-369.

Hardin, B. O., & Drnevich, V. P. (1972). Shear modulus and damping in soils: Design equations and curves. *Journal of the Soil Mechanics and Foundations Division, ASCE, 98*, 667-692.

Hashash, Y.M.A., Musgrove, M.I., Harmon, J.A., Groholski, D.R., Phillips, C.A., & Park, D. (2015). *DEEPSOIL 5.1 user manual*. Retrieved May 10, 2015, from https://nees.org/resources/5113/download/Tutorial__Manual_v5.pdf

Hashash, Y.M.A., Phillips, C., & Groholski, D. (2010). Recent advances in non-linear site response analysis. *Fifth International Conference on Recent Advances in Geotechnical Earthquake Engineering and Soil Dynamics*, Paper No. OSP 4.

Iguchi, M., & Luco, J.E., (1982). Vibration of flexible plate on viscoelastic medium. *Journal of Engineering Mechanics*, *108*, 1103-1120.

Kausel, E., Whitman, A., Murray, J., & Elsabee, F., (1978). The spring method for embedded foundations. *Nuclear Engineering and Design*, *48*, 377-392.

Kim, S., & Stewart, J.P., (2003). Kinematic soil-structure interaction from strong motion recordings. *Journal Geotechnical and Geoenvironmental Engineering*, *129*, 323-335.

Kramer, S.L. (1996). Soil-structure interaction. In *Geotechnical earthquake engineering* (294-303). New Jersey: Prentice Hall, Inc.

Liou, G.S., & Huang, P.H., (1994). Effect of flexibility on impedance functions for circular foundations. *Journal of Engineering Mechanics*, *120*, 1429-1446.

Luco, J.E., & Westmann, R.A., (1971). Dynamic response of circular footings. *Journal of Engineering Mechanics*, *97*, 1381-1395.

Lysmer, J., Tabatabaie, M., Tajirian, F., Vahdani, S., & Ostadan, F., (1981). *SASSI: A system for analysis of soil-structure interaction.* Retrieved April 15, 2015, from http://nisee.berkeley.edu/documents/elib/www/documents/GEOTECH/UCB-GT-81-02.pdf

Makris, N. & Gazetas, G. (1992). Dynamic pile-soil-pile interaction II: lateral and seismic response. *Earthqeake Engineering and Structural Dynamic, 20*, 145-162

Makris, N. & Gazetas, G. (1993). Displacement phase differences in a harmonically oscillating pile. *Geotechnique 43*, 135-150.

Marcuson, W.F., & Wahls, H.E., (1972). Time effects on dynamics shear modulus of clays. *Journal of Soil Mechanics and Foundations Division, 98*, (12), 1359-1373.

Masing, G. (1926). Eigenspannungen und verfestigung beim messing (Self stretching and hardening for brass), in: *Proceedings of the Second International Congress for Applied Mechanics*, (332–335), Switzerland: Zurich.

Mylonakis, G., Nikolaou, S., & Gazetas, G., (2006). Footings under seismic loading: Analysis and design issues with emphasis on bridge foundations. *Soil Dynamics and Earthquake Engineering*, *26*, 824-853.

Novak, M., Nogami, T., & Aboul-Ella, F., (1978). Dynamic soil reaction for plane strain case. *Journal of Engineering Mechanics, ASCE, 104:EM4*, 953-595.

Pais, A., & Kausel, E., (1988). Approximate formulas for dynamic stiffnesses of rigid foundations. *Soil Dynamics and Earthquake Engineering*, *7*, 213-227.

Pasific Earthquake Engineering Research Center, (2015). *PEER strong motion database*. Retrieved April 20, 2015, from http://ngawest2.berkeley.edu/

Poulos, H. G., (1968). Analysis of the settlement of pile groups. *Geotechnique 18,* 449-471.

Riggs, H.R., & Waas, G., (1985). Influence of foundation flexibility on soilstructure interaction. *Earthquake Engineering and Structural Dynamics*, *13*, 597-615.

Seed, H. B., & Idriss, I. M., (1970). Soil moduli and damping factors for dynamic response analyses. *Earthquake Engineering Research Center, University of California, Berkeley, 1970-12,* 40 (475/S41/1970). Retrieved May 13, 2015, from http://nisee.berkeley.edu/documents/EERC/EERC-70-10.pdf

Seed, H.B., Wong, R.T., Idriss, I.M., & Tokimatsu, K. (1986). Moduli and damping factors for dynamic analyses of cohesionless soils. *Journal of Geotechnical Engineering 112 (11),* 1016 –1032.

National Institute of Standards and Technology, NIST (2012). Soil-structure interaction for building structures. *Report NIST/GCR 12-917-21*, presented by NEHRP Consultants Joint Venture. Retrieved May 18, 2014, from http://www.nehrp.gov/pdf/nistgcr12-917-21.pdf.

Stewart, J. P., Seed, R. B., & Fenves, G. L. (1999). Seismic soil-structure interaction in buildings. II: Emprical findings. *Journal of Geotechnical and Geoenvironmental Engineering, ASCE, 125(1),* 38-48.

Stewart, J.P., & Kwok, O.L.A., (2008*). Nonlinear seismic ground response analysis: code usage protocols and verification against vertical array data.* Retrieved May 17, 2015, from http://escholarship.org/uc/item/7db3d49z#page-8

Veletsos, A.S., & Meek, J.W., (1974). Dynamic behavior of building-foundation systems. *Earthquake Engineering and Structural Dynamics*, *3*, 121-138.

Veletsos, A.S., & Nair, V.V., (1975). Seismic interaction of structures on hysteretic foundations. *Journal of Structural Engineering*, *101*, 109-129.

Villaverde, R., (2009). Structural response considering soil-structure interaction. In *Fundamental concepts of earthquake engineering* (571-647), Taylor & Francis: CRC Press

Vucetic, M., & Dobry, R., (1991). Effect of soil plasticity on cyclic response. *Journal of Geotechnical Engineering*, *117(1)*, 89–107.

Whitman, R.V., & Bielak, J. (1980). Foundations. In E. Rosenblueth, (Ed.). *Design of earthquake resistant structures*, New York: Halsted Press.

Wolf, J.P., & Von Arx, G.A., (1978). Impedance function of a group of vertical piles. *Proceedings: Specialty Conference on Soil Dynamics and Earthquake Engineering*, ASCE, Pasadena, California, 1024-1041.

Wong, H.L., & Luco, J.E., (1985). Tables of impedance functions for square foundations on layered media. *Soil Dynamics and Earthquake Engineering*, 4(2), 64-81.

Yamada, S., Hyodo, M., Orense, R.P., Dinesh, S.V., & Hyodo, T., (2008). Strain dependent dynamic properties of remolded sand-clay mixtures. *Journal Geotechnical and Geoenvironmental Engineering*, *134*, (7), 972-981.

APPENDIX A

Developed Algorithm for the Calculation of Dynamic Foundation Stiffness

Data Input

- **a)** ***Soil Profile****:* In this section, the user can define the shear wave velocity profile and soil profile. Besides, G/G_{max} reduction factor as an approximation to soil nonlinearity and average soil strength properties may also be defined using the interface as shown in Figure A.6. All data on the graphical interface can be saved and the saved data can be imported from this interface of the program.
- **b)** ***Structure Properties****:* Structure general characteristics are entered in this section (Figure A.2). If the piled foundation system will be used, the checkbox is marked and some important data is entered. All entered data can be saved to a file and then can be called up for use again.
- **c)** ***Pile Layout:*** If the pile foundation system will be used, the layout of pile group can be defined by the coordinates of each pile. All pile coordinates can be automatically created as array or prepared coordinate list in an Excel sheet, which can be imported to the software (Figure A.3).
- **d)** ***Stress Increase:*** The stress increase occurs in the soil media because of the net surcharge load transferred to the ground by the superstructure. This stress increase can be obtained at the desired coordinates and depth in the algorithm. It separates the foundation into finite meshes and calculates stress increase for each element. Superposition of these stress increases gives total stress increase below the foundation. If the size of the finite elements get decreased, more accurate results are obtained (Figure A.4).

Users are free to choose of two methods, which are “Pais and Kausel” and “Gazetas and Mylonakis”, to achieve the dynamic stiffness of foundation. In addition, one of the calculation option is the selection of constant frequency or frequency range. Overburden corrected V_s profile beneath the foundation due to the net surcharge load can be obtained according to Equation 3.9.

The main user interface was shown in Figure A.1. Steps 1~6 are followed for the calculation of the dynamic stiffness of the foundation or pile group. The table at the top right side of the screen shows some calculations of the corresponding layers. The frame on the bottom left side shows some data and calculations related to structure, soil, pile and foundation that will be used for following analysis steps. The frame on the bottom right side shows analysis results about pile foundation if the “Results” tab button was pressed.

In this algorithm, the method described in Figure 3.7 is used to determine the lateral spring. As shown in Figure A.10, the overall foundation dynamic stiffness and damping values distributed over the foundation footprint and side walls of the basement. The foundation area is divided into four zones for this distribution (Figure A.10). The spring stiffness of first region can be calculated directly from Equation 3.15. The spring stiffness of the second and the third regions (sideband of footprint) are increased by the rocking component of the oscillations. Thus the sideband spring stiffness is increased by a factor which is calculated from Equation 3.17 or 3.18 for related direction. The spring stiffness of the fourth regions are increased by a factor, which is average of the ones that were used in second and third region, since it is under the influence of the rocking component in both X and Y axis.

Similarly, dashpot values of these four region can be found as follow:

- Region 1: Equation 3.16 is used.
- Region 2, 3: Equation 3.19 and 3.20 are used.
- Region 4: Average of the Equation 3.19 and the 3.20 is used

Users can be follow results by clicking the related tab buttons, such as; “Foundation Dynamic Stiffness and Damping”, “Graphics” or “Spring Distributions” etc.

Requested dynamic stiffness calculations must be selected from the drop-down list box in the main interface. The calculation will automatically start after the selection process.

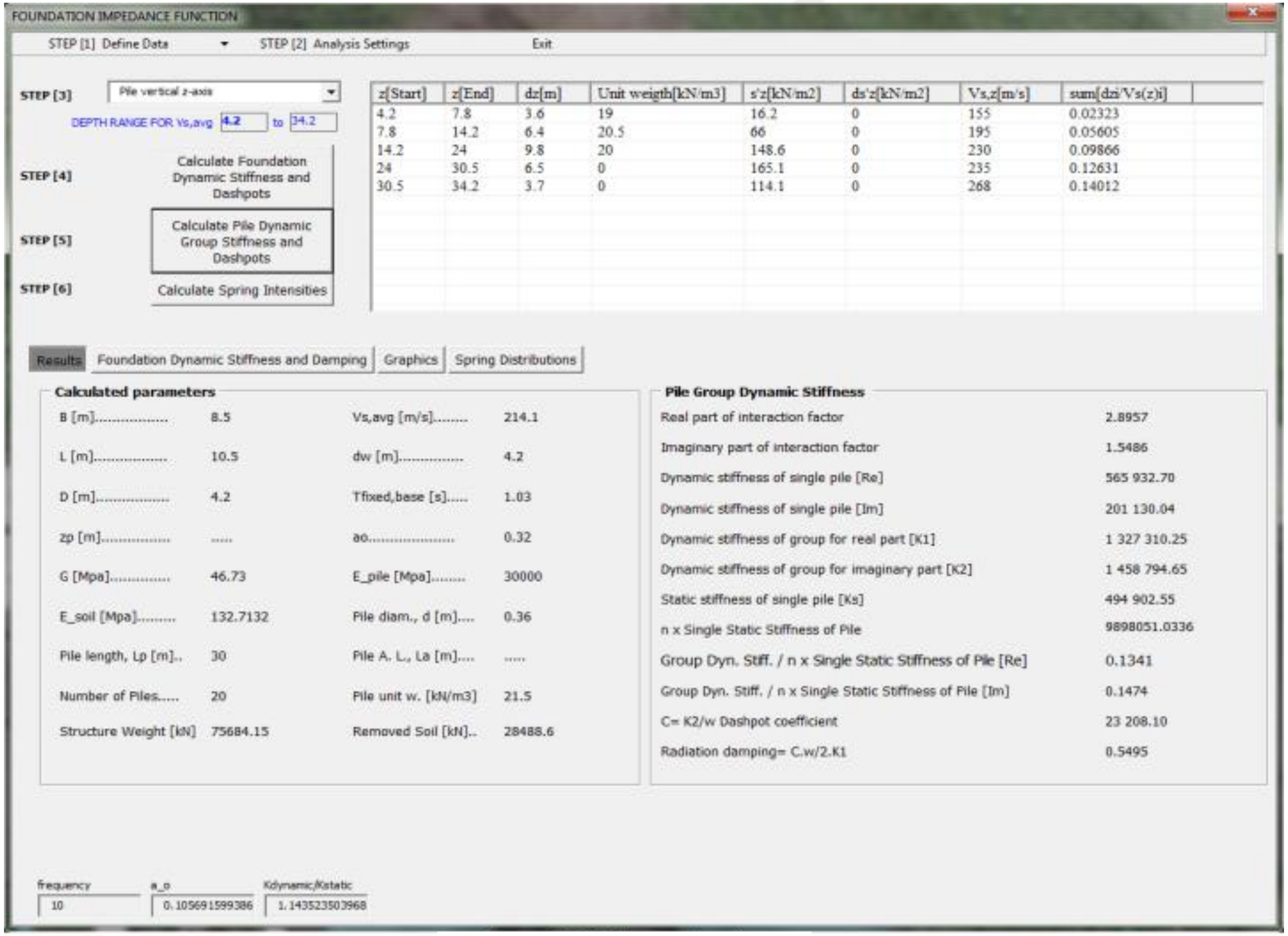

Figure A.1 Main user interface

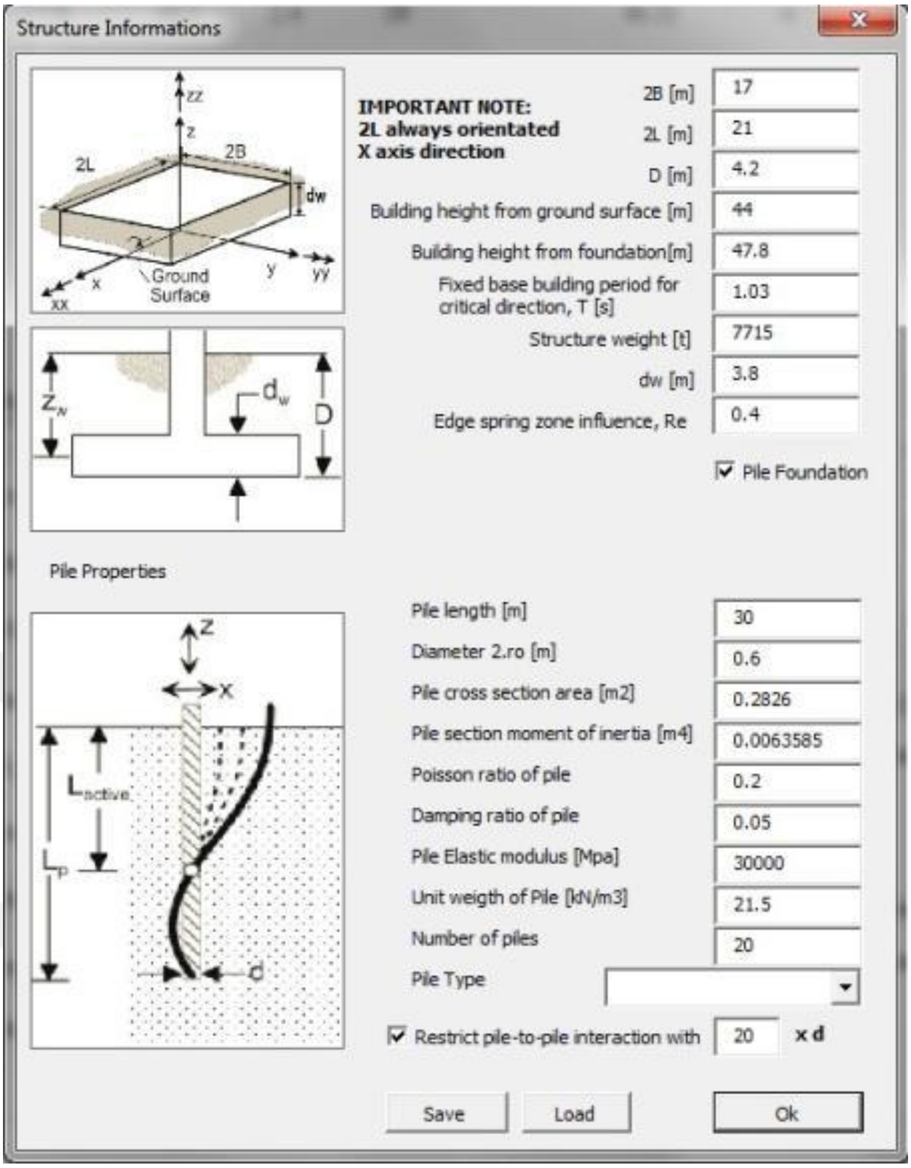

Figure A.2 Defining the general structure and pile properties

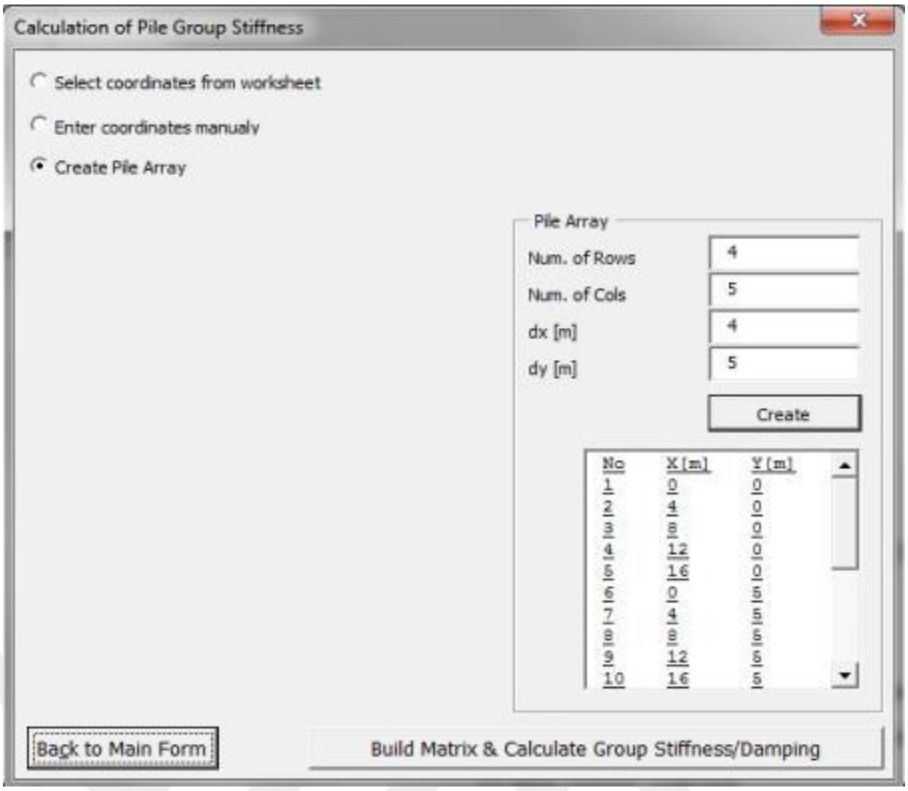

Figure A.3Defining pile layout properties

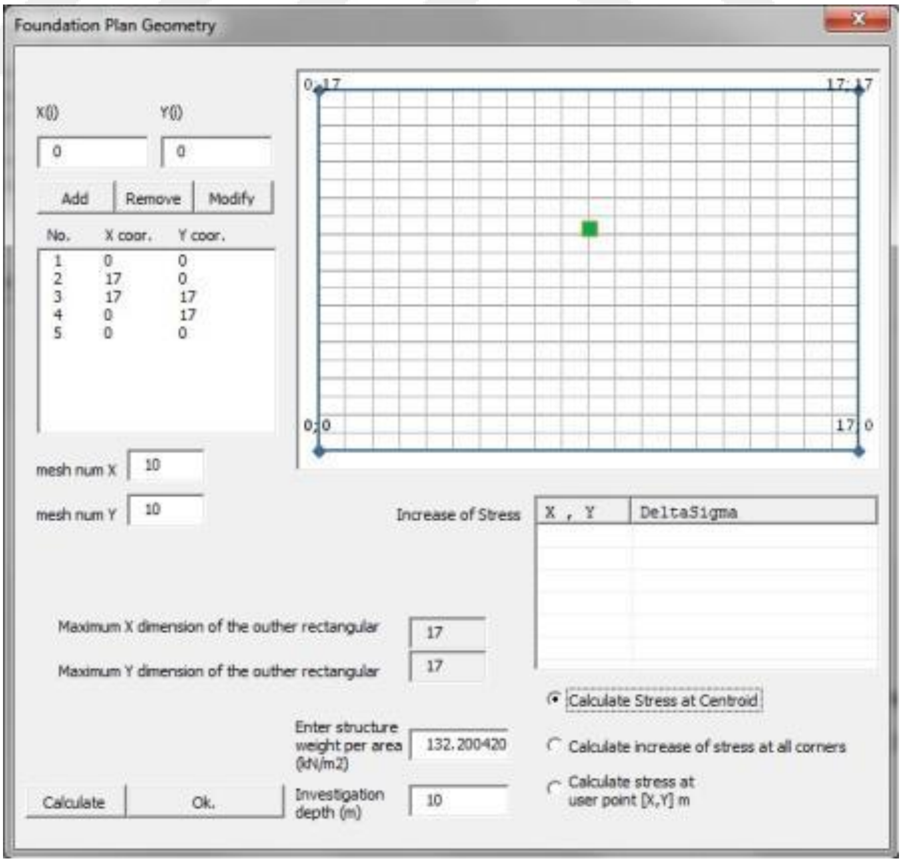

Figure A.4 Stress increase calculation interface

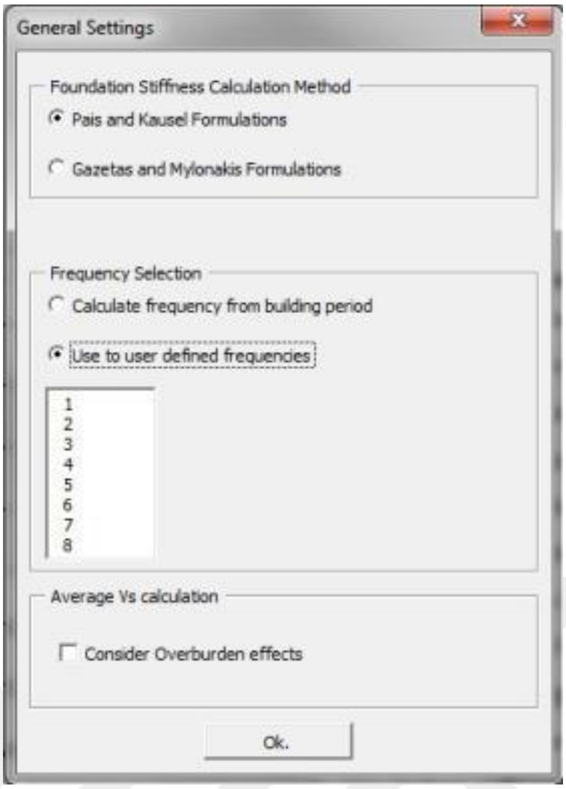

Figure A.5 Analysis options form

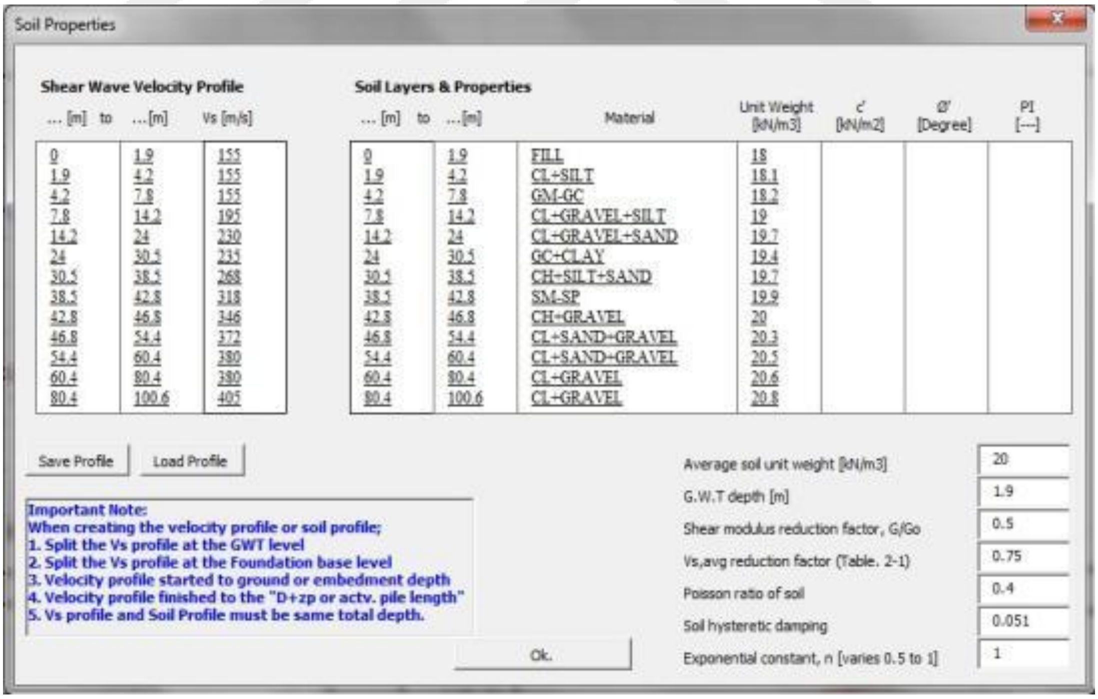

Figure A.6 Soil profile and shear wave velocity profile definition interface.

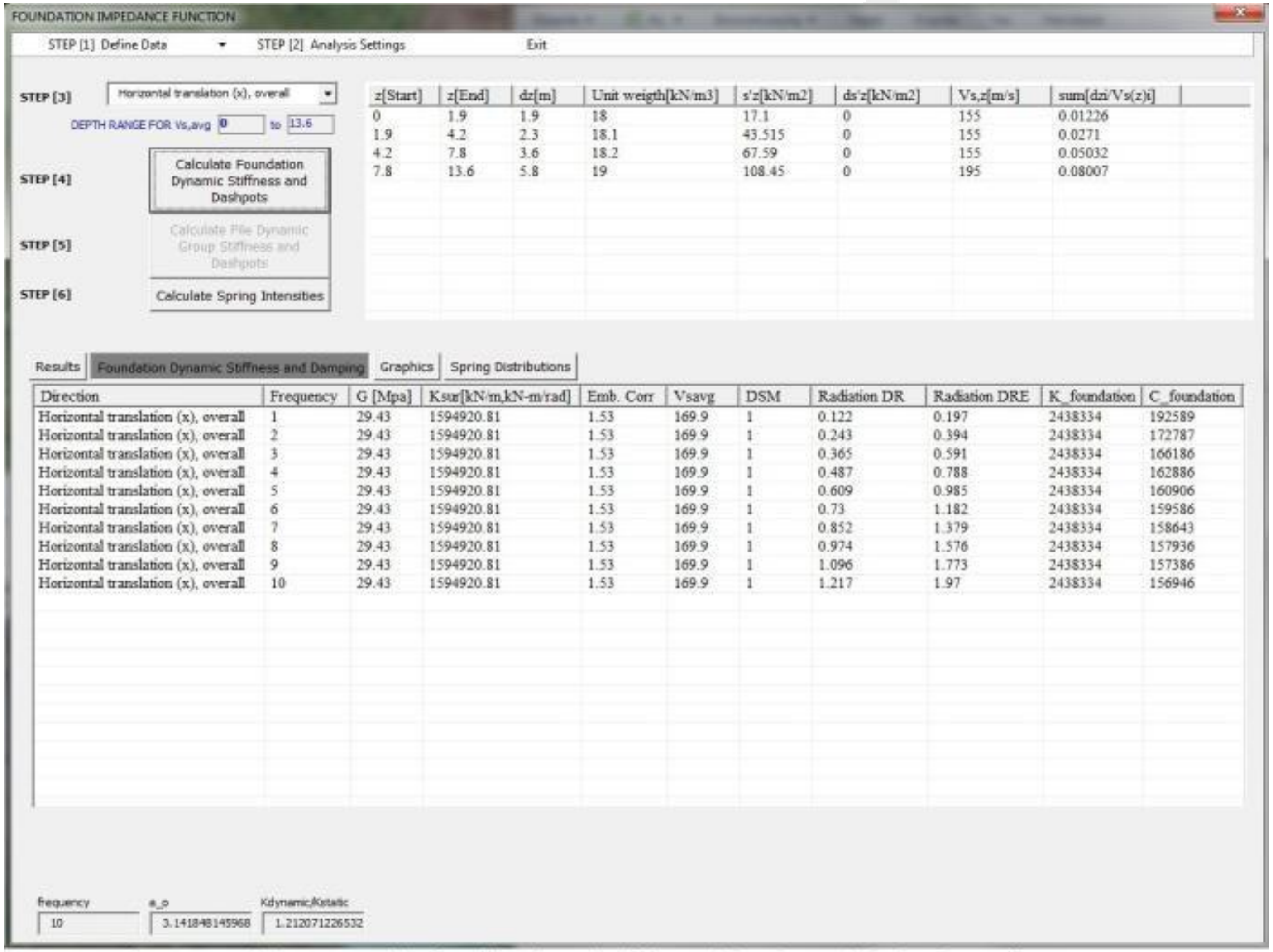

Figure A.7 Tabular output of the foundation dynamic stiffness and damping results in the relevant frequency range

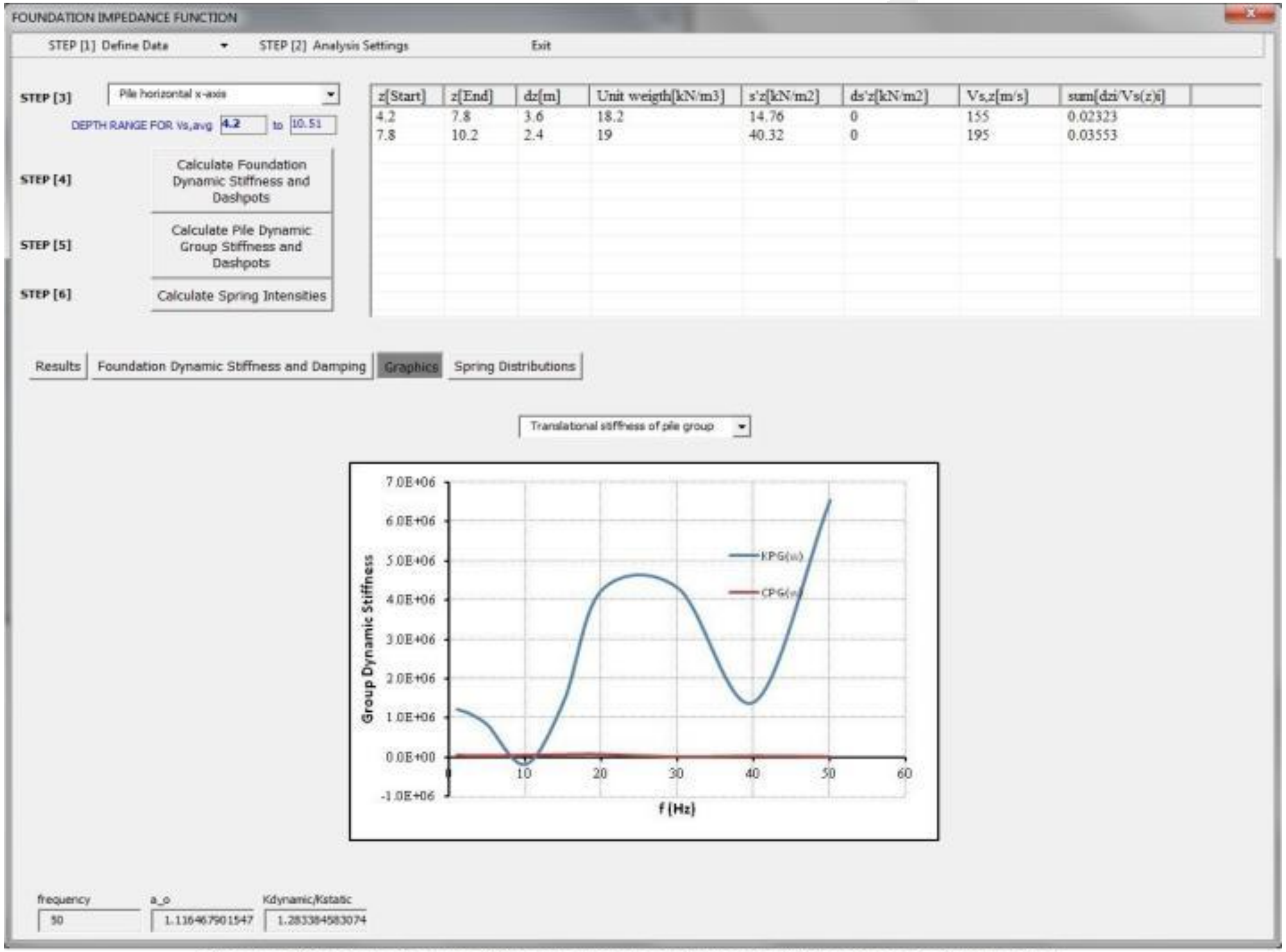

Figure A.8 Graphical output of the pile group lateral dynamic stiffness versus frequency

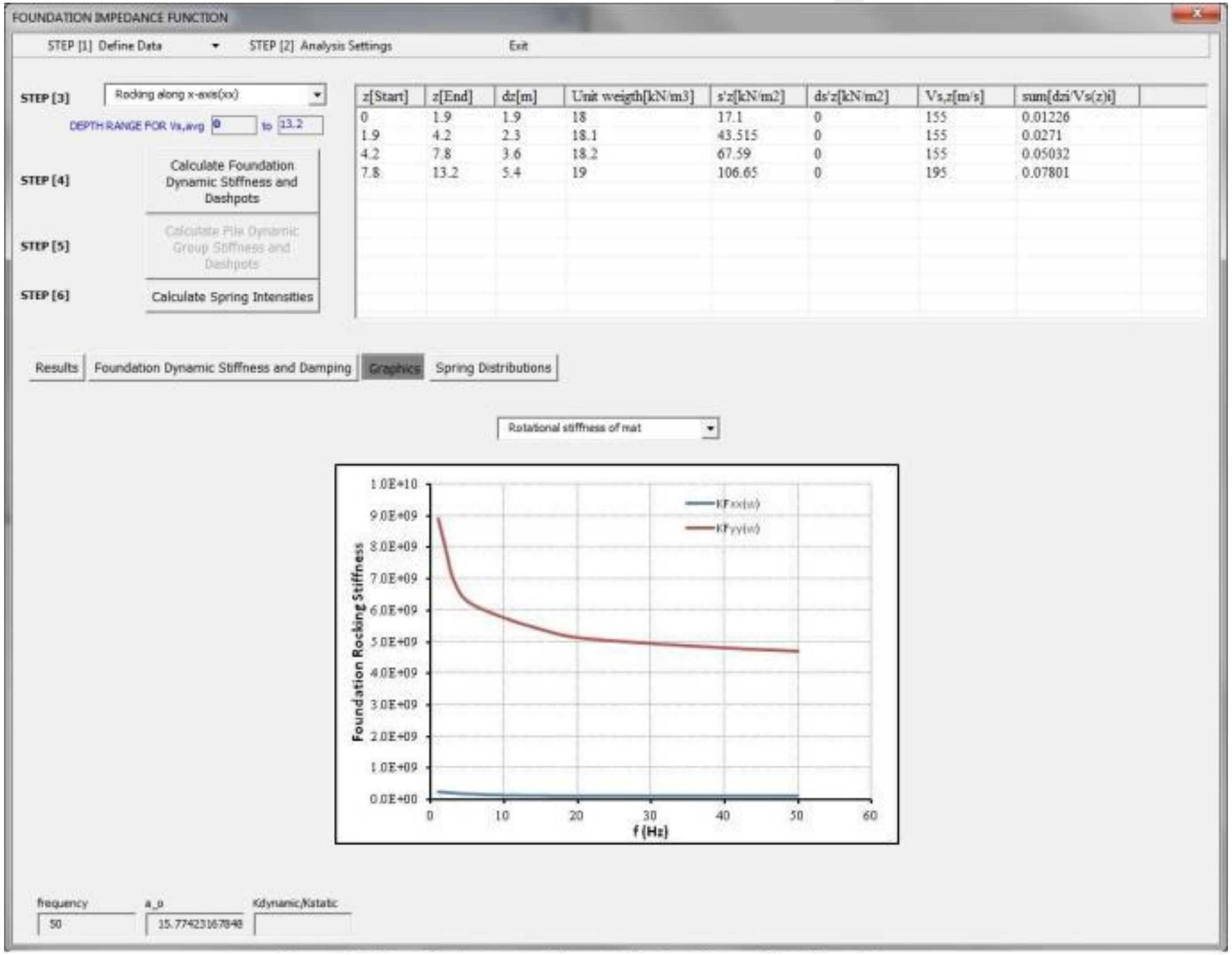

Figure A.9 Graphical output of the rotational stiffness of raft foundation versus frequency

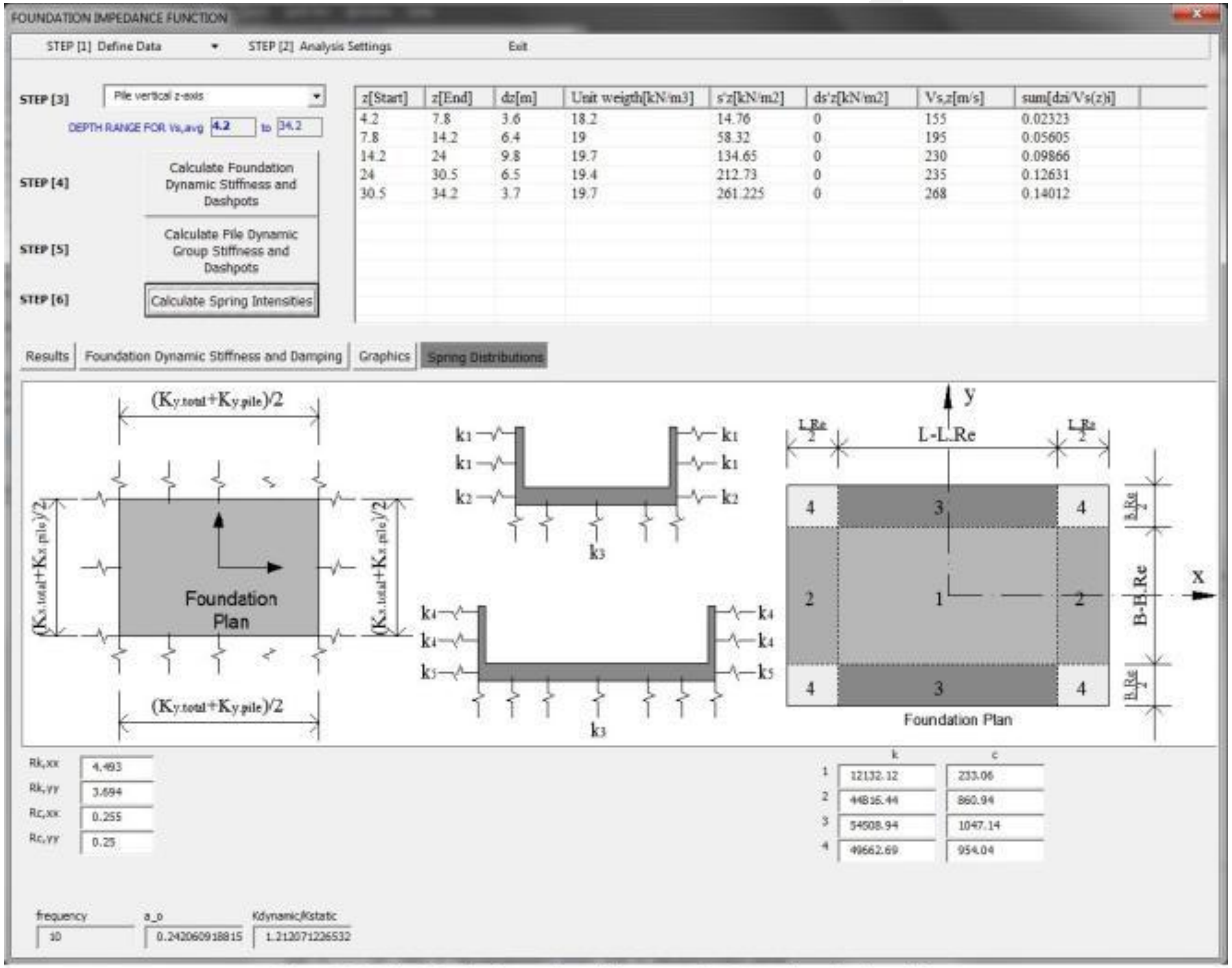

Figure A.10 Distributing the spring stiffness over the foundation base area and perimeter shear walls

APPENDIX B

Shear Modulus Reduction Curve and Damping Curve Parameters For Deep Soil Profile

Table B.1 Material model, G/G_{max} and damping curve parameters

Layer #	Depth (m)	Layer Name	Thickness (m)	Unit Weight (kN/m^3)	Shear Velocity (m/s)	Damping Ratio (%)	Ref. Strain (%)	Ref. Stress (Mpa)	Beta	s	b	d
1	0.0	FILL	0.95	18	155	2.200291	0.0362	0.18	1.575	0.915	0	0
2	1.0	FILL	0.95	18	155	1.325207	0.0034	0.18	0.24	0.63	0	0
3	1.9	CL with SILT	1.15	18.1	155	1.200737	0.0024	0.18	0.18	0.63	0	0
4	3.1	CL with SILT	1.15	18.1	155	1.120467	0.0058	0.18	0.3	0.63	0	0
5	4.2	GM-GC	1.2	18.2	155	0.657545	0.0044	0.18	0.345	0.615	0	0
6	5.4	GM-GC	1.2	18.2	155	0.654686	0.006	0.18	0.39	0.63	0	0
7	6.6	GM-GC	1.2	18.2	155	0.624163	0.0032	0.18	0.255	0.63	0	0
8	7.8	CL with G	1.28	19	195	0.933714	0.0048	0.18	0.225	0.645	0	0
9	9.1	CL with G	1.28	19	195	0.898373	0.0764	0.18	1.305	0.645	0	0
10	10.4	CL with G	1.28	19	195	0.867859	0.0968	0.18	1.485	0.645	0	0
11	11.6	CL with G	1.28	19	195	0.841255	0.1016	0.18	1.5	0.645	0	0
12	12.9	CL with G	1.28	19	195	0.817838	0.0844	0.18	1.305	0.645	0	0
13	14.2	CL with G+S	1.225	19.7	230	0.783056	0.1024	0.18	1.47	0.645	0	0
14	15.4	CL with G+S	1.225	19.7	230	0.764057	0.1052	0.18	1.47	0.645	0	0
15	16.7	CL with G+S	1.225	19.7	230	0.7467	0.0912	0.18	1.32	0.645	0	0
16	17.9	CL with G+S	1.225	19.7	230	0.731	0.095	0.18	1.335	0.645	0	0
17	19.1	CL with G+S	1.225	19.7	230	0.71643	0.1144	0.18	1.485	0.645	0	0
18	20.3	CL with G+S	1.225	19.7	230	0.703175	0.1168	0.18	1.485	0.645	0	0
19	21.6	CL with G+S	1.225	19.7	230	0.690755	0.0806	0.18	1.155	0.645	0	0
20	22.8	CL with G+S	1.225	19.7	230	0.679157	0.1192	0.18	1.47	0.645	0	0
21	24.0	GC	1.3	19.4	235	0.422661	0.002	0.18	0.15	0.63	0	0
22	25.3	GC	1.3	19.4	235	0.416452	0.0052	0.18	0.27	0.63	0	0
23	26.6	GC	1.3	19.4	235	0.408485	0.0048	0.18	0.255	0.63	0	0
24	27.9	GC	1.3	19.4	235	0.402995	0.0032	0.18	0.195	0.63	0	0
25	29.2	GC	1.3	19.4	235	0.395322	0.0054	0.18	0.27	0.63	0	0
26	30.5	CH	2	19.7	268	0.78737	0.118	0.18	1.155	0.66	0	0
27	32.5	CH	2	19.7	268	0.772694	0.1204	0.18	1.155	0.66	0	0
28	34.5	CH	2	19.7	268	0.759174	0.0972	0.18	0.99	0.66	0	0
29	36.5	CH	2	19.7	268	0.74672	0.1014	0.18	1.005	0.66	0	0
30	38.5	SM-SP	2.15	19.9	318	0.354146	0.005	0.18	0.24	0.63	0	0
31	40.7	SM-SP	2.15	19.9	318	0.347571	0.092	0.18	1.485	0.63	0	0
32	42.8	CH with G	2	20	346	0.682925	0.1258	0.18	1.155	0.66	0	0
33	44.8	CH with G	2	20	346	0.673467	0.1012	0.18	0.99	0.66	0	0
34	46.8	CL with S+G	2.533	20.3	372	0.606779	0.141	0.18	1.305	0.66	0	0
35	49.3	CL with S+G	2.533	20.3	372	0.59664	0.0736	0.18	0.84	0.66	0	0
36	51.9	CL with S+G	2.533	20.3	372	0.587357	0.175	0.18	1.47	0.66	0	0
37	54.4	CL with S+G	2	20.5	380	0.579468	0.1484	0.18	1.305	0.66	0	0
38	56.4	CL with S+G	2	20.5	380	0.57264	0.0988	0.18	0.99	0.66	0	0
39	58.4	CL with S+G	2	20.5	380	0.566286	0.1264	0.18	1.155	0.66	0	0
40	60.4	CL with G	2	20.6	380	0.498605	0.114	0.18	1.155	0.645	0	0
41	62.4	CL with G	2	20.6	380	0.510296	0.093	0.18	0.99	0.66	0	0
42	64.4	CL with G	2	20.6	380	0.505099	0.143	0.18	1.305	0.66	0	0
43	66.4	CL with G	2	20.6	380	0.499949	0.0972	0.18	1.005	0.66	0	0
44	68.4	CL with G	2	20.6	380	0.495197	0.1776	0.18	1.485	0.66	0	0
45	70.4	CL with G	2	20.6	380	0.49049	0.097	0.18	0.99	0.66	0	0
46	72.4	CL with G	2	20.6	380	0.486108	0.1516	0.18	1.32	0.66	0	0
47	74.4	CL with G	2	20.6	380	0.481744	0.1012	0.18	1.005	0.66	0	0
48	76.4	CL with G	2	20.6	380	0.477669	0.1262	0.18	1.155	0.66	0	0
49	78.4	CL with G	2	20.6	380	0.473646	0.1008	0.18	0.99	0.66	0	0
50	80.4	CL with G	2.02	20.8	405	0.469678	0.1284	0.18	1.155	0.66	0	0
51	82.4	CL with G	2.02	20.8	405	0.465893	0.08	0.18	0.84	0.66	0	0
52	84.4	CL with G	2.02	20.8	405	0.462207	0.1282	0.18	1.14	0.66	0	0
53	86.5	CL with G	2.02	20.8	405	0.458575	0.1586	0.18	1.305	0.66	0	0
54	88.5	CL with G	2.02	20.8	405	0.455083	0.1052	0.18	0.99	0.66	0	0
55	90.5	CL with G	2.02	20.8	405	0.451754	0.134	0.18	1.155	0.66	0	0
56	92.5	CL with G	2.02	20.8	405	0.448499	0.1094	0.18	1.005	0.66	0	0
57	94.5	CL with G	2.02	20.8	405	0.445253	0.136	0.18	1.155	0.66	0	0
58	96.6	CL with G	2.02	20.8	405	0.442191	0.111	0.18	1.005	0.66	0	0
59	98.6	CL with G	2.02	20.8	405	0.439163	0.138	0.18	1.155	0.66	0	0
60	100.6	CL with G+M	2.2	21.1	482	0.453317	0.1442	0.18	1.155	0.66	0	0

Table B.1 Material model, G/G_{max} and damping curve parameters (Continued)

61	**102.8**	CL with G+M	2.2	21.1	482	0.449942	0.0896	0.18	0.84	0.66	0	0
62	**105.0**	GC	2	20.6	496	0.263622	0.1096	0.18	1.335	0.645	0	0
63	**107.0**	CL with M	4	21.1	540	0.442933	0.1478	0.18	1.155	0.66	0	0
64	**111.0**	GC	3	20.6	600	0.257701	0.108	0.18	1.305	0.645	0	0
65	**114.0**	CL with M+G	5.2	21.8	760	0.433083	0.0936	0.18	0.84	0.66	0	0
66	**119.2**	CL with M+G	5.2	21.8	760	0.426314	0.154	0.18	1.155	0.66	0	0
67	**124.4**	CL with M+G	5.2	21.8	760	0.420116	0.1268	0.18	1.005	0.66	0	0
68	**129.6**	CL with M+G	5.2	21.8	760	0.41424	0.1946	0.18	1.32	0.66	0	0
69	**134.8**	CL with M+G	5.2	21.8	760	0.408733	0.0996	0.18	0.84	0.66	0	0
70	**140.0**	CL	13	22	760	0.387622	0.1056	0.18	0.84	0.66	0	0
71	**153.0**	CL	10	22	668	0.377468	0.176	0.18	1.155	0.66	0	0
72	**163.0**	GP	5	22	600	0.223607	0.1258	0.18	1.32	0.645	0	0
73	**168.0**	CL	4	22	600	0.368027	0.181	0.18	1.155	0.66	0	0
74	**172.0**	CL	46	22	650	0.351116	0.1906	0.18	1.155	0.66	0	0
75	**218.0**	GC	4	22	660	0.199863	0.0936	0.18	1.02	0.645	0	0
76	**222.0**	CLAYSTONE	18	22.5	732	1.778919	0.2512	0.18	0.45	0.75	0	0
77	**240.0**	D1	40	23	800	1.778919	0.2512	0.18	0.45	0.75	0	0
78	**280.0**	D2	40	23	870	1.778919	0.2512	0.18	0.45	0.75	0	0
79	**320.0**	D3	40	23	920	1.778919	0.2512	0.18	0.45	0.75	0	0
80	**360.0**	D4	40	23	980	1.778919	0.2512	0.18	0.45	0.75	0	0
81	**400.0**	D5	40	23	1420	1.778919	0.2512	0.18	0.45	0.75	0	0
82	**440.0**	D6	40	23	1420	1.778919	0.2512	0.18	0.45	0.75	0	0
83	**480.0**	D7	40	23	1420	1.778919	0.2512	0.18	0.45	0.75	0	0
84	**520.0**	D8	40	23	1420	1.778919	0.2512	0.18	0.45	0.75	0	0
85	**560.0**	D9	40	23	1420	1.778919	0.2512	0.18	0.45	0.75	0	0
86	**600.0**	D10	40	23	1420	1.778919	0.2512	0.18	0.45	0.75	0	0
87	**640.0**	D11	100	24	1620	1.778919	0.2512	0.18	0.45	0.75	0	0
88	**740.0**	D12	100	25	1620	1.778919	0.2512	0.18	0.45	0.75	0	0
89	**840.0**	D13	100	26	2150	0.790888	0.35	0.18	0.345	0.795	0	0
90	**940.0**	D14	100	27	2150	0.790888	0.35	0.18	0.345	0.795	0	0
91	**1040.0**	D15	100	30	2150	0.790888	0.35	0.18	0.345	0.795	0	0

APPENDIX C

Foundation Input Motions Obtained from Method-I and Method-II

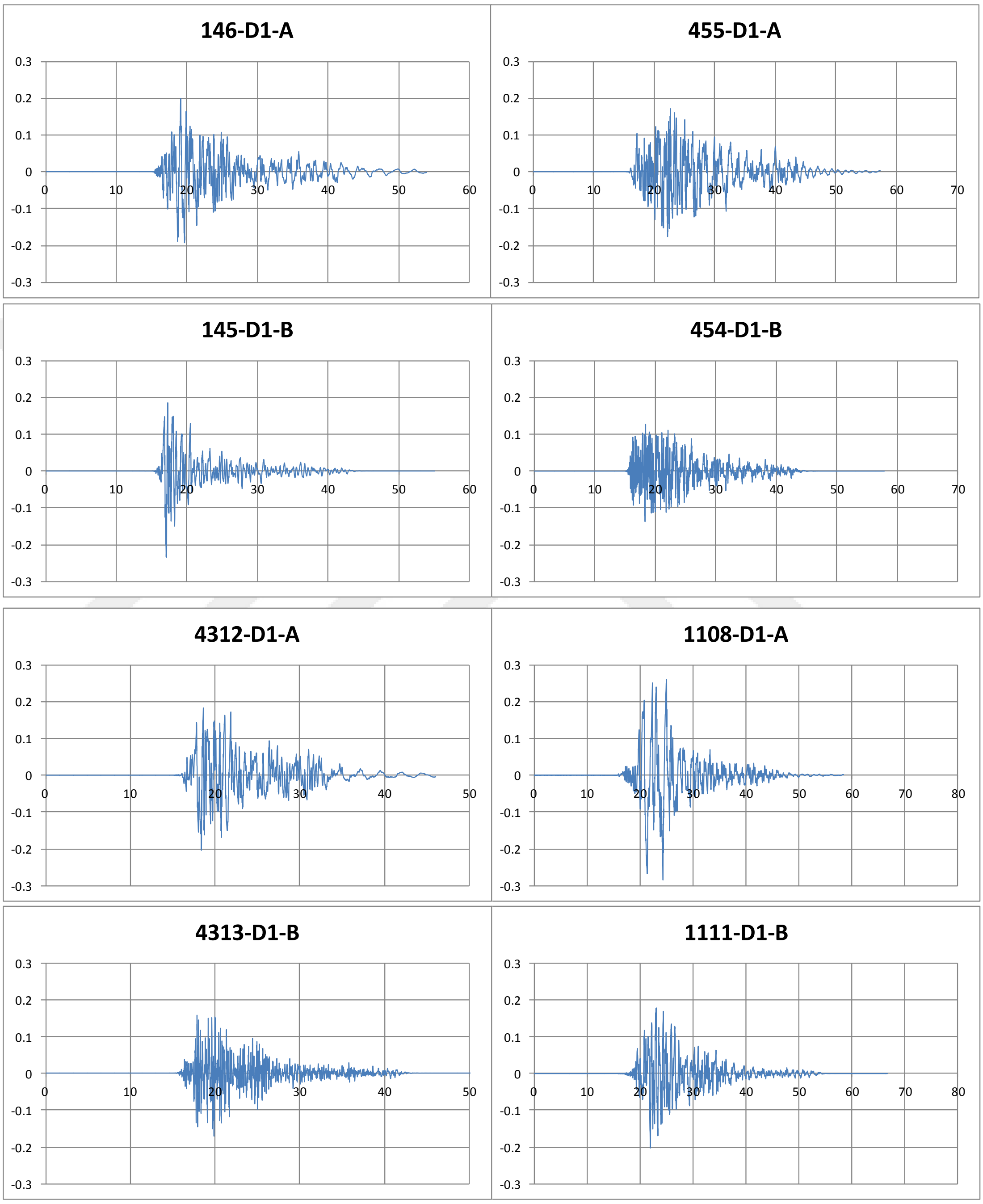

Figure C.1 D1 earthquake intensity level foundation base time histories were obtained from the site response analysis according to the Method-I and Method-II.

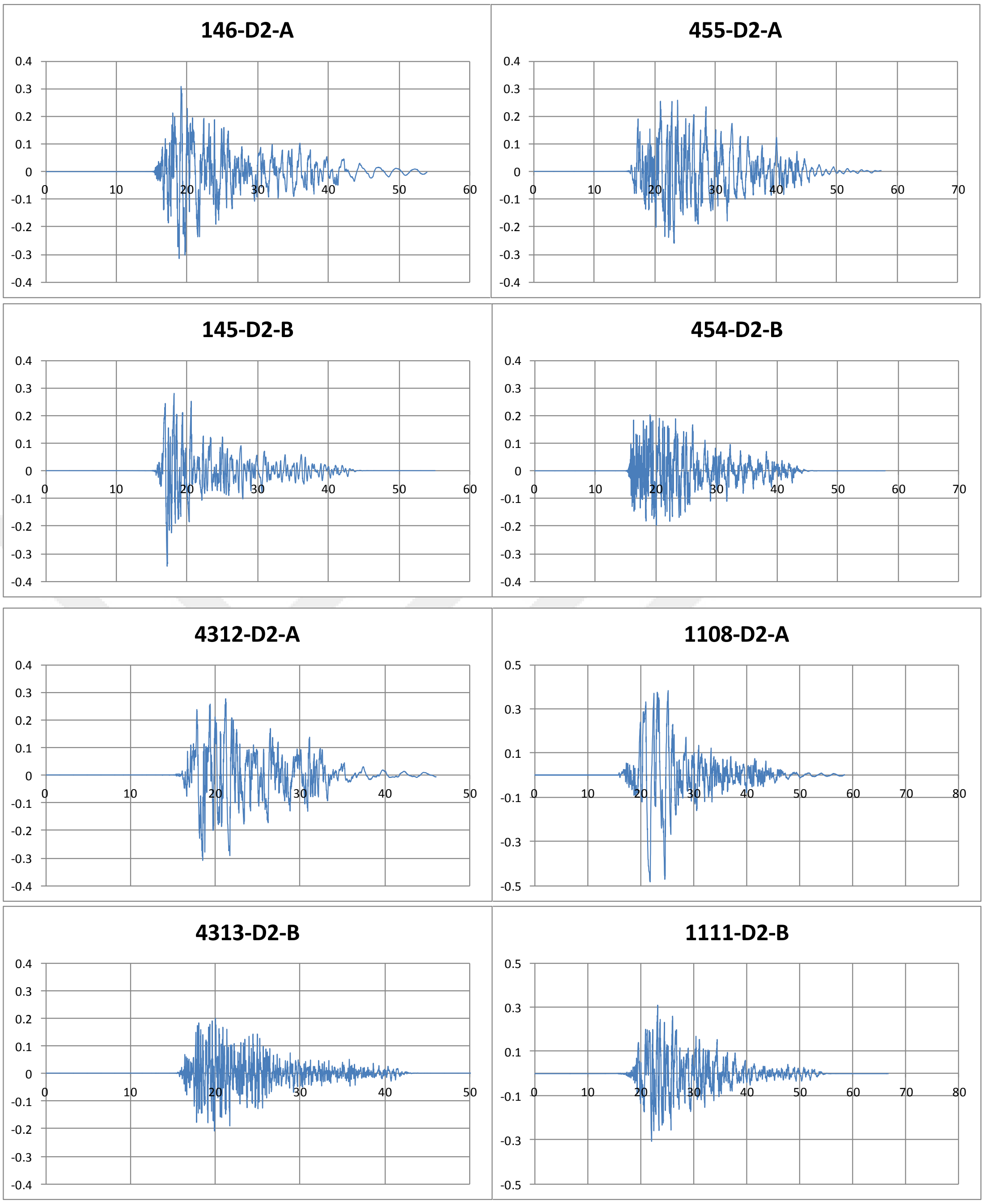

Figure C.2 D2 earthquake intensity level foundation base time histories were obtained from the SRA according to the Method-I and Method-II.

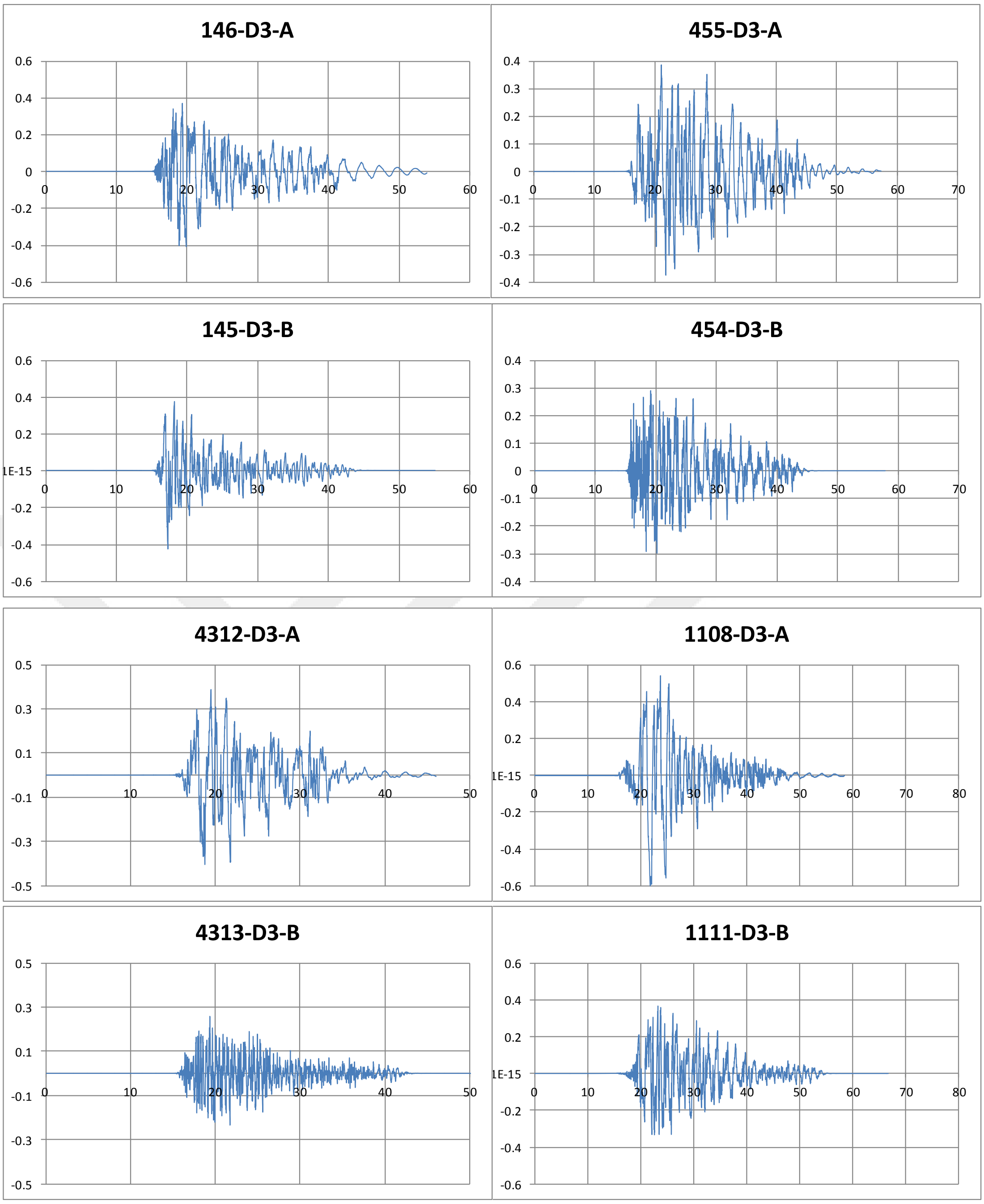

Figure C.3 D3 earthquake intensity level foundation base time histories were obtained from the SRA according to the Method-I and Method-II.

APPENDIX D

Graphical Output of The Dynamic Stiffness of The Foundation According to the Developed Algorithm and DYNAN Software

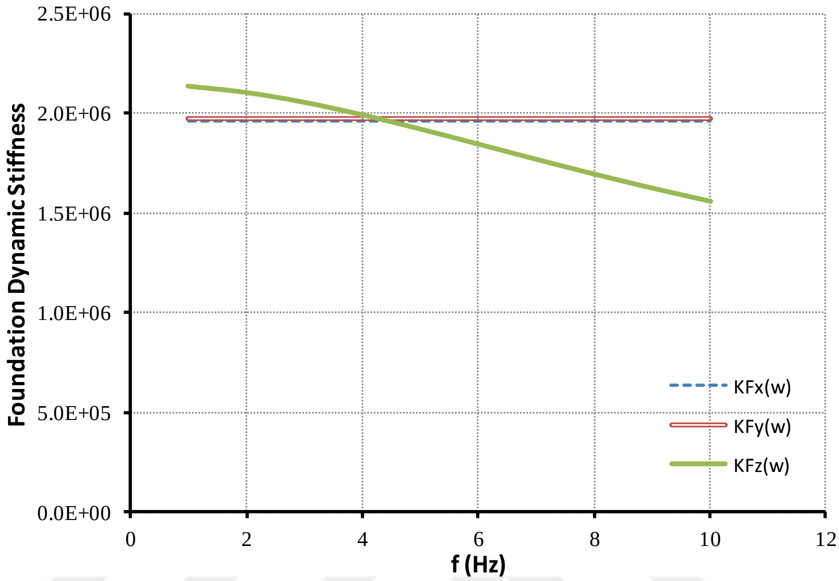

Figure D.1 Foundation translational dynamic stiffness changes in frequency according to Pais and Kausel formulation (Developed Algorithm).

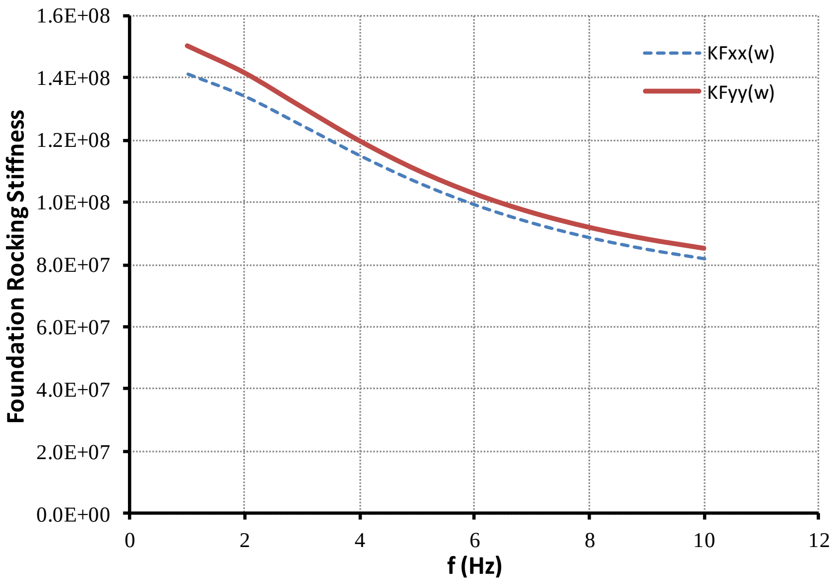

Figure D.2 Foundation rotational dynamic stiffness changes with frequency according to Pais and Kausel formulation (Developed Algorithm).

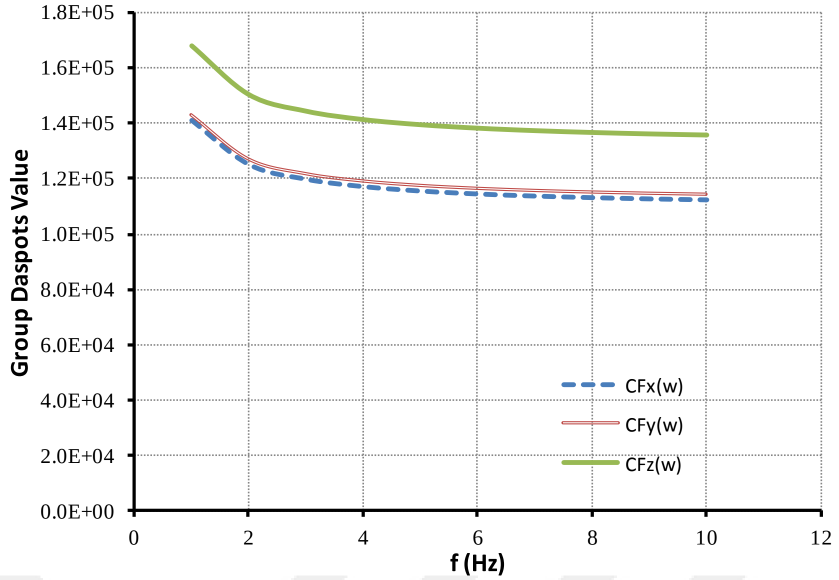

Figure D.3 Foundation translational damping changes with frequency according to Pais and Kausel formulation (Developed Algorithm).

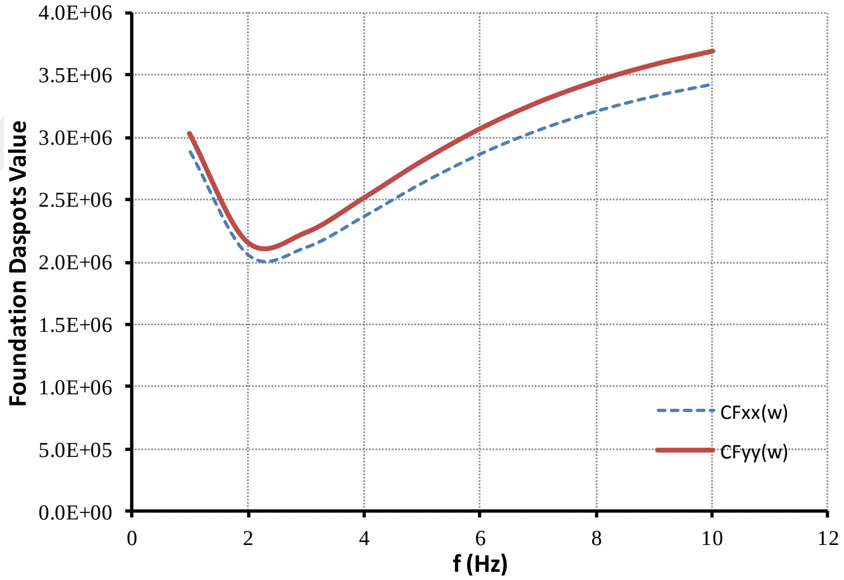

Figure D.4 Foundation rotational damping changes with frequency according to Pais and Kausel formulation (Developed Algorithm).

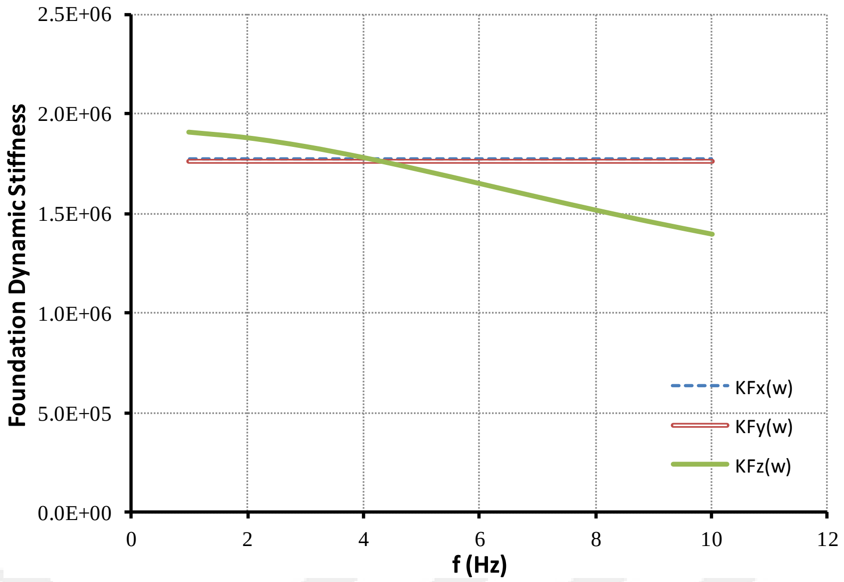

Figure D.5 Foundation translational dynamic stiffness changes in frequency according to Mylonakis and Gazetas formulation (Developed Algorithm).

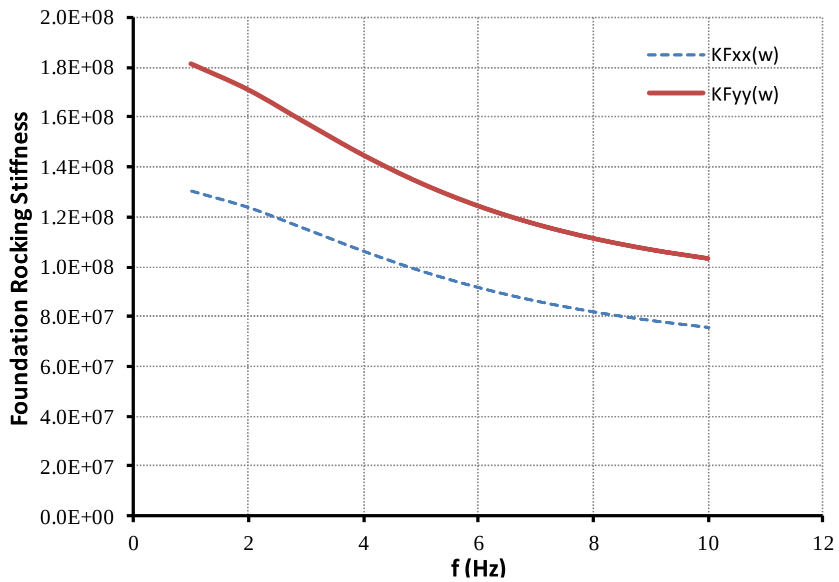

Figure D.6 Foundation rotational dynamic stiffness changes in frequency according to Mylonakis and Gazetas formulation (Developed Algorithm).

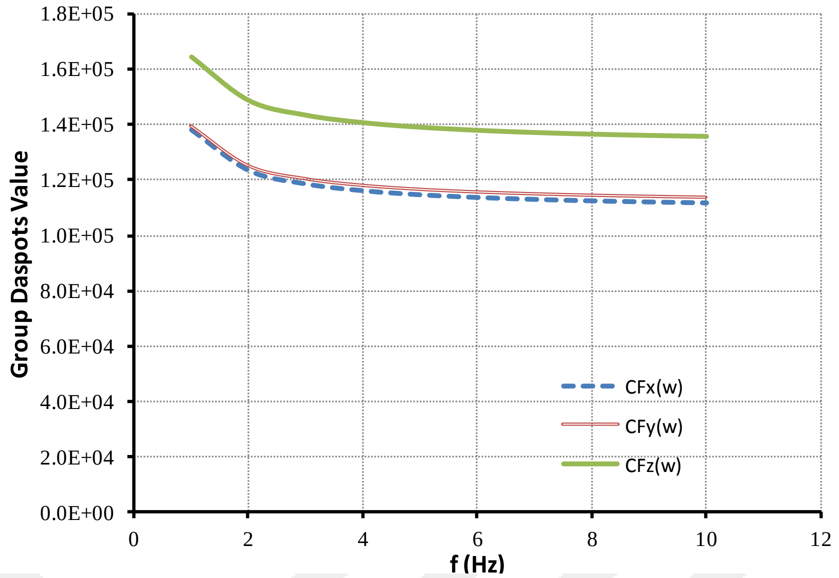

Figure D.7 Foundation translational damping changes in frequency according to Mylonakis and Gazetas formulation (Developed Algorithm).

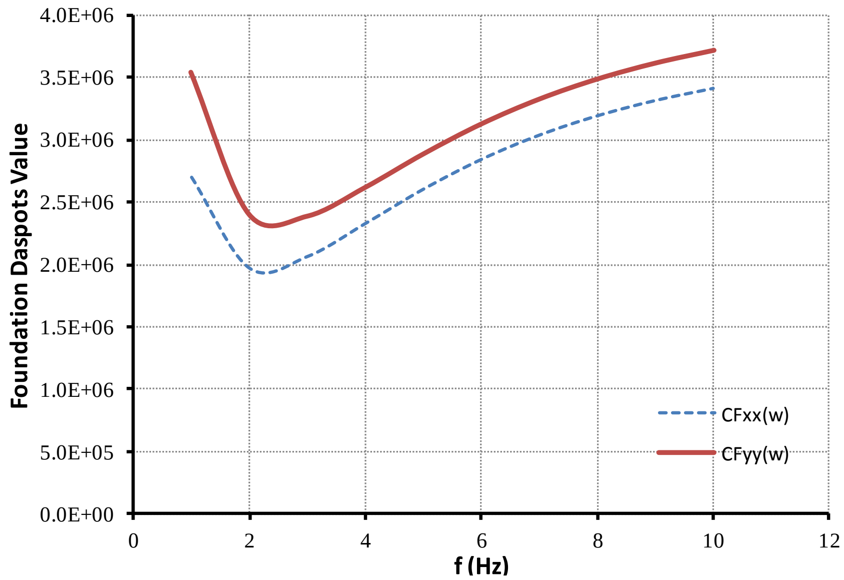

Figure D.8 Foundation rotational damping changes in frequency according to Mylonakis and Gazetas formulation (Developed Algorithm).

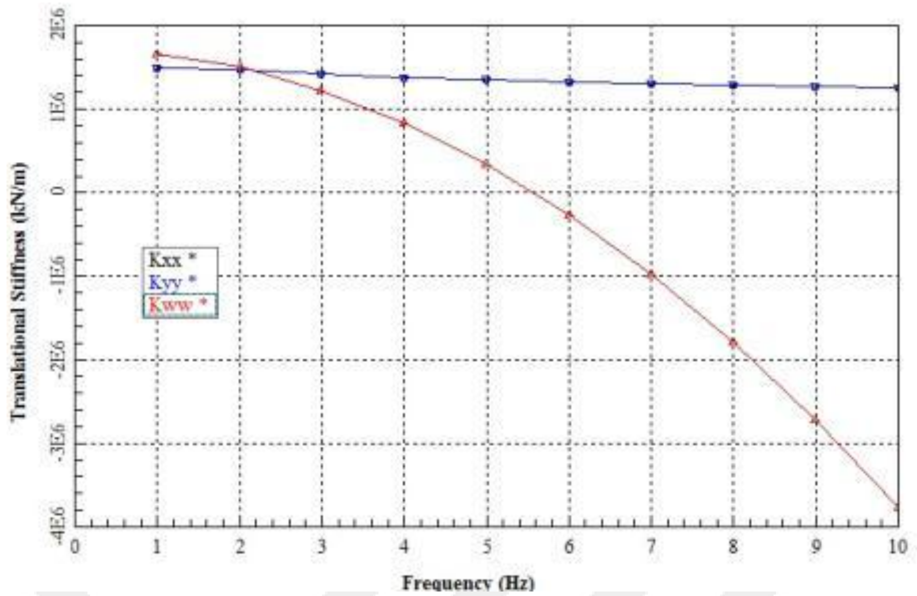

Figure D.9 Foundation translational stiffness changes in frequency according to DYNAN software

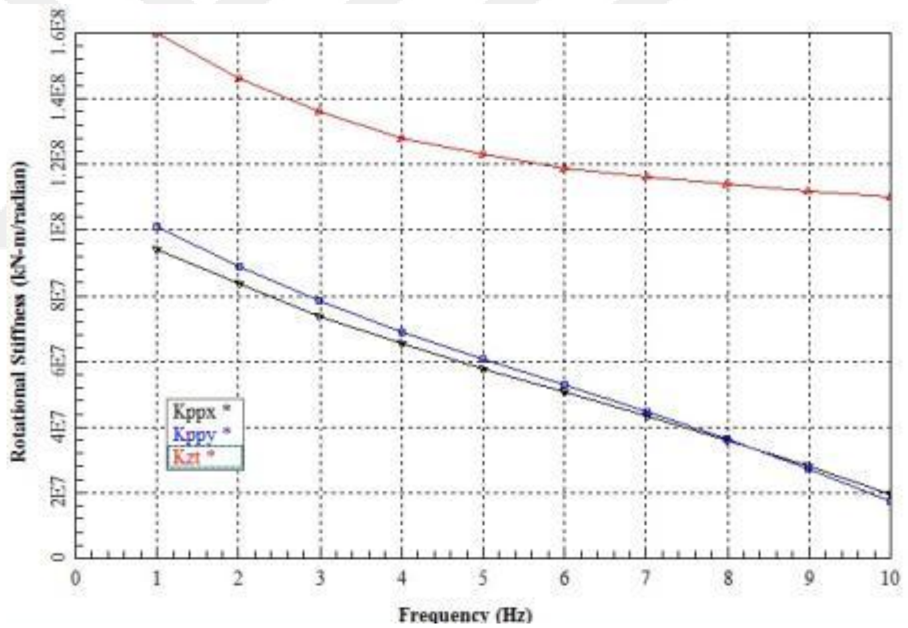

Figure D.10 Foundation rotational stiffness changes in frequency according to DYNAN software

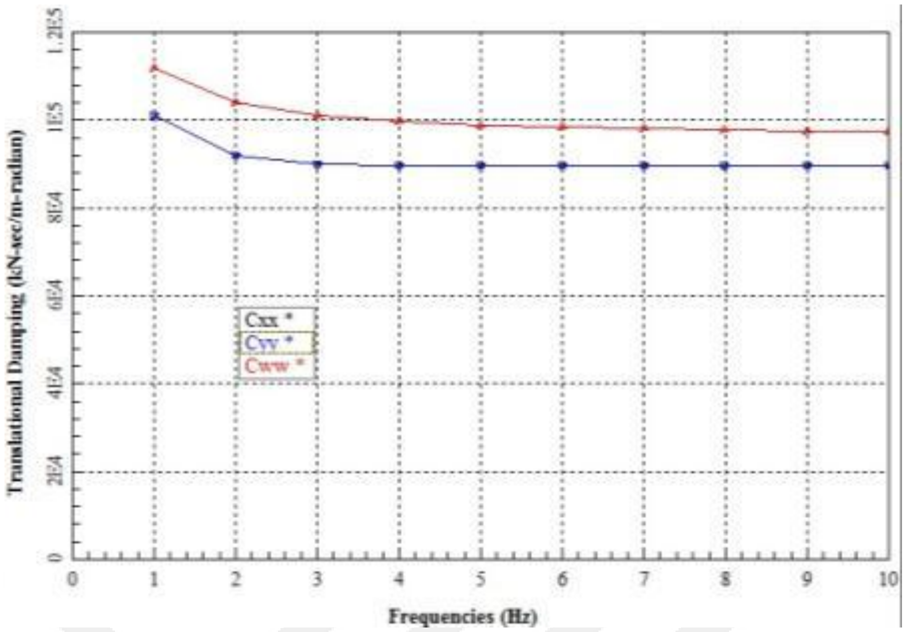

Figure D.11 Foundation translational damping changes in frequency according to DYNAN software

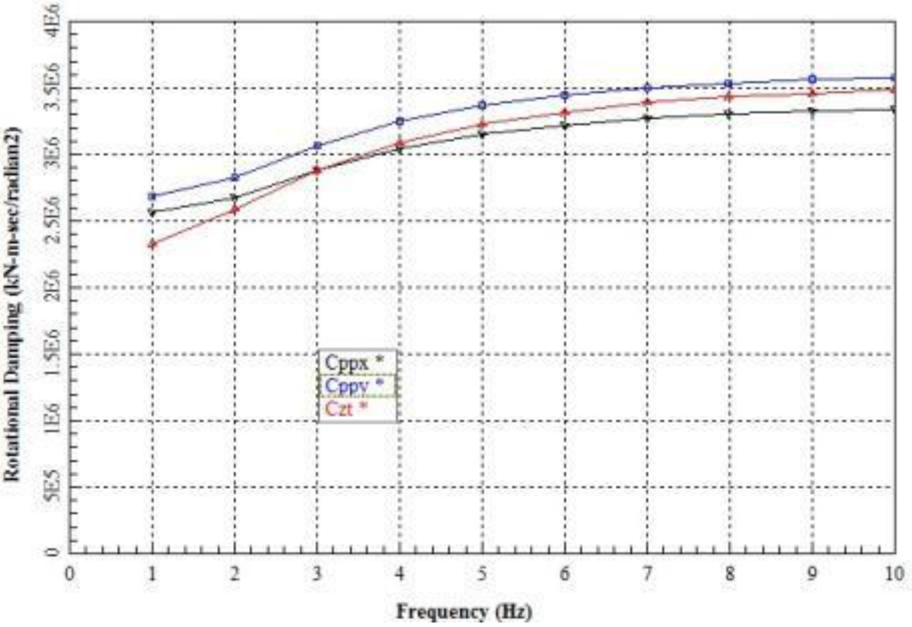

Figure D.12 Foundation rotational damping changes in frequency according to DYNAN software

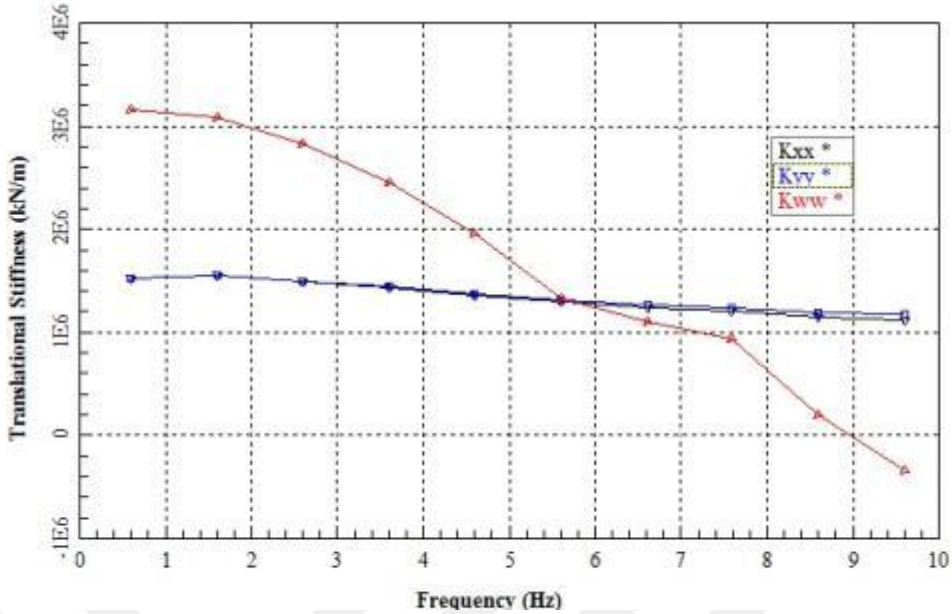

Figure D.13 Piled foundation translational stiffness changes in frequency according to DYNAN software

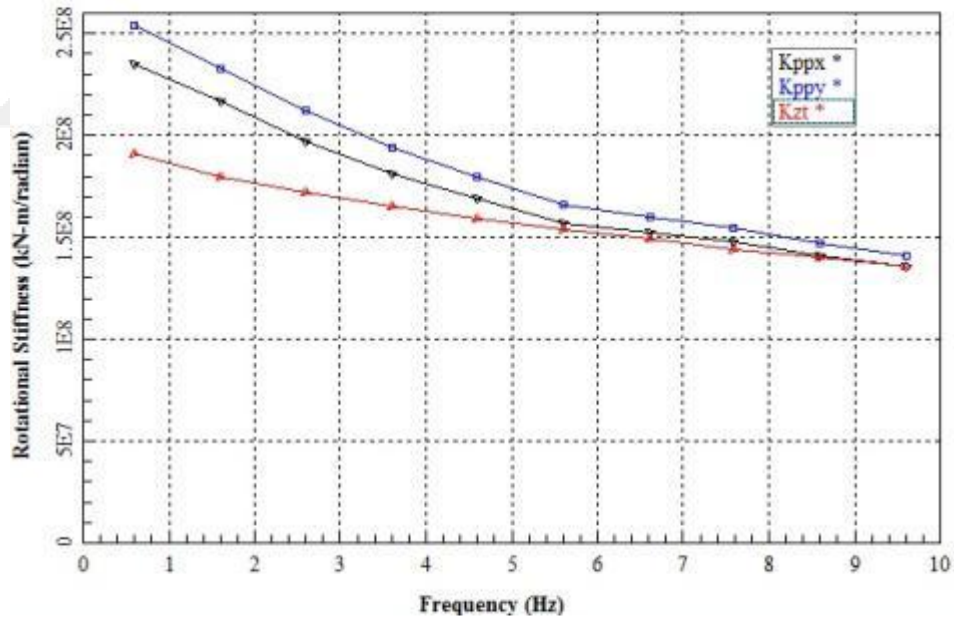

Figure D.14 Piled foundation rotational stiffness changes in frequency according to DYNAN software

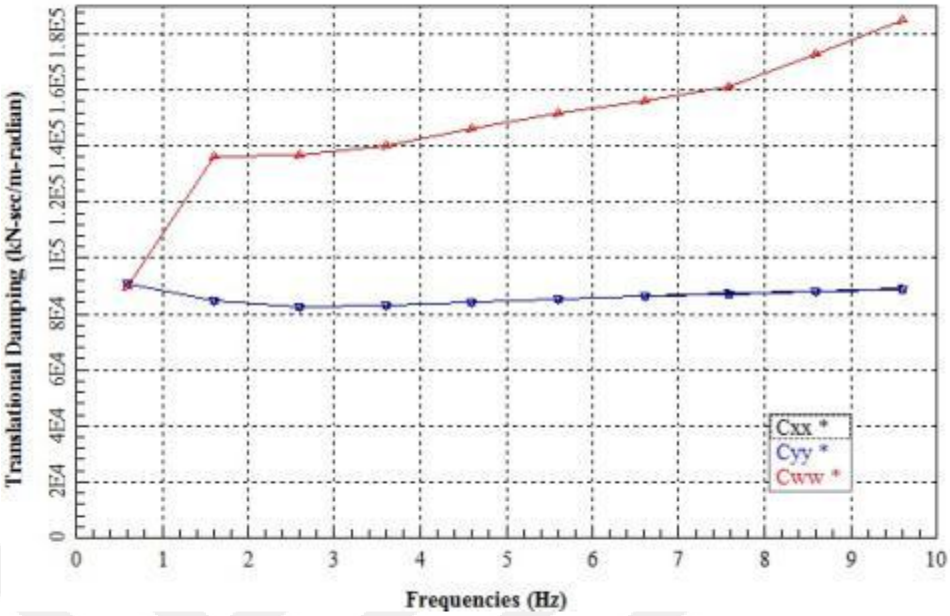

Figure D.15 Piled foundation translational damping changes in frequency according to DYNAN software

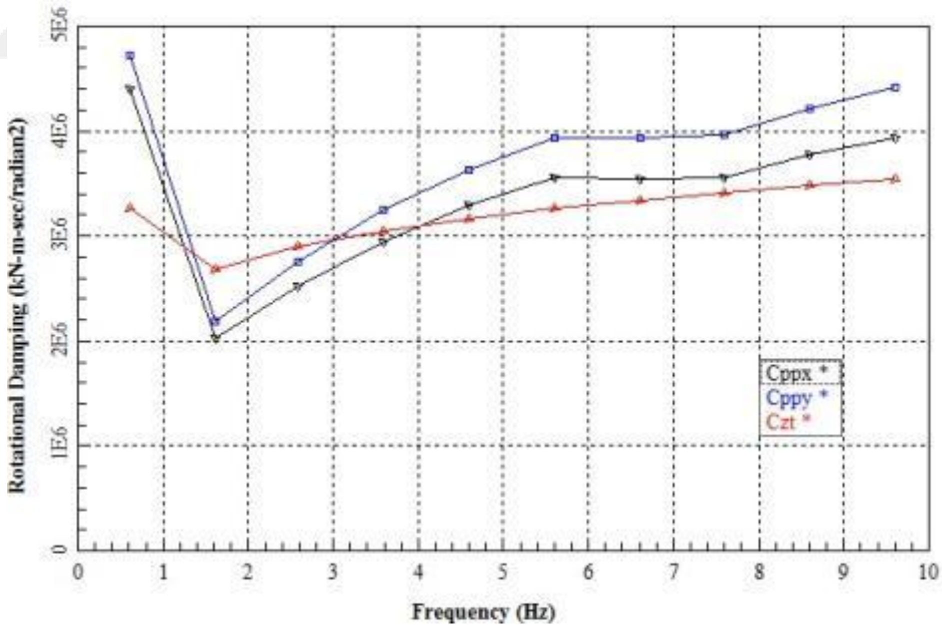

Figure D.16 Piled foundation rotational damping changes in frequency according to DYNAN software

APPENDIX E

Hand Calculation of The Rigid Footing Dynamic Stiffness of The Example Building

Required Data for Dynamic Stiffness Calculations

The foundation half size in the short direction, B (m): 7.2

The foundation half size in the long direction, L (m): 7.625

The foundation embedment depth, D (m): 4.2

Average Soil Poisson's ratio: 0.4

Flexible base period of structure, T_f (second): 1.66

Soil average unit weight (kN/m^3): 20

Average Shear Wave Velocity of the Active Profile Depth

Table E.1 Calculation of the active profile depth, z_p (m):

Vibration Mode	**Equations**	**z_p (m)**	**D+z_p (m)**
Horizontal translation x, y	$\sqrt{BL}$	$=\sqrt{7.2*7.625}=7.41$	7.41+4.2=11.61
Vertical Translation z	$\sqrt{BL}$	$=\sqrt{7.2*7.625}=7.41$	7.41+4.2=11.61
Rocking along xx	$\sqrt[4]{B^3L}$	$=\sqrt[4]{7.2^3*7.625}=7.3$	7.3+4.2=11.50
Rocking along yy	$\sqrt[4]{BL^3}$	$=\sqrt[4]{7.2*7.625^3}=7.52$	7.52+4.2=11.72

The profile depth is discretized into layers having thickness Δ_{zi} and velocity $V_{s,(z)i}$ as shown in Table E.2~E.4. Vs,avg values were calculated from equation 3.10

Table E.2 Translation x, y, z $V_{s,avg}$ calculations

z_i	**z_{i+1}**	**$\Delta z_i = z_{i+1} - z_i$**	**$V_{s(z)i}$**	**$\Delta z_i / V_{s(z)i}$**	**$V_{s,avg}$**
m	**m**	**m**	**m/s**	**m/m/s**	**m/s**
0	1.9	1.9-0=1.9	155	1.9/155=0.0123	11.61/0.0698=166.3
1.9	4.2	4.2-1.9=2.3	155	2.3/155=0.0148	
4.2	7.8	7.8-4.2=3.6	155	3.6/155=0.0232	
7.8	11.6	11.6-7.8=3.8	195	3.8/195=0.0195	
				Σ=0.0698	

Table E.3 Rocking mode (xx) Vs,avg calculations

z_i	z_{i+1}	$\Delta z_i = z_{i+1} - z_i$	$V_{s(z)i}$	$\Delta z_i / V_{s(z)i}$	$V_{s,avg}$
m	**m**	**m**	**m/s**	**m/m/s**	**m/s**
0	1.9	1.9-0=1.9	155	1.9/155=0.0123	11.5/0.0693=165.9
1.9	4.2	4.2-1.9=2.3	155	2.3/155=0.0148	
4.2	7.8	7.8-4.2=3.6	155	3.6/155=0.0232	
7.8	11.5	11.5-7.8=3.7	195	3.7/195=0.019	
				Σ=0.0693	

Table E.4 Rocking mode (yy) Vs,avg calculations

z_i	z_{i+1}	$\Delta z_i = z_{i+1} - z_i$	$V_{s(z)i}$	$\Delta z_i / V_{s(z)i}$	$V_{s,avg}$
m	**m**	**m**	**m/s**	**m/m/s**	**m/s**
0	1.9	1.9-0=1.9	155	1.9/155=0.0123	11.7/0.0703=166.4
1.9	4.2	4.2-1.9=2.3	155	2.3/155=0.0148	
4.2	7.8	7.8-4.2=3.6	155	3.6/155=0.0232	
7.8	11.7	11.7-7.8=3.9	195	3.9/195=0.02	
				Σ=0.0703	

Calculation of the Shear Modulus of the Active Profile Depth

For translational vibration mode:

$$G_{\max} = \rho_s * V_{s,avg}^2 = \left(\frac{20}{9.81}\right) * 166.3^2 = 56382.7\, kN/m2 = 56.4 MPa$$

For rocking x axis:

$$G_{\max} = \rho_s * V_{s,avg}^2 = \left(\frac{20}{9.81}\right) * 165.9^2 = 56111.7\, kN/m2 = 56.1 MPa$$

For rocking y axis:

$$G_{\max} = \rho_s * V_{s,avg}^2 = \left(\frac{20}{9.81}\right) * 166.4^2 = 56450.5\, kN/m2 = 56.5 MPa$$

Reduction in the shear modulus for considering soil nonlinearity

From Table 3.5 for site class D and for PGA≈0.5g ;

G/Gmax was selected 0.5. Thereby, shear modulus can be obtained as follows;

Translational vibration modes (x, y, z): G = 56.4 * 0.5 = 28.2 MPa

Rocking along xx axis: G = 56.1*0.5 = 28.05 MPa

Rocking along yy axis: G = 56.5*0.5 = 28.25 MPa

Static Stiffness Of The Surface Foundation (Table 3.1 Pais and Kausel)

Static stiffness of the foundation must be calculated for obtaining the dynamic stiffness of the foundation. Thereby, static stiffness of the raft foundation can be obtained for relevant vibration modes as follows;

$$K_{x,sur} = \frac{GB}{2-v}\left[6.8\left(\frac{L}{B}\right)^{0.65} + 2.4\right] = \frac{28.2*7.2}{2-0.4}\left[6.8\left(\frac{7.625}{7.2}\right)^{0.65} + 2.4\right] = 1200255 = 1.2E+6\ kN/m$$

$$K_{y,sur} = \frac{GB}{2-v}\left[6.8\left(\frac{L}{B}\right)^{0.65} + 0.8\left(\frac{L}{B}\right) + 1.6\right] = \frac{28.2*7.2}{2-0.4}\left[6.8\left(\frac{7.625}{7.2}\right)^{0.65} + 0.8\left(\frac{7.625}{7.2}\right) + 1.6\right]$$

$$= 1206248 = 1.2E+6\ kN/m$$

$$K_{z,sur} = \frac{GB}{1-v}\left[3.1\left(\frac{L}{B}\right)^{0.75} + 1.6\right] = \frac{28.2*7.2}{1-0.4}\left[3.1\left(\frac{7.625}{7.2}\right)^{0.75} + 1.6\right] = 1636587 = 1.64E+6\ kN/m$$

$$K_{xx,sur} = \frac{GB^3}{1-v}\left[3.2\left(\frac{L}{B}\right) + 0.8\right] = \frac{28.05*7.2^3}{1-0.4}\left[3.2\left(\frac{7.625}{7.2}\right) + 0.8\right] = 73093363 = 7.31E+7\ kN/m$$

$$K_{yy,sur} = \frac{GB^3}{1-v}\left[3.73\left(\frac{L}{B}\right)^{2.4} + 0.27\right] = \frac{28.25*7.2^3}{1-0.4}\left[3.73\left(\frac{7.625}{7.2}\right)^{2.4} + 0.27\right] = 79968005 = 8E+7\ kN/m$$

Embedment Correction Factors for Static Stiffness of Rigid Footings (Table 3.2 Pais and Kausel)

$$\eta_X \approx \eta_y = \left[1 + \left(0.33 + \frac{1.34}{1+L/B}\right)\left(\frac{D}{B}\right)^{0.8}\right] = \left[1 + \left(0.33 + \frac{1.34}{1+7.625/7.2}\right)\left(\frac{4.2}{7.2}\right)^{0.8}\right] = 1.64$$

$$\eta_Z = \left[1 + \left(0.25 + \frac{0.25}{L/B}\right)\left(\frac{D}{B}\right)^{0.8}\right] = \left[1 + \left(0.25 + \frac{0.25}{7.625/7.2}\right)\left(\frac{4.2}{7.2}\right)^{0.8}\right] = 1.32$$

$$\eta_{xx} = \left[1+\frac{D}{B}+\left(\frac{1.6}{0.35+L/B}\right)\left(\frac{D}{B}\right)^2\right] = \left[1+\frac{4.2}{7.2}+\left(\frac{1.6}{0.35+7.625/7.2}\right)\left(\frac{4.2}{7.2}\right)^2\right] = 1.97$$

$$\eta_{yy} = \left[1+\frac{D}{B}+\left(\frac{1.6}{0.35+(L/B)^4}\right)\left(\frac{D}{B}\right)^2\right] = \left[1+\frac{4.2}{7.2}+\left(\frac{1.6}{0.35+(7.625/7.2)^4}\right)\left(\frac{4.2}{7.2}\right)^2\right] = 1.92$$

Static Stiffness of the Embedded Rigid Footings

For each degree of freedom;

$$K_{emb} = \eta K_{sur}$$

$$K_{x,emb} = \eta_x K_{x,sur} = 1.64*1200255 = 1968418 = 1.97E+6\ kN/m$$

$$K_{y,emb} = \eta_y K_{y,sur} = 1.64*1206248 = 1978247 = 1.98E+6\ kN/m$$

$$K_{z,emb} = \eta_z K_{z,sur} = 1.32*1636587 = 2160295 = 2.16E+6\ kN/m$$

$$K_{xx,emb} = \eta_{xx} K_{xx,sur} = 1.97*73093363 = 143993925 = 1.44E+8\ kN/m$$

$$K_{yy,emb} = \eta_{yy} K_{yy,sur} = 1.92*79968005 = 153538570 = 1.54E+8\ kN/m$$

Dynamic Stiffness Modifiers for Rigid Footings

Angular frequency:

$$\omega = 2*\pi/T = 2*\pi/1.66 = 3.785$$

Dimensionless frequency:

$a_0 = \omega * B/V_{s,avg} = 3.785*7.2/166.3 = 0.164$ for translational vibration modes

$a_0 = \omega * B/V_{s,avg} = 3.785*7.2/165.9 = 0.164$ for rocking along x axis

$a_0 = \omega * B/V_{s,avg} = 3.785*7.2/166.4 = 0.164$ for rocking along y axis

A coefficient where used in the formulas can be calculated as follow;

$$\psi = \sqrt{2(1-v)/(1-2v)} = \sqrt{2(1-0.4)/(1-2*0.4)} = 2.449$$

Dynamic stiffness modifiers for translational x and y axis;

$$\alpha_x = \alpha_y = 1$$

For translational z axis;

$$\alpha_z = 1 - \left[\frac{\left(0.4 + \frac{0.2}{L/B}\right) a_0^2}{\left(\frac{10}{1+3(L/B-1)}\right) + a_0^2} \right] = 1 - \left[\frac{\left(0.4 + \frac{0.2}{7.625/7.2}\right) * 0.164^2}{\left(\frac{10}{1+3(7.625/7.2-1)}\right) + 0.164^2} \right] = 0.998$$

For rocking along x axis;

$$\alpha_{xx} = 1 - \left[\frac{\left(0.55 + 0.01\sqrt{L/B-1}\right) a_0^2}{\left(2.4 - \frac{0.4}{(L/B)^3}\right) + a_0^2} \right] = 1 - \left[\frac{\left(0.55 + 0.01\sqrt{7.625/7.2-1}\right) * 0.164^2}{\left(2.4 - \frac{0.4}{(7.625/7.2)^3}\right) + 0.164^2} \right] = 0.993$$

For rocking along y axis;

$$\alpha_{yy} = 1 - \left[\frac{(0.55) a_0^2}{\left(0.6 + \frac{1.4}{(L/B)^3}\right) + a_0^2} \right] = 1 - \left[\frac{(0.55) * 0.164^2}{\left(0.6 + \frac{1.4}{(7.625/7.2)^3}\right) + 0.164^2} \right] = 0.992$$

Dynamic Stiffness of The Rigid Footings

$$K_x = K_{x,emb} * \alpha_x = 1968418 * 1 = 1968418 = 1.97E + 6\ kN/m$$

$$K_y = K_{y,emb} * \alpha_y = 1978247 * 1 = 1978247 = 1.98E + 6\ kN/m$$

$$K_z = K_{z,emb} * \alpha_z = 2160295 * 0.998 = 2155974 = 2.16E + 6\ kN/m$$

$$K_{xx} = K_{xx,emb} * \alpha_{xx} = 143993925 * 0.993 = 142985968 = 1.43E + 8\ kN/m$$

$$K_{yy} = K_{yy,emb} * \alpha_{yy} = 153538570 * 0.992 = 152310261 = 1.52E + 8\ kN/m$$

Radiation Damping Ratios for Embedded Footings (adapted from Pais and Kausel, 1988)

For translational x axis direction;

$$\beta_x = \left[\frac{4\left[L/B + (D/B)(\psi + L/B)\right]}{\left(K_{x,emb}/GB\right)} \right] \left[\frac{a_0}{2\alpha_x} \right]$$

$$= \left[\frac{4\left[7.625/7.2 + (4.2/7.2)(2.449 + 7.625/7.2)\right]}{\left(1968418/28.2*1000*7.2\right)} \right] \left[\frac{0.164}{2*1} \right] = 0.105$$

For translational y axis direction;

$$\beta_y = \left[\frac{4\left[L/B + (D/B)(1 + \psi L/B)\right]}{\left(K_{y,emb}/GB\right)} \right] \left[\frac{a_0}{2\alpha_y} \right]$$

$$= \left[\frac{4\left[7.625/7.2 + (4.2/7.2)(1 + 2.449*7.625/7.2)\right]}{\left(1978247/(28.2*1000*7.2)\right)} \right] \left[\frac{0.164}{2*1} \right] = 0.106$$

For translational z axis direction;

$$\beta_z = \left[\frac{4\left[\psi(L/B) + (D/B)(1 + L/B)\right]}{\left(K_{z,emb}/GB\right)} \right] \left[\frac{a_0}{2\alpha_z} \right]$$

$$= \left[\frac{4\left[2.449(7.625/7.2) + (4.2/7.2)(1 + 7.625/7.2)\right]}{\left(2160295/(28.2*1000*7.2)\right)} \right] \left[\frac{0.164}{2*0.998} \right] = 0.117$$

For rocking along x-x axis;

$$\beta_{xx} = \left[\frac{\frac{4}{3}\left[\frac{D}{B} + \left(\frac{D}{B}\right)^3 + \psi\frac{L}{B}\left(\frac{D}{B}\right)^3 + 3\left(\frac{D}{B}\right)\left(\frac{L}{B}\right) + \psi\left(\frac{L}{B}\right)\right] a_0^2}{\left(\frac{K_{xx,emb}}{GB^3}\right)\left[\left(\frac{1.8}{1+1.75\left(L/B-1\right)}\right)+a_0^2\right]} + \frac{\left(\frac{4}{3}\right)\left(\psi\frac{L}{B}+1\right)\left(\frac{D}{B}\right)^3}{\left(\frac{K_{xx,emb}}{GB^3}\right)} \right]\left[\frac{a_0}{2\alpha_{xx}}\right]$$

$$= \left[\frac{\frac{4}{3}\left[\frac{4.2}{7.2} + \left(\frac{4.2}{7.2}\right)^3 + 2.449\left(\frac{7.6}{7.2}\right)\left(\frac{4.2}{7.2}\right)^3 + 3\,\frac{4.2}{7.2}\left(\frac{7.6}{7.2}\right) + 2.45\left(\frac{7.6}{7.2}\right)\right] 0.16^2}{\left(\frac{143993925}{28.05*1000*7.2^3}\right)\left[\left(\frac{1.8}{1+1.75\left(7.625/7.2-1\right)}\right)+0.164^2\right]} + \frac{\left(\frac{4}{3}\right)\left(2.449\,\frac{7.625}{7.2}+1\right)\left(\frac{4.2}{7.2}\right)^3}{\left(\frac{143993925}{28.05*1000*7.2^3}\right)} \right]\left[\frac{0.164}{2*0.993}\right]$$

$$= 0.006$$

For rocking along yy axis;

$$\beta_{yy} = \left[\frac{\left(\frac{4}{3}\right)\left[\left(\frac{L}{B}\right)^3\left(\frac{D}{B}\right) + \psi\left(\frac{D}{B}\right)^3\left(\frac{L}{B}\right) + \left(\frac{D}{B}\right)^3 + 3\left(\frac{D}{B}\right)\left(\frac{L}{B}\right)^2 + \psi\left(\frac{L}{B}\right)^3\right] a_0^2}{\left(\frac{K_{yy,emb}}{GB^3}\right)\left[\left(\frac{1.8}{1+1.75\left(L/B-1\right)}\right)+a_0^2\right]} + \frac{\left(\frac{4}{3}\right)\left(\frac{L}{B}+\psi\right)\left(\frac{D}{B}\right)^3}{\left(\frac{K_{yy,emb}}{GB^3}\right)} \right]\left[\frac{a_0}{2\alpha_{yy}}\right]$$

$$= \left[\frac{\frac{4}{3}\left[\left(\frac{7.6}{7.2}\right)^3\frac{4.2}{7.2} + 2.5\left(\frac{4.2}{7.2}\right)^3\frac{7.6}{7.2} + \left(\frac{4.2}{7.2}\right)^3 + 3\,\frac{4.2}{7.2}\left(\frac{7.6}{7.2}\right)^2 + 2.5\left(\frac{7.6}{7.2}\right)^3\right] 0.16^2}{\left(\frac{153538570}{28.25*1000*7.2^3}\right)\left[\left(\frac{1.8}{1+1.75\left(7.63/7.2-1\right)}\right)+0.16^2\right]} + \frac{\left(\frac{4}{3}\right)\left(\frac{7.63}{7.2}+2.5\right)\left(\frac{4.2}{7.2}\right)^3}{\left(\frac{153538570}{28.25*1000*7.2^3}\right)} \right]\left[\frac{0.16}{2*0.99}\right]$$

$$= 0.006$$

Calculating Dashpot Coefficients

$$C_j = 2K_j\left(\frac{\beta_{j,radiation} + \beta_{j,hysteresis}}{\omega}\right)$$

$$C_x = 2*1968418\left(\frac{0.105+0.05}{3.785}\right) = 161218 = 1.61E+5 \ \ kN/m/_{rad/s}$$

$$C_y = 2*1978247\left(\frac{0.106+0.05}{3.785}\right) = 163068 = 1.63E+5 \ \ kN/m/_{rad/s}$$

$$C_z = 2*2155974\left(\frac{0.117+0.05}{3.785}\right) = 190250 = 1.90E+5 \ \ kN/m/_{rad/s}$$

$$C_{xx} = 2*142985968\left(\frac{0.006+0.05}{3.785}\right) = 4095604 = 4.09E+6 \ \ kN/m/_{rad/s}$$

$$C_{yy} = 2*152310261\left(\frac{0.006+0.05}{3.785}\right) = 453630 = 4.54E+5 \ \ kN/m/_{rad/s}$$